SOFT CARBON NANOTUBE FIBER ELECTRODES FOR MULTIMODAL NEURAL INTERFACING

A Dissertation
Presented to
The Academic Faculty

by

Linlin Lu

In Partial Fulfillment
of the Requirements for the Degree
of Philosophy in the
Department of Biomedical Engineering

Peking University & Georgia Institute of Technology & Emory University
August 2019

SOFT CARBON NANOTUBE FIBER ELECTRODES FOR MULTIMODAL NEURAL INTERFACING

Approved by:

Dr. Xiaojie Duan, Advisor
Department of Biomedical Engineering
Peking University

Dr. Antony K. Chen
Department of Biomedical Engineering
Peking University

Dr. Garrett B. Stanley, Co-Advisor
Department of Biomedical Engineering
Georgia Institute of Technology

Dr. Youfan Hu
School of Electronics Engineering and Computer Science
Peking University

Dr. Haifeng Chen
Department of Biomedical Engineering
Peking University

Date Approved: [May 30, 2019]

ACKNOWLEDGEMENTS

Five years of doctoral life flies. Looking back on the years passed, I feel full of emotion when the thesis was about to be completed. First of all, I sincerely thank my advisor, Dr. Duan Xiaojie, who has devoted herself to the design and finalization on the thesis. Dr. Duan has set a lifelong learning model for me. She is a great lady who succeeds in balancing family and scientific career. Her encouragement as a female scientist will inspire me to strive hard and innovate on the road of science and research. Thank the great laboratory mates at Duan lab, Fu Xuefeng, Guan Qian, Meng Xuejuan, Zhao Siyuan, Liu Xiaojun, Zhang Jing, Chu Fangbing, Xu Zheng, Li Gen, Wei Shiyuan, Tushar Sachdev, Wang Puxin.

I would like to express my sincerest thanks to Professor Garrett B. Stanley at Georgia Institute of Technology for his full support to me and for providing me with the conditions for all the experiments, from ideas, funds, personnel to experimental instruments, and to his laboratory members, Yijuin Liew, Christian Waiblinger, Elaida Dimwamwa, Aurelie Pala, Michael F. Bolus, Nathaniel C Wright, Audrey Sederberg, Clarissa Whitmire, Peter Y. Borden and Adam A. Willats. I learnt a lot from Garrett. Words cannot express how grateful I am for him as my co-advisor.

Special thanks go to Fu Xuefeng and Yijuin Liew. Xuefeng is my collaborator in many experiments. She is positive and optimistic and passionate about life and science. The days we spent together are full of joy. Yijuin is a great mentor who instructs me a lot not only on electrophysiological recording experiments, but also on how to more effectively and scientifically communicate with all kinds of personnel. I feel lucky for encountering them in my life.

Thanks to the confocal microscopy manager Lv Hongxia, classmate Zhao Zhizhen who helped me on laser cutter device, Dang Wenhui who showed me how to use atomic

force microscope, Zhang Yongyi et al. in Suzhou Institute of Nano-tech and Nano-bionics who provided carbon nanotubes, my roomate Xu Jiajun.

I would like to thank my friends in Atlanta. They are like family to me. Their names are listed here: Zhang Huicong, Peng Xirui, Song Tianze, Zhao Lihan, Shen Xing, Yang Mengmeng, Zhou Bangtian, Wu Yuemin, Chen Qiaoshan, Yang Rui, Chen Jiamin, Lin Yutao, etc. Thanks to the big warm family in Atlanta.

Finally, I would like to thank my family. Their support is the driving force for me to move forward.

TABLE OF CONTENTS

LIST OF TABLES

LIST OF FIGURES

LIST OF SYMBOLS AND ABBREVIATIONS

CNT	Carbon nanotube
MR	Magnetic resonance
MRI	Magnetic resonance imaging
PEO	Polyethylene oxide
PFA	Paraformaldehyde
S1	The first somatosensory cortex
VPm	Ventral posteromedial nucleus
MHb	Medial habenular nucleus
LHb	Lateral habenular nucleus
CSF	Cerebrospinal fluid
EIS	Electrochemical impedance spectroscopy
CV	Cyclic voltammetry
CSC	Charge storage capacity
CIL	Charge injection limit
GE	Gradient echo
SE	Spin echo
TR	Time of repetition
TE	Time of echo
SNR	Signal-to-noise ratio
LFP	Local field potential
EEG	Electroencephalograph
ECoG	Electrocorticogram

S1Tr	The trunk region of primary somatosensory cortex
VPL	Ventral posterolateral thalamic nucleus
CA1	Field CA1 of the hippocampus
CA2	Field CA2 of the hippocampus
CA3	Field CA3 of the hippocampus
PCA	Principal component analysis
PC1	The first principal component
PC2	The second principal component
GFAP	Glial fibrillary acidic protein (astrocyte marker)
NeuN	Neuronal nuclei (neuronal nuclear marker)
Iba1	Ionized calcium binding adaptor molecule 1 (microglia marker)
DAPI	4', 6-diamidino-2-phenylindole
OCT	Optimal cutting temperature
NIOSH	National Institute for Occupational Safety and Health
SD	Standard deviation
SEM.	Standard error of mean
SEM	Scanning electron microscope
ANOVA	Analysis of variance
SR	Slow rate
sccm	Standard cubic centimeters per minute
PSTH	Peristimulus time histogram
E	Young's modulus
δ	Skin depth
L	Inductance
I_{max}	Maximum eddy current

μ_0	Magnetic permeability of vacuum
ε_i	Electromotive force
RES_{sample}	Resistance of the sample
τ	Decay time constant
ω	Angular frequency
μ	Magnetic permeability
μ_r	Relative magnetic permeability
χ	Susceptibility
ρ	Resistivity

SUMMARY

Electrodes made of stainless steel, noble metals and crystalline silicon have been widely used for neural recording and neural stimulation in neuroscience study and clinical application. However, the high stiffness and large size of these electrodes challenges their capability of forming chronically stable neural-electrode interfacing for reliable and stable neural recording and stimulation. What's more, these electrodes may cause magnetic field distortions and introduce large blind areas around the electrodes during magnetic resonance imaging (MRI), while MRI allows global brain activity detection and serves as an important and commonly used tool in neuroscience researches and clinical applications. Therefore, a neural electrode that integrates MRI compatibility and forms stable chronic neural interface for neural recording and stimulation is highly desired.

Carbon nanotube (CNT) fiber is an excellent material candidate for the purpose due to its high softness, excellent electrochemical properties and close-to-tissue magnetic susceptibility. The aim of the thesis study is to develop soft and ultrasmall CNT fiber based neural electrodes for multimodal neural interfacing, such as MRI study, neural recording, etc. The thesis developed the fabrication and implantation technologies of standalone CNT fiber electrodes, demonstrated their electrochemical properties, mechanical compliance in vitro and biocompatibility in vivo, examined and explained their MRI compatibility in vivo, explored their multiple advantages for acute and chronic neural recording in vivo. The main accomplishments are as follows:

(1) Fabrication, implantation technologies and characterization of CNT fiber electrodes. CNT fibers were fabricated from millions of tiny CNTs and coated with parylene-C via chemical vapor deposition for insulation, followed by blade cutting on the fibers for exposing the recording sites. A shuttle-assisting method was utilized for implantation, where CNT fiber electrodes were firstly combined with stiff tungsten wires by gluing with biocompatible and dissolvable adhesive polymer materials, then being inserted together with the tungsten wire which acted as a shuttle, and finally the tungsten shuttle was extracted out and left the CNT fiber electrodes inside. The nitric acid treated CNT fiber electrodes showed 0.11 times, 178 times, and 34 times the impedance, charge storage capacity and charge injection limit respectively of PtIr electrodes of a similar size. The low impedance favors for neural recording. And the high charge storage capacity and high charge injection limit favor for neural stimulation. The bending stiffness per width were 8.16k nN • m, 0.16k nN • m, 153k nN • m, 39k nN • m and 460k nN • m respectively for 20 μ m CNT fiber electrodes, 5 μ m CNT fiber electrodes, PtIr electrodes, carbon fiber electrodes and silicon electrodes. The orders of magnitude smaller bending stiffness demonstrated the softness of CNT fiber electrodes, favorable for reducing tissue damage, mitigating inflammatory responses and facilitating chronic stable neural interface.

The histological studies at 6-week post electrodes implantation showed 2-fold reduction compared to PtIr electrodes for the accumulated astrocytes and activated microglia, which are inflammatory cells produced during foreign body reaction. The neuron lost zone of CNT fiber electrodes was 40% smaller than that of PtIr electrodes. The results at 12-week post implantation of PtIr electrodes showed further neurodegeneration with 1.3-fold neuron lost zone increase while CNT fiber electrodes showed no significant

further degeneration. These results proved that the CNT fiber electrodes manifested improved and more stable chronic neural interfacing, facilitating chronic studies on neural activities.

(2) Standalone CNT fiber electrodes demonstrated MRI compatibility. 20 μm diameter CNT fiber electrodes in T2 anatomical images under 7.0 T MRI scan showed 40% artifact size of PtIr electrodes with a similar electrode size. The CNT fiber electrodes were barely visible in T1-weighted MRI scanning, compared to 922 μm artifact size existed for PtIr electrodes. The main reason for CNT fiber electrodes' better MRI compatibility is due to their much closer magnetic susceptibility to tissue. Though the eddy currents in both electrodes, which may contribute to the artifacts, are quite small and disappear fast, the calculation showed that the CNT fiber electrodes have ~ 1% eddy current amplitude, ~ 1% current decaying time constant and ~ 1/10 skin depth compared with those of the PtIr electrodes. Therefore, the CNT fiber electrodes exhibited much superior MRI compatibility, favoring and enabling many applications, such as verification and adjustment of the implantation position of deep brain stimulating electrodes with MRI, mapping large-scale neural activity from functional MRI with electrophysiological recording results with high temporal and spatial resolution, localization of seizure foci for clinical treatment, etc.

(3) Acute and chronic neural recordings in vivo. Representative single unit neural signals responding to whisker stimulation recorded in ventral posteromedial (VPm) thalamic nucleus in rats demonstrated the CNT fiber electrodes' ability for precisely targeting planned brain areas in the brain as VPm area is small (~ 1-2 mm) and deep (~5

mm) in the brain. Other recordings in the somatosensory area of S1 served as a good justification of the CNT fiber electrodes' single unit signal detection sensitivity, as the relatively smaller spikes amplitude generated from neurons in S1 requires higher electrical detection sensitivity.

The multi-depth electrophysiological recording results demonstrated the CNT fiber electrodes' ability of fine-tuning the implantation position of the microelectrodes after implantation, which offers advantage for both recording and stimulating neural electrodes. Note that many state-of-the-art flexible electrodes require about 2 weeks for tissue recovery after implantation before the first successful electrophysiological recording, while the CNT fiber electrodes obtain real time electrophysiological recording during implantation. What's more, many flexible electrodes lack the capability of fine-tuning of implanted position or the implantation are constrained within a very shallow depth, the CNT fiber electrodes are robust enough to be fined-tuned and a 7 mm implantation depth is attainable, enabling deep brain study.

The chronic recording examples showed the longevity of the CNT fiber electrodes for stably recording single unit signals for 4-6 months without repositioning. For further analyzing the electrophysiological recordings, principal component analysis was performed, and four different features of the sorted single units were calculated. These analyses manifested that some of the recorded single units for that rat recorded for 4 months were possibly from the same neuron, which demonstrated the potential of CNT fiber electrodes for tracking same neurons, favoring many fundamental neuroscience studies, such as investigating the mechanisms of aging of neurons, studying the action potential firing changes of neurons with repeated stimulation, etc.

In addition, ultrasmall electrodes made with 5 μm diameter CNT fiber cores were achieved and the single unit recording capability verified in vivo. The ultrasmall sized CNT fiber electrodes allow for high spatial recording resolution, low tissue damage and mild inflammatory responses, and more electrodes being integrated in a limited space.

In conclusion, the thesis study extensively explored the possibilities of soft CNT fiber electrodes, which showed multiple excellent advantages for multimodal neural interface. The thesis study laid the foundation for further exploration and development of CNT fiber based neural interface, and provided an outstanding tool for future neuroscience study, brain-computer-interface research and clinical application.

CHAPTER 1. INTRODUCTION

The thesis study focuses on developing soft carbon nanotube (CNT) fiber electrodes for multimodal neural interface. In this chapter, the neural interface is firstly introduced in the first subsection, including the complexity of the brain study, electrical signals in the brain and a brief introduction of neural electrodes. In the second subsection, two important factors of neural electrodes, electrochemical and mechanical considerations are presented together with multiple possible sources of failures. In the third subsection, previous studies of CNT fibers are discussed, especially the most relevant studies on CNT fibers for neural interfacing. The fourth subsection reveals significances and innovations of the thesis study. Thesis organization is presented in the last subsection.

1.1 Background

1.1.1 The complexity of the brain study

The brain as the most complex organ in the human body and other vertebrate animals, serves as the center of neural systems. Approximately 14-16 billion neurons exist in the cerebral cortex and about 55-70 billion neurons exist in the cerebellum. [1] Each neuron connects and communicate with about several thousand other neurons by synapses. The human brain has many types of neurons, such as basket cells, pyramidal cells, and chandelier cells, which are named by shape. We don't know exactly how many kinds of cells there are in the brain, for example, Cajal-Retzius cells, which play a critical role in the brain development, are scarcely distributed in the brain. Figure 1 illustrate several types of neural cells. We don't know how many other types of cells have not been discovered yet

and/or why so many cells are needed for the brain functioning. Not only do we need to figure out what's in the brain, but we also need to know how each part connect with each other, how it changes over time or stimulation, how information is stored and transmitted, and how other cells and connections in the brain change when a connection is interrupted. Until we figure this out, it is impossible for us to expect to know how the whole brain works. The field of neuroscience requires huge amounts of data. On the one hand, we need advanced tools to get more data, and on the other hand, we need to understand the theory behind these data, using methods including learning from psychology, cognitive science, Mathematics, computer science, linguistics, evolutionary theory, and so on. Theory, experiment, and the interactions of theory and experiment are all important.[1]

There are multiple strategies to study the brain. Figure 2 shows four generalized modalities of neural study, including electrical, optical, magnetic resonance and molecular modalities. For electrical neural recording since 1950s, the amounts of neurons being simultaneously recorded has doubled about every 7 years. Jason E. Chung et al. reported polymer electrode arrays of 1024 recording channels, capable of tracking populations of individual neurons for more than one week, the longevity of tracking single-unit for 160 days post-implantation, simultaneously recording 375 single units from multiple regions in awake and freely behaving rats. [2] For optical imaging methods, signals resulting from fluorescent indicators endowed by the activities of neurons are detected by photodetectors. For magnetic resonance imaging, radio-frequency emissions due to nuclear spins under magnetic field was detected and utilized to rebuild the magnetic resonance images. For the molecular based techniques, multiple creative neural activity detecting strategies were

conceived, for example, by correlating the nucleotide misincorporation probabilities of DNA or RNA cells to the activity of neurons. [3-5]

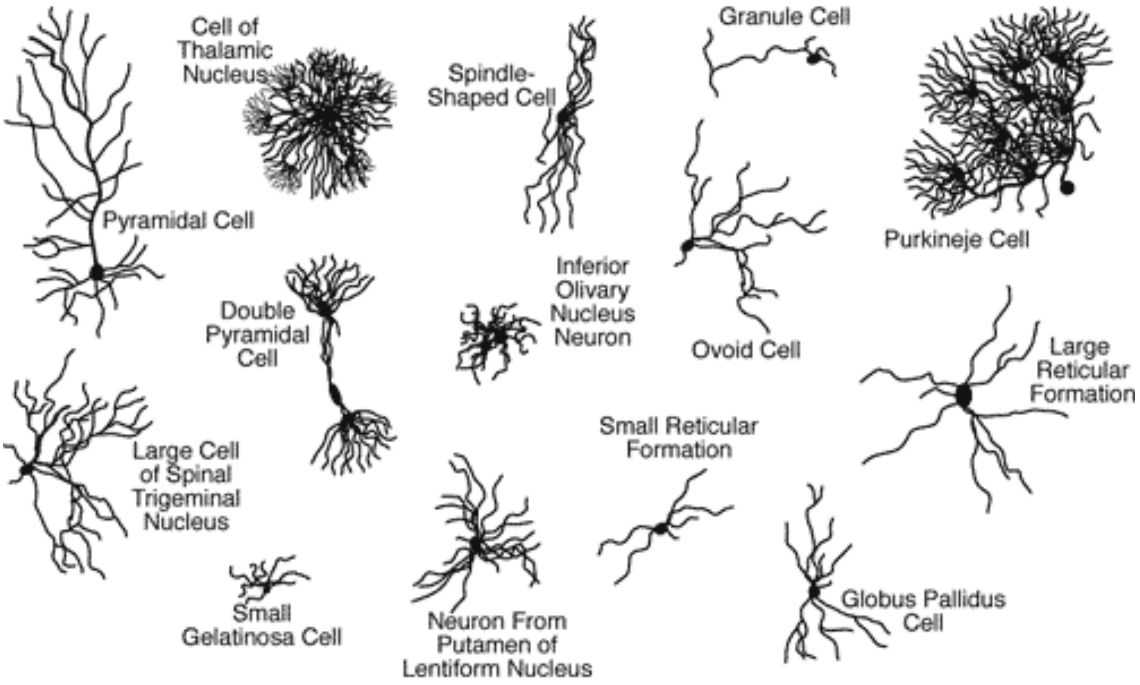

Figure 1. Typical neuron types. Figure from curriculum of Robert Stufflebeam. http://www.mind.ilstu.edu/curriculum/neurons_intro/neurons_intro.php

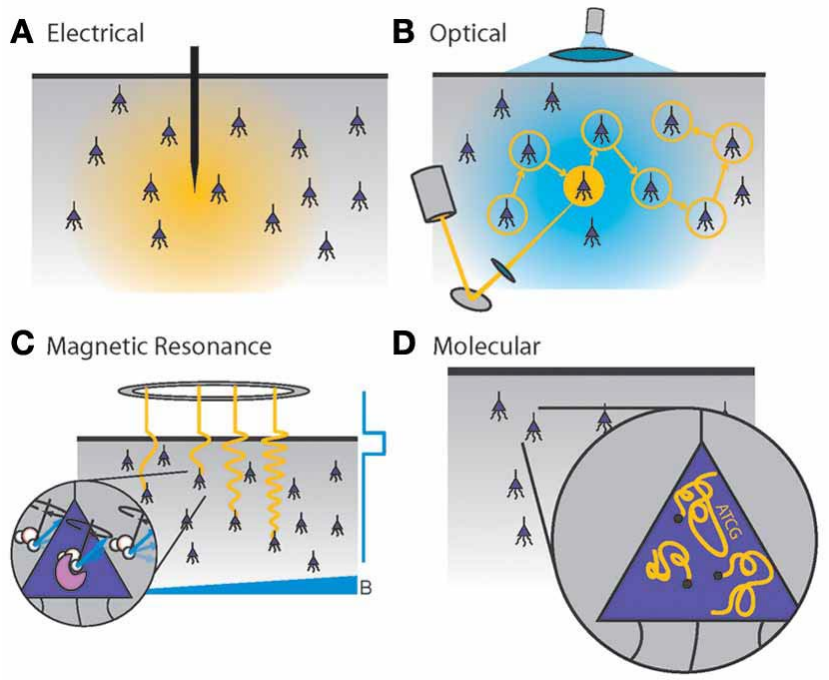

Figure 2. Four common neural recording modalities. Figure from Adam H. Marblestone. [6]

Each recording modality has its assumptions, disadvantages and disadvantages as described below for each recording modality.[6] (1) Extracellular electrical recording. The assumptions include two aspects, a. Decay profile of the extracellular voltage. b. Estimated noise levels at the recording sites. The maximum recording distance between the electrodes and recorded neurons is about 100-200 μm for detecting reliable and sortable single unit signals. The advanced multi-electrode arrays are capable of recording hundreds of neurons at single unit level at tens of micron spatial resolution and at sub-millisecond temporal resolution. (2) Optical imaging. We assume that the values of scattering and adsorption of light can be estimated as a function of wavelength. Currently, light-sheet illumination could enable simultaneous recording of ~ 100,000 neurons in behaving zebrafish at a 1.25 s timescale,[7] while 1-photon fiber scopes enable simultaneous recording of thousands of

neurons in behaving mice at a time scale of ~ 100 ms.[8] (3) MRI. Advanced MRI technologies with a magnetic field of 7 T, 8 Tor even 11.75 T have been developed, though not for clinical use. However, it's still far from achieving single neuron accuracy.[6] (4) Molecular neural recording. The assumptions include that polymerase biochemical parameters correlate with neural activities. Substantial progress has been made in DNA read-and write technology while trade-offs also exist between throughput and spatial resolution. Molecular recoding technique offers a brand perspective to decipher the neural activities.[9]

1.1.2 Electrical signals in the brain

Four categories of neural recording technologies were mentioned in the above subsection, including electrical, optical, magnetic resonance related, and molecular technologies. There is a vast of opportunities in every technological field. Material advancement in recent years provides a huge opportunity for electrical recording technologies, which is my major focus. Therefore, this subsection introduces various of electrical signals in the brain.

Briefly, this subsection contains the following contents: (1) A very brief introduction of the electrical generation in the brain. (2) Three commonly mentioned electrical recording techniques, EEG, ECoG, depth electrodes for recording local field potential and spikes (action potential) categorized by the placement of electrodes. (3) Principles of action potential or to say, spikes. The action potential is specifically presented as it is the major electrical signals involved in my thesis study. (4) Two critical parameters (recording

distance between electrodes and recorded neurons and the firing rate of neurons) for successful neural action potential recording are discussed.

As the center of nervous systems of all vertebrates and most invertebrates, there are many electrical activities in the brain. The human central nervous system is mainly composed of two kinds of cells, namely neurons and glial cells. The function of neurons is to receive stimulation and transmit excitability. Glial cells provide support, nutrition and protection functions for neurons. Neurons are composed of cell bodies and protrusions, which are divided into dendrites and axons. There is frequent electrical activity in the cerebral cortex. Neurons in the cerebral cortex have self-generating electrical activity, so the cerebral cortex often has a constant rhythmic potential change called spontaneous brain electrical activity.

There are a variety of electricity recording methods available for measuring neural activity in the brain. According to the position where the recording electrode is placed in the brain, the signal recorded can be categorized as electroencephalograph (EEG), which is recorded by potential change on the scalp by bipolar or unipolar electrodes, electrocorticogram (ECoG), which performs potential recording directly on the surface of the cortex, and local field potential (LFP) and spikes recorded by intracortical electrodes inside the brain tissue. The demonstration of these three kinds of signals and probes are shown in Figure 8. Compared to EEG and ECoG, intracortical electrodes can record voltage signals with higher temporal resolution and spatial resolution. EEG and ECoG usually record the collective electrical activity of neurons, rather than the electrical activity of individual cells, because the recording sites of EEG and ECoG are far from the neurons, and the recording sites are generally larger than that of intracortical electrodes. The

intracortical electrodes are capable of not only recording local field potential (LFP), but also recording the action potential (spikes), that is, the firing of a single cell. The firing of individual neuron is the basic component of the neural network. Understanding the firing patterns of single neurons is an important method to understand the information transmission by electrical signals in the brain and to study the cognitive science and brain-machine interface.

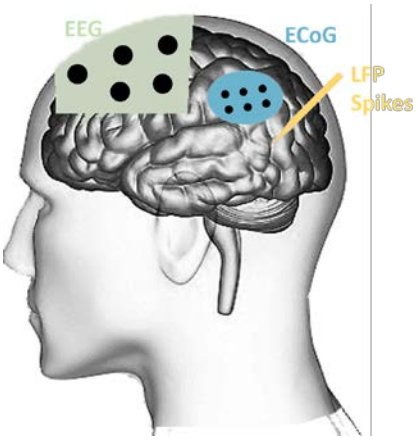

Figure 3. Schematics of EEG, ECoG, LFP and Spikes recording probes and positions in the brain.

The action potential is a type of brain electricity that records the electrical activity of a single cell. The generation process of an action potential includes the depolarization and hyperpolarization of cell membrane when the neurons are stimulated from a resting state to an excited state, that is, a process in which the negative potential in the membrane rapidly disappears. However, this process often exceeds zero, causing the membrane to change from a negative potential to a positive potential. This reversal process is called reverse polarization or hyperpolarization. Therefore, the firing of an action potential is a continuous process of depolarization and reverse polarization of the membrane. At this time, a large amount of Na+ outside the cell membrane flows into the cell, and the cell

membrane at this time is called a sodium membrane; The cell membrane, in turn, selectively allows a large amount of K+ to flow out of the cell, called the potassium membrane. The **Figure 18** shows the change of membrane potential of action potential.

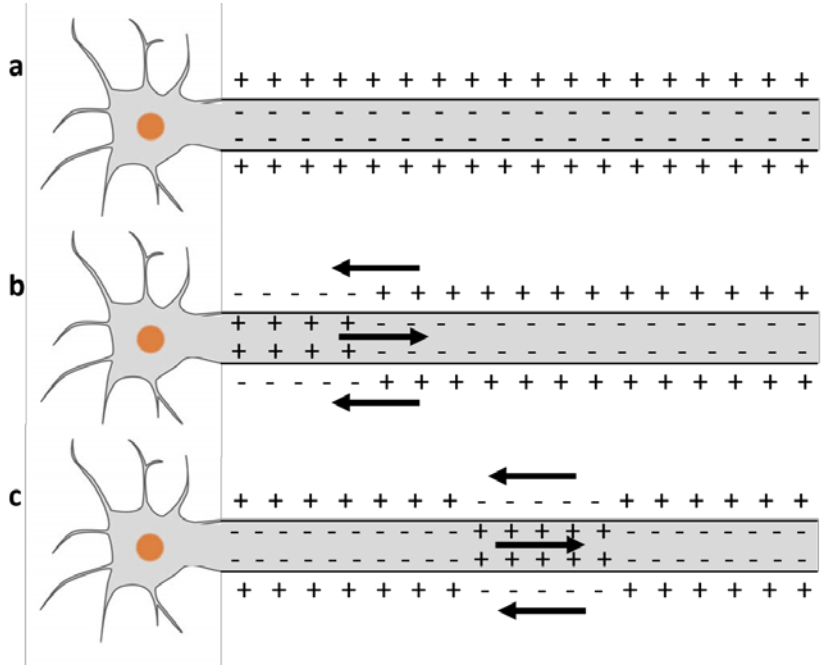

Figure 4. Membrane ionic changes during an action potential. (a) shows the resting potential of neural membrane. (b) shows the initiation of action potential. (c) shows the transmission of action potential.

The distance between the electrode-neuron has a great influence on the type and size of the neural signals that the electrodes can record. Gyorgy Buzsaki et al studied electrode recording neural signals in CA1 pyramidal cells and estimated the performance of electrodes characterized by the recorded spike amplitudes as a function of distance between the electrodes and neurons recorded as shown in Figure 9. Briefly, the tetrode can record larger than 60 μV amplitude signals within no more than 50 μm radius area around the electrodes. From ~ 50 μm - ~ 140 μm radius area, signals with amplitude less than 60 μV could be recorded. if the distance of the electrode from the cell is greater than 140 μm,

the extracellular recorded spike will not be distinguished from the background noise, that means no effective spike signal will be recorded.[10] Zoltan Somogyvari et al. The simulated method was used to estimate the electrode-cell distance at which the electrode can measure the effective spike. The maximum estimated distance is 72 μm.[11] Adam H. Marblestone et al. estimated the maximum distance between electrode and neurons recorded for recording spikes is about 100 μm - 200 μm.[6]

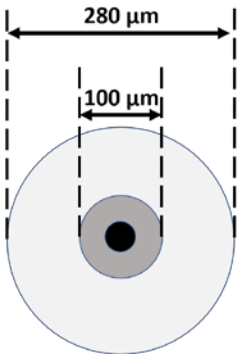

Figure 5. The three categories of different performance of electrodes as a function of distance between electrodes and recorded neurons reported by Gyorgy Buzsaki et al. The black area represents the area of tetrode. The dark grey area represents the area within which larger than 60 μ V amplitude spikes can be recorded. The light grey area represents where less than 60 μ V amplitude but clusterable spikes can be recorded.

In addition to the distance between the electrode neurons affecting the signal quality of the recorded spikes, the firing rate of the neurons themselves is one of the most important factors affecting the recorded signals. The frequency of neurons' firing in the brain is hugely different between different cell types, in different brain regions, or under different brain state. Studies on the firing rate of neurons in the brain found by some researchers is listed in the table below.[6] It can be seen from the table that firing rate of neurons ranges from almost no firing at all to a firing frequency of > 500 Hz, and the difference is huge. Also, a majority of spikes are fired by a minority of neurons.[12-15] The reason that firing

rate of neurons is critical for neural recording is that it is not possible for the experimenters to record any spikes if the firing rate of neurons close to the recording sites of implants is very low, for example, the nearby neurons don't fire spontaneously or don't fire due to trauma or damage caused by either implantation procedures or concussions.

Table 2. Various firing rates of neurons discovered by researchers.

Firing Rate (Hz)	Note	Researchers
< 0.1	These cells make up to ~ 90% of certain cell types in some brain areas	Shoham et al., 2006;[16] Barth and Poulet, 2012.[17]
~ 0.16	Neocortex in primates	Lennie, 2003.[18]
~ 0.5	Cerebellar granule cells, which constitute about half of the neurons in the brain.	Chadderton et al., 2004.[19]
5	Estimated average firing rate	Sarpeshkar, 2010;[20] Harris et al., 2012.[21]
⩾ 500	-	Gittis et al., 2010.[22]

Besides, it is worth mentioning that the firing rate of neurons is a very important essential attribute of the electrophysiological data for extracellular action potential recording. Because the waveforms of the action potential recorded is generally only used to sort the signals into different units, or different cell sources. At present, when the sorting

process is completed, usually only the firing rate and the firing time stamps are useful for the interpretation of information and information transmission.

1.1.3 Neural Electrodes

After the electrical signals in the brain being introduced, now we focus on the neural electrodes, as this is my major focus among many disciplines created by neuroscience and neural engineering. In this subsection, a brief literature review from conventional neural electrodes to advanced technologies on neural electrodes will be presented.

Conventional neural electrodes are made from stainless steel, noble metals and silicon, etc.[23] The Utah electrode array (Figure 1) and Michigan electrodes (Figure 2) are two common types of conventional electrodes.

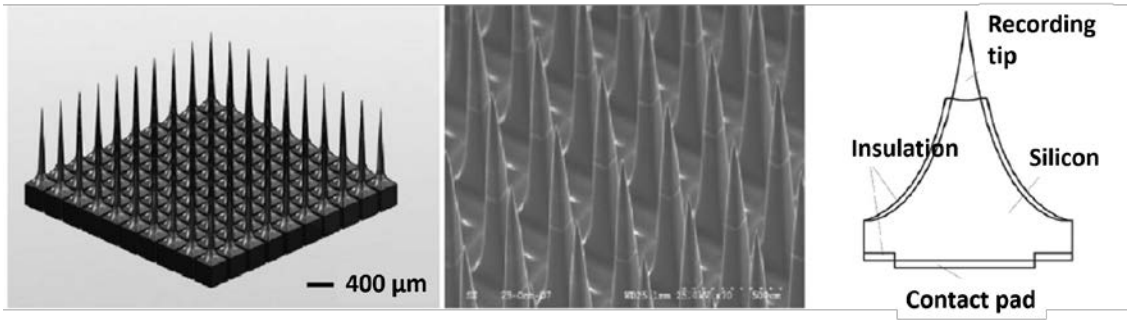

Figure 6. Illustration of Utah electrodes. Schematics drawing of an electrode array, images of SEM and representative cross-sectional structure. The figure was adapted from Zoltan Fekete paper.[24]

Figure 7. Illustration of Michigan electrodes. Schematics drawing of a Michigan electrode, images of SEM and representative cross-sectional structure. The figure was adapted from Zoltan Fekete paper.[24]

With a much larger stiffness compared to tissue, they are not mechanically compatible with biological systems. Chronic implantation of implants made from these materials will cause neural tissue damage and cause long-lasting inflammation response around the implanted electrodes. Thus, the electrodes cannot record from stable positions in the tissue owing to the relative shear force between the stiff electrodes and the much softer tissue.

The goal for neural recording electrodes is to chronically and stably record from as many neurons as possible in the expected recording area with high-quality neural signals and causing less tissue damage. The initial trauma generated during implantation of the electrodes is related to the size of the electrodes. The bending stiffness is inversely proportional to the fourth power of the diameter of the electrodes.[25, 26] In addition, the smaller the exposed recording sites, the finer resolution the electrodes can reach. Kipke and co-workers developed an ultrasmall microelectrode utilizing 7-µm-diameter carbon fibers as the core with a total diameter 8.5 µm. They recorded stably for over five weeks in

rodents.[27] Chong Xie and co-workers developed ultraflexible nanoelectronic thread probes which has glial scar-free neural integration. They used a 7 μm carbon fibre as the insertion shuttle to drag the ultraflexible electronics inside the tissue, which results in small footprint of the insertion track. They reported absence of chronic neuronal degradation and glial scar. The demonstrated their electrodes can reliably track single units for months.[28] J. A. Rogers and co-workers developed mesh-like flexible electronics by using biodegradable silk as a substrate and remove the unnecessary part of the substrate on the electronics. The mesh structure hugely increases the flexibility of the electronics and they can better fit the curvature of the brain tissue, which makes it possible to develop large-scale neural electrodes to record from large brain area.[29] Lieber and co-workers developed three dimensional mesh electronics, with structural and mechanical properties similar to neural tissue. They implant the mesh electronics using syringes. The in-vivo study showed that their electronics are capable of mapping brain activity at the single-neuron level for at least four months.[30] Janos Voros and co-workers developed high-density stretchable electrode grids. They used silicone as the substrate and embedded gold-coated titanium dioxide nanowires as the core material. Their electrode density reached 38/mm² and can stably record for 3 months.[31] J. A. Rogers and Brian Litt and their co-workers developed silicon nanomembrane transistors based neural electronics with thousands of sensors. These sensors can record brain activities such as sleep spindles, electrographic seizures.[32] Guosong Hong et al. in 2019 reviewed developed high spatial integrated, multiple functional and long-term stable neural recording electrode technologies. [33] Figure 8 adapted from the review demonstrate the discoveries and breakthroughs achieved by the development of neural recording electrodes, together with

three the improvement in the spatial integration, temporal stability and the functional integration with the development of recording electrodes.

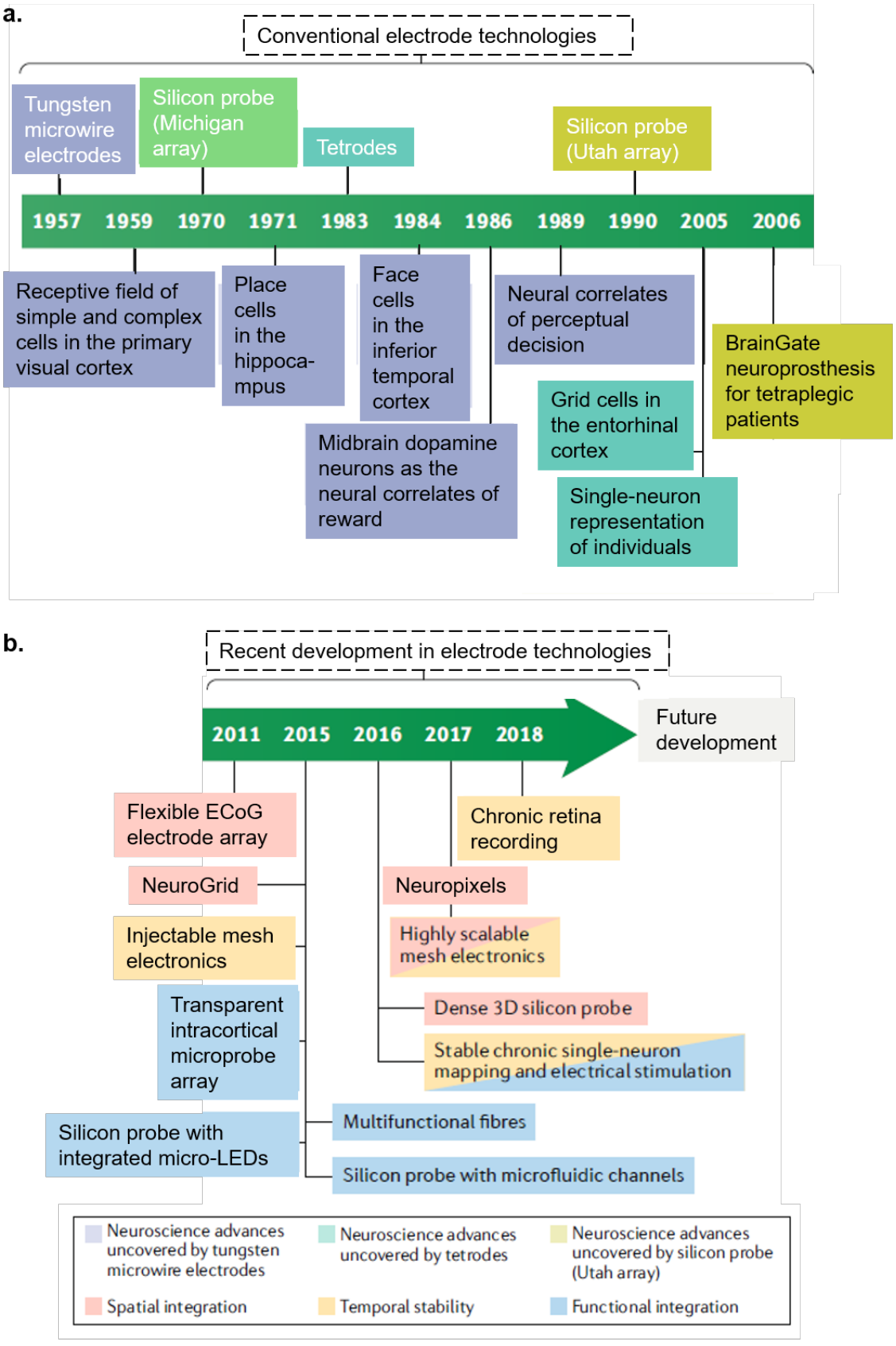
a.
Conventional electrode technologies
Tungsten microwire electrodes
Silicon probe (Michigan array)
Tetrodes
Silicon probe (Utah array)
1957
1959
1970
1971
1983
1984
1986
1989
1990
2005
2006
Receptive field of simple and complex cells in the primary visual cortex
Place cells in the hippoca-mpus
Face cells in the inferior temporal cortex
Midbrain dopamine neurons as the neural correlates of reward
Neural correlates of perceptual decision
Grid cells in the entorhinal cortex
Single-neuron representation of individuals
BrainGate neuroprosthesis for tetraplegic patients
b.
Recent development in electrode technologies
2011
2015
2016
2017
2018
Future development
Flexible ECoG electrode array
NeuroGrid
Injectable mesh electronics
Transparent intracortical microprobe array
Silicon probe with integrated micro-LEDs
Chronic retina recording
Neuropixels
Highly scalable mesh electronics
Dense 3D silicon probe
Stable chronic single-neuron mapping and electrical stimulation
Multifunctional fibres
Silicon probe with microfluidic channels
Neuroscience advances uncovered by tungsten microwire electrodes
Neuroscience advances uncovered by tetrodes
Neuroscience advances uncovered by silicon probe (Utah array)
Spatial integration
Temporal stability
Functional integration

Figure 8.(Continued) Conventional and recent advanced electrode technologies. Figure adapted from: Guosong Hong et al. review *Novel electrode technologies for neural recordings*.[33]

1.2 Fundamentals of Neural Electrodes

1.2.1 Electrochemical Fundamentals

Electrical transmission between electrodes and tissue is critical for the stimulating and recording neural electrodes functioning. For the electrode, it is the electrons that playing a role in the electrical transmission. For the tissue, it is all kinds of ions in the extracellular fluid, such as sodium, potassium and chloride, that transfer charges. In the electrode-tissue interface, a double-layer capacitor forms between the conducting elements such as electrons in the electrode and the conducting elements in the tissue such as the electrolytes. There is potential change which forms an electric field at the interface because the interface is where two different phases happens. When there are potential changes, charge transferring happens between the two phases. There are mainly two kinds of charge transferring. When the potential difference between the double layer is relatively small, non-Faradaic reactions happen, while charges are redistributed for the two layers. In this case, the charges can be recovered when the potential is reversed. However, when the potential difference is relatively huge, Faradaic reactions happen and the electrons between the two layers are transferred. In the second case, reduction and oxidation reactions take place. As to whether the Faradaic process is reversible or not, it depends on how soon the reduction and oxidation products move far away. If the products diffuse far away soon, then the process is not reversible as it is not possible to recruit those far-away particles for reaction. Otherwise, the products can be reversed. One thing worth mentioning is that the

Faradaic reactions create potentially products that are damaging to electrodes or tissues, which should be considered when designing electrodes, especially stimulating electrodes, which inject currents into the tissue.[34]

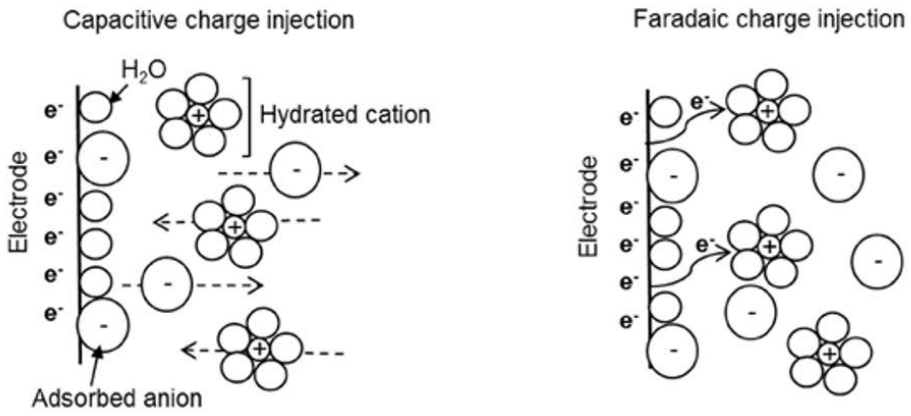

Figure 9. Schematics drawing of electrode-electrolyte interface.

The double-layer capacitor is extremely important for stimulating electrodes. For recording electrodes, usually the currents at the electrode-tissue interface are quite small and no Faradaic reaction will happen so the critical parameter for the recording electrode is the impedance of the electrodes. The recording site should be smaller than approximately 2000-4000 μm^2.[35] It is believed that the higher the impedance of the electrodes, the smaller the signal-to-noise ratio they record from neurons.[35]

1.2.2 Mechanical Considerations

Mechanical mismatch between neural electrodes and tissue is considered as an important factor for failure of electrodes, owing to several reasons. (1) Implants with mismatched mechanical properties to tissue are prone to cause more severe foreign body reaction, thereby causing severe sustained inflammatory response. As a result of the

inflammatory response, astrocytes accumulate around the implants and form a thick layer, called glial scar, which may increase the impedance of the implanted electrodes and thus shielding the recording sites of electrodes from conducting signals from the nearby neurons. Moreover, the inflammatory response may also cause neuronal degradation around the implant, causing the silence or damage of neurons and thus stopping the spike firing of neurons, leading to no signals recorded by the electrodes. (2) The relative shear force due to mechanical mismatch between tissue and implanted electrodes results in relative motion between them, even the force generated by breathing could lead to a micromotion between electrodes and tissue as demonstrated in a review by Aziliz Lecomte.[36] The relative movement leads to a larger damage to the tissue along the implanting path, larger neuronal lost zone and fewer healthy neurons, and a larger distance between the closest firing viable neurons and the electrode recording sites, thus preventing the electrodes from recording effective signals from the neurons. Breathing and heart beat induced pressure are about tens of microns and 0.2 μm respectively as shown in Figure 10a.[37] Finite element simulation results shown in Figure 10b demonstrates that the strains generated by tethering forth on stiff electrodes is mainly on the inserted tip of the implants, while the major strain generated by soft electrodes mainly constrains on the upper tissue.[38] For the two different distribution of strains phenomena, the situation is better for the soft electrodes as much less strain generated around the recording sites. (3) The mechanical- mismatch caused relative movement leads to inaccurate recording positions of the electrodes. As the position changes, the neurons being recorded changes, and even the recorded brain regions might change. This phenomenon makes it impossible to record reliably and stably from the same groups of neurons, not to mention from the same neurons, thus precluding researches that require

long-term study on certain types of neurons, such as the research on chronic response of neurons to repeatedly appearing stimuli, changes in synaptic plasticity over long-time scale due to the behaviour of learning and memory, the aging of neurons.[39-41] All these mentioned researches are of great interest for neural scientists.

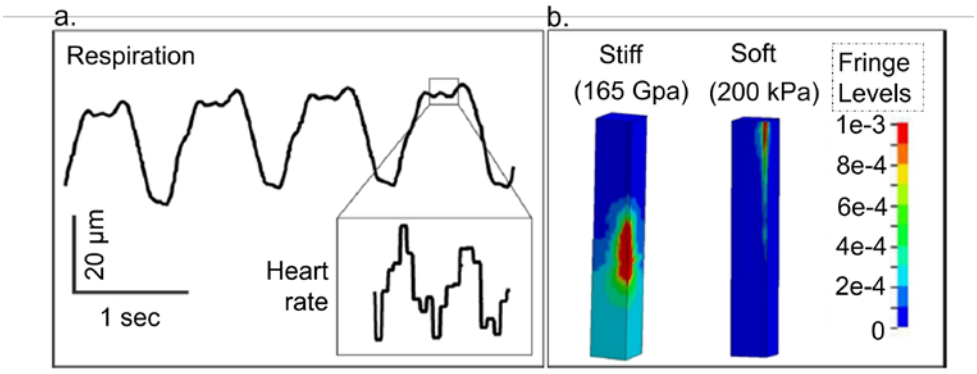

Figure 10. (a) Schematic drawing of respiration and heart beats induced micromotion. (b) Finite element simulation of fringes caused by stiff and soft probes. Figure reproduced from [36]. The original versions of a and b are respectively from [37] and [38]

We now know that mechanical properties play a very important role in the tissue-electrode interface and electrode longevity. Many materials of implants are mechanically mismatched from tissues. Then how to reduce the mismatch between the mechanical mismatch? Generally, three strategies have been approved to be effective.

The first effective method is to make small-sized microelectrodes. (1) The small-sized electrode has a small implantation path, and it is obvious that the initial direct damage to the tissue is small, as fewer neurons in the implantation path get damaged around the implanted electrode, and more healthy neurons survive, thus contributing to an effective neural electrical signal being recorded at the electrode. (2) A critical physical property for characterizing the flexibility of the electrode is bending stiffness, which is proportional to

the fourth power of the size of the electrode. For example, an electrode with a diameter of 100 μm has a bending stiffness 10,000 than that of a 10 μm diameter electrode. The relative movement between the implanted electrode and the tissue is affected by the bending stiffness, and the smaller the bending stiffness, the smaller the relative movement between the electrode and the tissue, resulting in a smaller secondary damage to the tissue post implantation. (3) In addition, small-sized electrodes are more flexible so that the inflammatory response induced is less severe and the implants are less likely to be wrapped by thick glial scar. As we know that glial scar increases the impedance of the electrode and thus decreasing the SNR detected by the electrodes. Therefore, a small-sized flexible electrode has a great advantage in neural recording.

The second effective strategy is to utilize materials with small Young's modulus. In the case of the same size, the electrode with a smaller Young's modulus is softer and closer to the mechanical properties of the brain tissue, and thus the inflammatory reaction is smaller, resulting in less tissue damage and more healthy neurons surrounding the implanted electrodes. The foreign body reaction induced by stiff and compliant implant with the same electrode size are respectively demonstrated in Figure 11a and Figure 11b. The stiff electrode induced inflammation zone, represented by the light blue region, is significantly larger than that induced by compliant electrode. In the inflammation zone, the red cells represent activated microglia and macrophages while the orange cells surrounding the electrodes represent reactive astrocytes. Nothing that the number and density of astrocytes surrounding the stiff electrode is much more than that surrounding the compliant electrode. As a result of the inflammation response, those aggregated astrocytes form a layer called glial scar surrounding the electrode. The much denser glial scar around the stiff

electrode leads to the decrease of signal qualities recorded by the electrode. In addition, the neurons in blue color are the source of signals we recorded using the electrodes. As shown in Figure 11, the neurons are outside of the inflammation zone, which means that the larger the inflammation region, the longer distance between the electrode recording site and the neurons being recorded, the worse signals to record on the electrodes. Therefore, compliant materials are desired and effective in reducing inflammation response of the tissue and improve the signal qualities recorded on the recording site of the implanted electrodes.

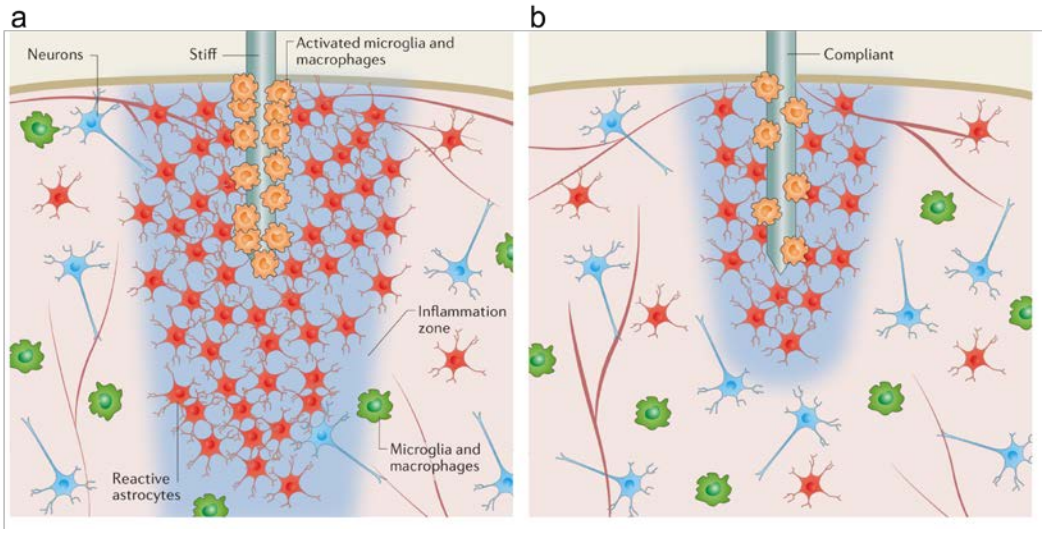

Figure 11. Foreign body reactions induced by stiff and compliant implant. Figure from [42]

The electrode material allows the implanted electrodes to be extended without substantial relative motion when the tissue is in motion, resulting in less damage and easier electrode maintenance at the initial implantation site. The two materials in the figure are the same size, but the Young's modulus is different.

The third strategy is to make improvements in the design of the structure of the electrodes. Figure 12 shows several common structures for increasing the flexibility and

elasticity. Materials with the porous feature and the curvatures transform from rigid to flexible and stretchable materials, which facilitate its compliance with tissue and reduce the potential relative micromotion between the implanted electrodes and tissue.

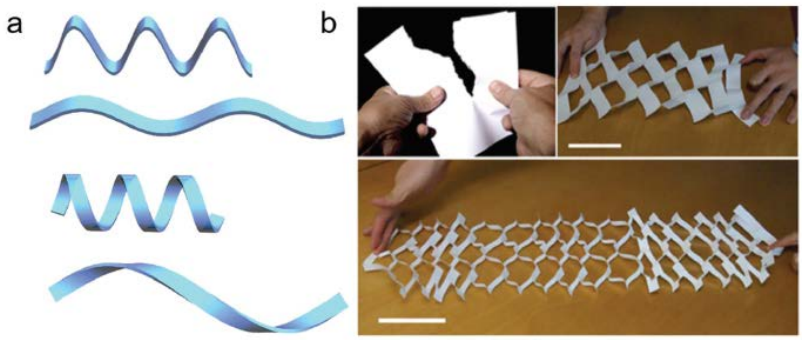

Figure 12. Pattern designs for increasing flexibility and elasticity of electrodes. Figure a and b are from [43], with the original version of b. from [44]

1.2.3 Sources of Failures of Neural Electrodes

Implanted neural electrodes are used in prosthetic devices to record electrophysiological signals for several decades. However, reliable and chronic recording from individual neurons remains a huge challenge. The sources of failures of the electrodes include electrode assembly failure, tissue response caused failure and blood-brain-barrier damage caused failure.

Many of the electrode assembly failure occurred at the connectors, grounding wires, insulation layer corrosion. For the connectors and grounding wires failures, it is probably due to the mechanical stress caused in the electrodes as animals or patients implanted with electrodes move around and result in inevitable physical damage to the electrodes assembly. As for the insulation layer corrosion, several factors may contribute in the failure

of the electrodes. Firstly, the corrosion of the insulation layer exposes larger area of the recording sites. As we know that the recording sites are limited in a certain range and should not exceed a certain area for detecting individual neural signals. With the larger exposed recording sites, the electrodes will be recording signals from a larger area of the tissue. And the result will be an integration of the signals detected at larger areas of neurons. The summation of the signals may lead to unsortable neural signals, thus resulting in the failure of the electrodes' functionality in detecting single neurons. For stimulating electrodes, the exposed larger area may lead to imprecise stimulation. Besides, corrosion of the insulation material may bring toxic products, which may cause the neural damage, neuron loss, or affecting the normal spike firing of neurons in the vicinity of the electrodes.[45, 46]

It is widely believed that chronic tissue response is the major contributor for electrodes' failure.[47-49] Briefly, upon the implantation of electrodes, microglial cells will be activated as fast as 1-day post implantation.[49] Microglia recruit astrocytes for the wound healing process. Microglia and microphases will remain surrounding the vicinity of the electrodes over chronic time. Astrocytes will tightly form a glial scar, which is a dense layer, around the electrodes. This dense layer will push the potentially firing neurons away from the electrodes recording sites, increasing the distance between neurons and electrodes. Besides, the glial scar also increases the impedance of the electrodes, which makes it more difficult to record signals from neurons. There are multiple factors accounting for the tissue response. One is the mechanical mismatch between the electrodes and tissue. Electrodes are too stiff to be compliant with the tissue, leading to relative movement between the implanted electrodes and tissue when concussions occur. The concussions may result from

animals' breathing, running or hitting hard objects, etc. It's inevitable if the mechanical mismatch exists. Another reason for the tissue response is the toxicity of the implants, which will kill or damage originally healthy neurons.

During the penetration of the electrodes, the blood-brain-barrier is inevitably damaged, causing leak of fluids inside the blood vessels to the brain tissue. The blood-brain-barrier damage sustains during the chronic implantation time, causing persistent negative impacts on the function of electrodes.[50, 51]

1.3 Previous Studies of CNT Fibers

Carbon nanotube (CNT) fibers are made of millions of carbon nanotubes. Carbon nanotube is a new kind of carbon materials with nanoscale size and complete molecular tubular structure. As early as in 1952, scientists in the former Soviet Union observed the structure of carbon nanotubes under projection electron microscopy and published it in Russian journals. But Jie Sishen et al. synthesized high quality and ordered carbon nanotube arrays on planar substrate film using catalysts until 1996.[52] In 2004, Zhang et al. continuously extracted thin ribbons from super-aligned carbon nanotube arrays. The carbon nanotubes connect with each other head to tail through van der Waals forces and twisted into a fiber, the CNT fiber.[53]

Four subsections in this section include: (1) The excellent properties of CNT fibers that favour their application in neural interface (2) In vivo applications and the toxicity study of CNT fibers, excluding the biocompatibility concern for applications involved with the implanted CNT fibers (3) Previous studies involving CNT fibers for neural interface application (4) Discussion.

1.3.1 Excellent Properties of CNT Fibers

Excellent mechanical and electrochemical properties of CNT fibers are due to their unique constitution and structure. The carbon nanotube fibers are mechanically strong and flexible. CNT has strong carbon-carbon bonds, which results in a tensile strength in the range of 11-63 GPa, and the unique atomistic structures of carbon nanotubes result in a high tensile elongation break of 10-30%. The electrical conductivity of CNT is about 3×10^4 S/cm. There are generally three methods for the fabrication of continuous CNT fibers from millions to trillions of CNTs. Method 1, spinning fibers from CNT solutions,[54-56] and treating by enhanced nanotube alignment, hot drawing to enhance the mechanical performance.[57, 58] Method 2, spinning from aligned CNT arrays by twisting[53] and shrinking with liquid[59, 60], tension[61, 62] during drawing the fibers from the arrays. Method 3, spinning from CNT aerogel in a reactor at high temperature.[63-65] The CNT alignment can be enhanced by increasing the spinning speed and the fibre density increases by treating the fibre with acetone vapor. The electrochemical and mechanical properties are dependent on the CNT fibre fabricating method as demonstrated in Figure 13. Many of them are excellent enough for the electrochemical and mechanical requirements for neural interface, by comparing with advanced neural electrodes, such as some successful types of carbon fibre electrode, which has a 1.0×10^4 S/cm electrical conductivity, 1-2% tensile elongation to break.[66]

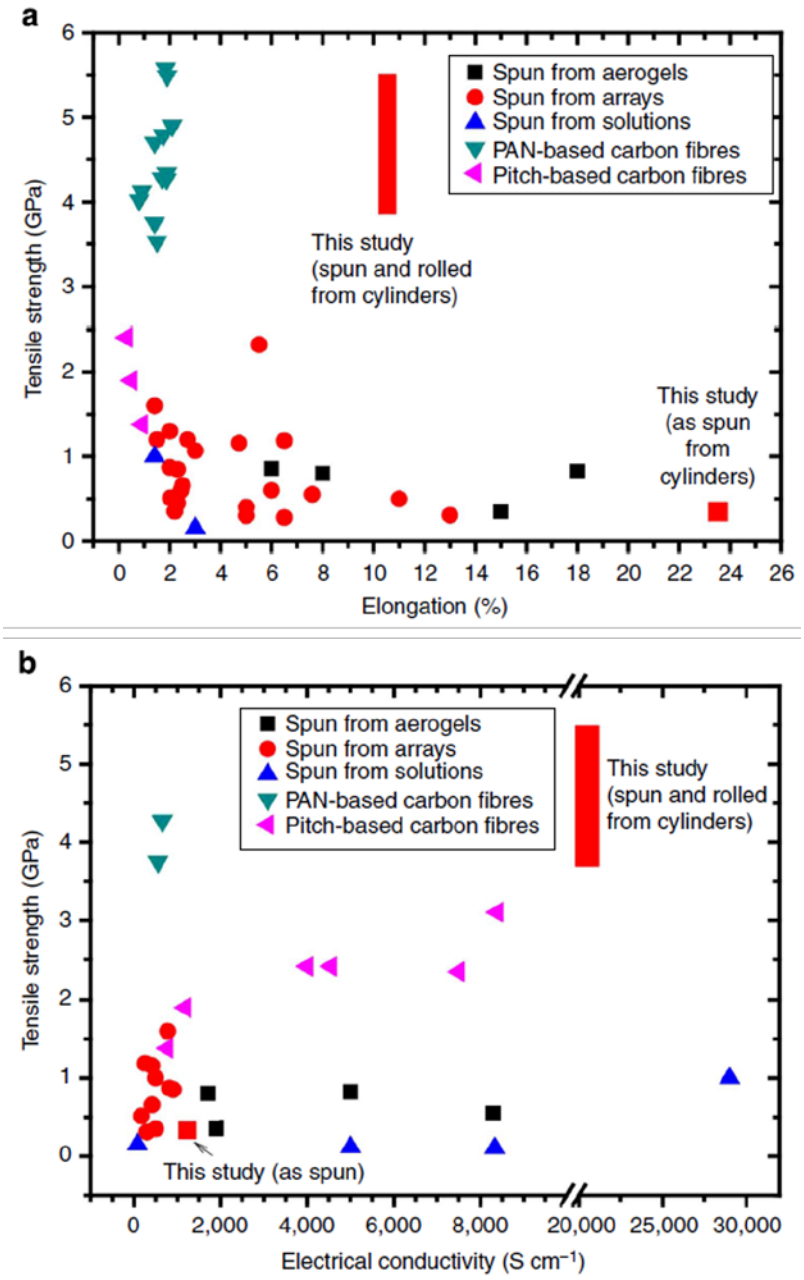

Figure 13. Mechanical properties (a) and electrical conductivity (b) of CNT fibers reported in literatures. Figure from [66]

In addition, CNT fibre induces much less MRI artifacts than traditional PtIr electrode for deep brain stimulation (DBS). A rapidly developing therapy for many neurological diseases is DBS, with stimulating neural electrodes implanted in patients'

brain. Traditional DBS electrodes made of PtIr may induce severe artifacts due to field distortions in the vicinity of the implanted electrodes. The dominant cause for the magnetic field distortions is believed to be magnetic susceptibility between the electrodes and the surrounding tissue.[67] The susceptibilities of brain tissue, PtIr and CNT fibre are estimated to be -9.05 ppm, 231 ppm and -26 ppm.[67] Therefore, CNT fibre may induce much less magnetic field distortions in theory. Jiang et al. compared the artifacts by PtIr and CNT fiber 1 week and 6 weeks post implantation produced in rat brains in a 3.0 T MRI scanner. CNT fibers showed much reduced artifacts than PtIr in both timepoints as shown in Figure 14. The same lab also demonstrated the much-reduced MRI artifacts of CNT fiber than PtIr post 12 weeks implantation in another study using a 3.0 T MRI.[68] The stable less induced MRI artifacts provides CNT fiber a great advantage over other electrode materials, considering the huge demanding needs on MRI compatible electrodes.

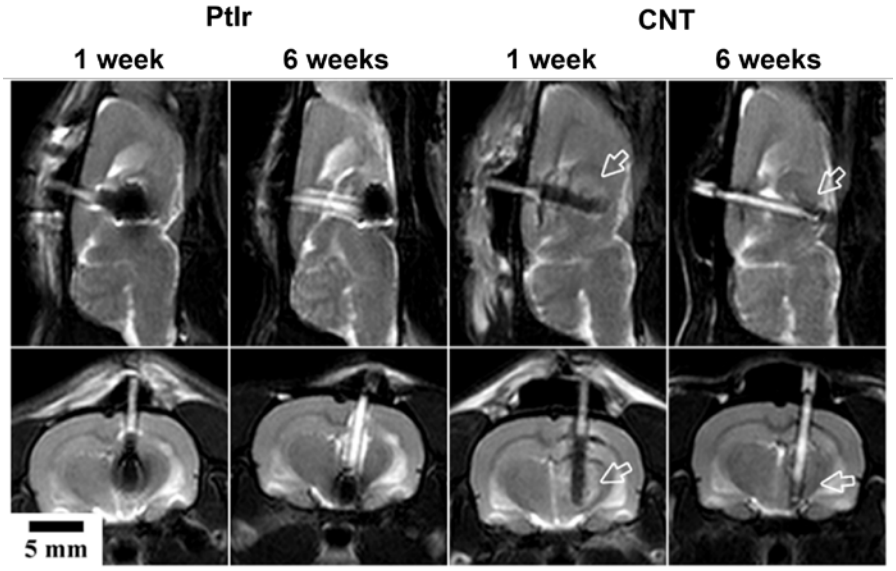

Figure 14. CNT fiber and PtIr artifact electrode artifact study 1- and 6-weeks post implantation. Figure from [67]

1.3.2 In Vivo Toxicity Study of CNT Fibers

As stated in the above subsection, CNT fiber is a promising material for neural interface, the toxicity of CNT fibers is therefore a critical concern of researchers for applying CNT fibers in biological tissues.

Rober A. Dubin et al. performed in vitro cell growth experiments and demonstrated that CNT fibers are nontoxic to mammalian cells and neurons. The CNT fibers supported the spreading and growth of mammalian cells and facilitated the adhesion of neurites.[69] Yi Guo et al. performed in vivo experiments and demonstrated that CNT fibers induced less inflammatory responses compared to traditional PtIr, indicating better biocompatibility of CNT fibers than PtIr.[68] The CNT fibers and PtIr were implanted in rat brain, and the results of 1 week and 12 weeks post implantation, showed significantly lower inflammatory marker (CD68) and reduced fibrous tissue formation as shown in Figure 15.

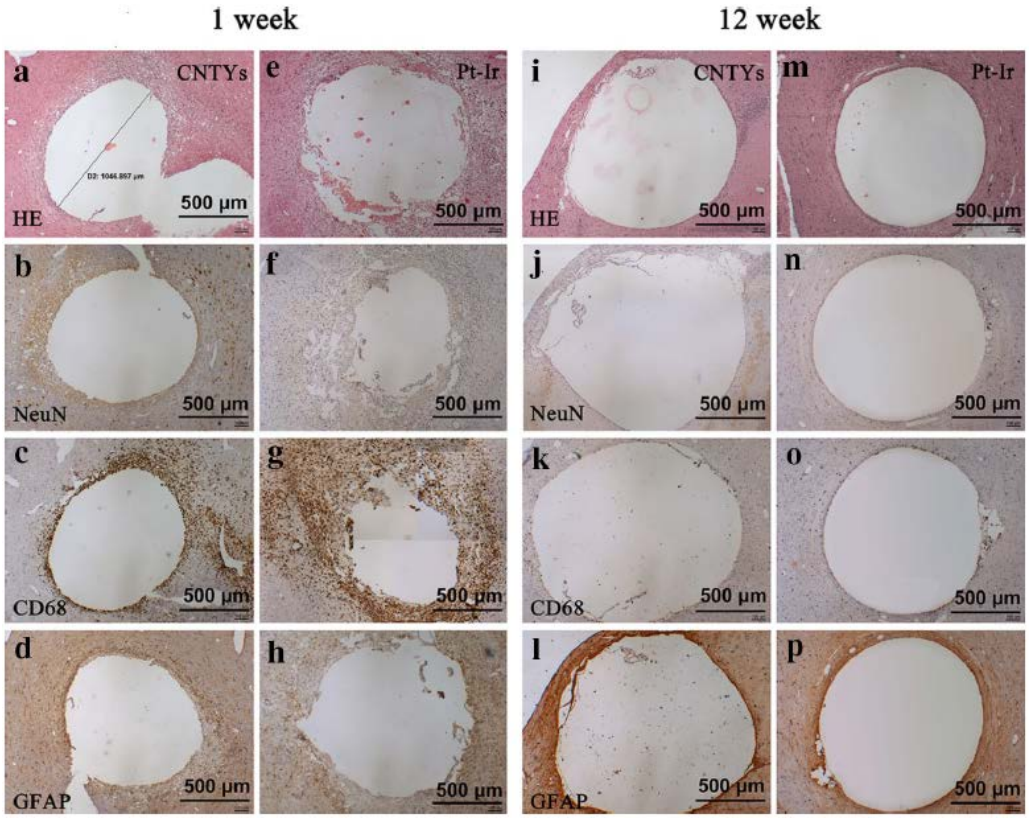

Figure 15. Histological studies of implanted CNT fibers and PtIr electrodes 1 week and 12 weeks post implantation.

1.3.3 Previous Studies of CNT Fiber as Electrode Material for Neural Interface

With the excellent electrochemical and mechanical properties, CNT fibers are promising candidates for application in neural interface. Here I present the most relevant study to my thesis regarding CNT fiber electrodes, which was published in ACS Nano magazine in 2015.

Flavia Vitale et al. first demonstrated stimulating and recording using CNT fibers electrodes. [70] For stimulating experiments, a diameter of 43 μm CNT fiber was used for stimulating neural electrodes, implanted by attaching to a 100 μm diameter polyimide (PI) shuttle. The stimulating CNT fiber electrodes showed comparable effects compared with

PtIr electrodes, but with less inflammation results. For neural recording experiments, CNT fiber electrodes with a diameter of 12.6 μm were not used alone, but together with three other 12 μm diameter NiCr electrodes to form tetrodes (four-channel electrodes). The recordings were performed 2 weeks after implantation and recorded every 1 to 2 days for 2 weeks as shown in Figure 16.

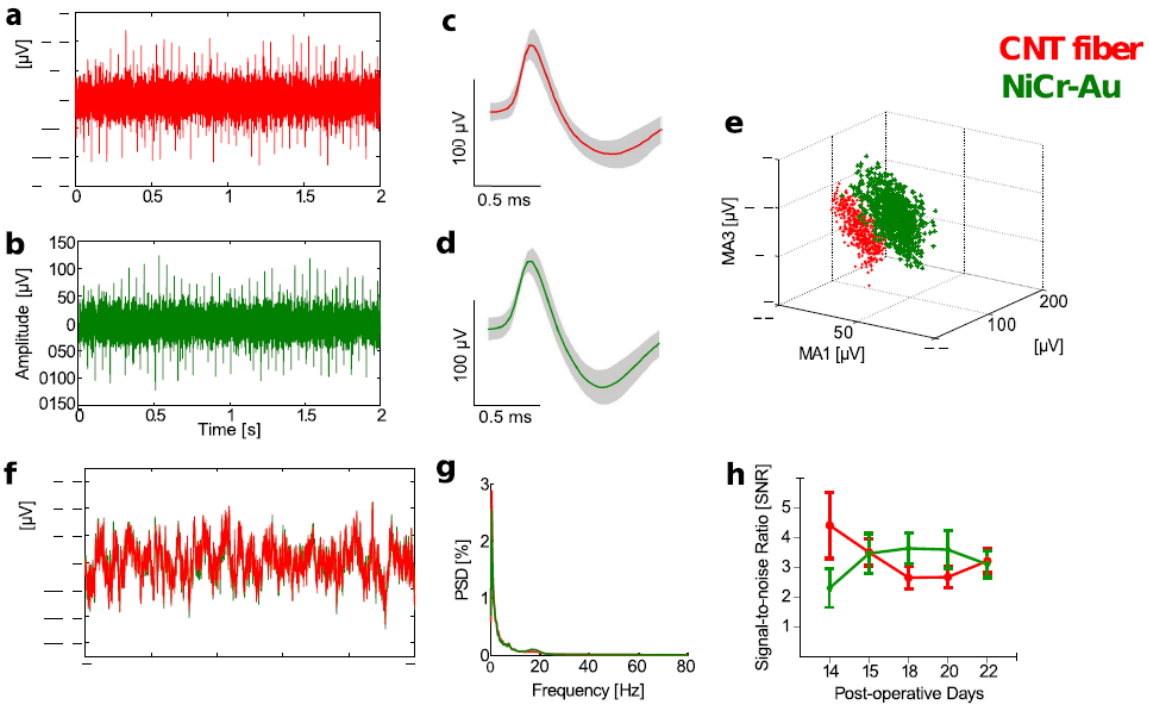

Figure 16. Flavia Vitale et al. demonstrated neural recording with CNT fiber electrodes. Figure from [70]

However, the neural recording results is far from convincing. The author claimed quantitatively and qualitatively comparable electrophysiological recording to NiCr-Au electrodes recording. The single units shown in Figure 16a&c and 16b&d for CNT fiber electrodes and NiCr-Au electrodes have a peak-to-peak amplitude of 124.4±15.5 μV, 123.0±17.7 μV respectively. And the SNR of CNT fiber electrodes and NiCr-Au electrodes are 3.21 and 3.1 respectively. The super similar values of amplitude and SNR are very

suspicious, and even more suspicious when comparing the voltage traces in Figure 16a&b with a 20 Hz noise appearing equally spaced as shown in Figure 17. The claimed detected single units, or spikes, perfectly match with the 20 Hz noise. Thus, the recorded signals claimed in the study are very suspicious to be noise in fact. The claim of recording for two continuous weeks with single units detected is therefore suspicious too.

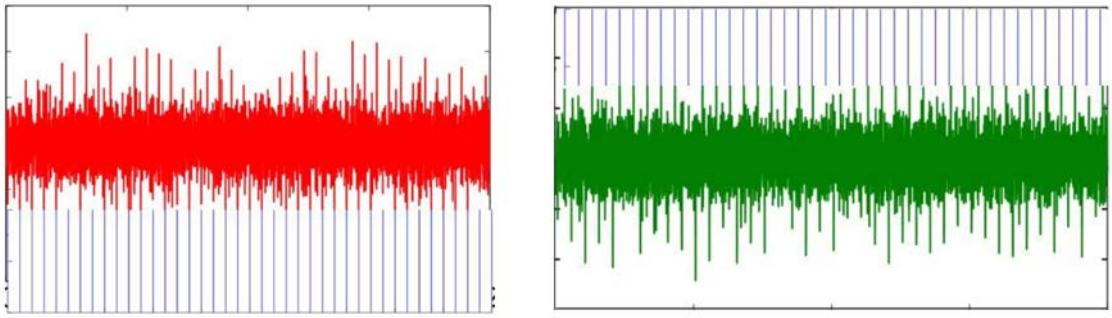

Figure 17. Neural recording results from Vitale et al., *ACS Nano*, 2015, superimposed with the lines showing the equally spaced time points of 20 Hz noises. The noises were generated by Matlab.

1.4 Significances and Innovations of the Thesis

Soft MRI compatible microelectrodes capable of chronically recording neural activity are greatly desired for neural interface. CNT fiber is an excellent material candidate for neural interface due to its high softness, low impedance, high charge injection capacity and close magnetic susceptibility to water/tissues. The thesis focuses on the development and application of CNT fiber electrodes. In the thesis, neural electrodes from 5-20 μm CNT fibers are fabricated and characterized on mechanical properties, electrochemical properties, MRI compatibility and neural tissue biocompatibility. Acute neural recordings performed in the whisker pathway on rats using 15 μm and 5 μm CNT fiber electrodes achieved high quality whisker responsive single-unit neural signals. Multi-depth neural

recording demonstrated that CNT fiber microelectrodes are strong enough to be repositioned along the insertion track post implantation into the brain tissue and adaptive electrode-neural interface is formed. Chronic study on rats with CNT fiber electrodes demonstrated the longevity and stability of the CNT fiber electrodes for months. In the section, significances and innovations of the thesis are demonstrated.

1.4.1 Significances

The thesis study of CNT fiber electrodes is of great significances in the following aspects:

(1) The soft and flexible CNT fiber electrodes enable chronic reliable and stable neural recording. The technology of achieving chronic reliable and stable neural electrical signals is critical and greatly desired in not only fundamental neuroscience, such as tracking the changes of aging neurons or regenerated neurons, studying the synaptic plasticity over long-time scale and adaptation of neurons to repeatedly appearing stimuli, but also it is of great advantage in brain-computer-interface , clinical trials and treatments of neurological diseases. Figure 18 shows a brain computer interface example of a patient suffering from severed spinal cord. An array of silicon electrodes was implanted in his brain. However, the silicon array with higher stiffness than CNT fiber electrodes, may cause relative micromotion due to the shear force between the electrode array and the tissue over time, leading to decreased signal quality and increased inflammation response and thus the electrode may need to be replaced after a period of time. However, if CNT fiber electrodes were implanted instead, which achieves reliable and stable signals over chronic

time, there will be no need for replacing the electrodes over a much longer period, thus avoiding the secondary surgery for the patients.

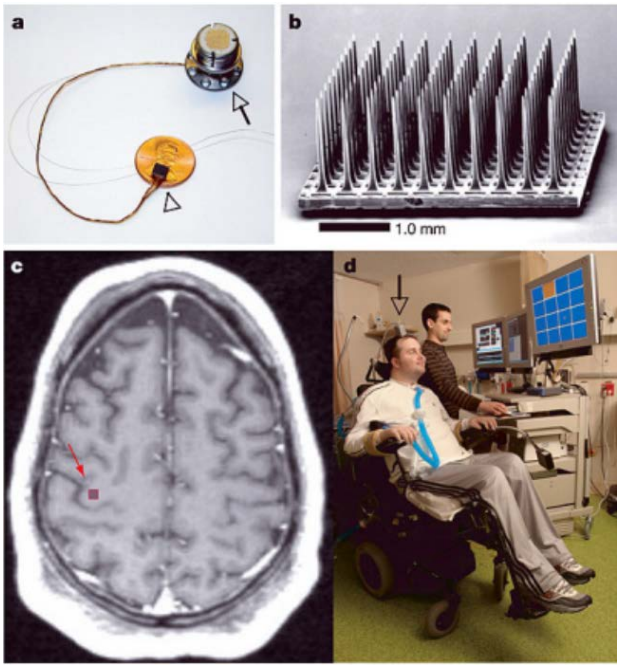

Figure 18. BrainGate system. A neuromotor prosthetic device implanted in a patient as brain-computer interface. Figure from: Mo Costandi, a neuroscience writer. https://neurophilosophy.wordpress.com/2006/07/13/brain-machine-interface-controls-movement-of-prosthetic-limb/

(2) The CNT fiber electrodes with an ultrasmall CNT fiber core with a 5μm diameter was successfully fabricated and demonstrated in single unit neural recording. Ultrasmall sized neural electrodes provide several advantages, (a). High spatial resolution due to the ultrasmall recording sites makes it possible to record sortable single unit spikes from area in the brain where neurons are small-sized and densely packed, such as the medial habenula (MHb) region near the third ventricle of the brain. (b). The ultrasmall size leads to a small bending stiffness of the CNT fiber electrodes, facilitating stable tissue-electrode interface, thus causing less tissue damage, less inflammation response and better

longevity of the electrodes. (c). Ultrasmall size of single electrode makes it possible to fabricate multi-channel electrodes with a small diameter, as we desire to record more channels with the same size of implant. For example, 10 CNT fiber electrodes with 10 μm diameters takes the same space in the tissue as a 100 μm PtIr electrode.

(3) The methods of fabrication and implantation of the CNT fiber electrodes are demonstrated and the chronic performances of the CNT fiber electrodes in neural recording are evaluated across multiple animals. These studies provide a reference on methods and precautions of using CNT fiber electrodes, facilitating the commercialization, clinical wide use, and further application study of the CNT fiber electrodes.

(4) The developed CNT fiber electrodes enable simultaneous neural recording, DBS and MRI scan. (a). Simultaneous use of DBS and MRI. MRI is a frequently used clinical examination for patients with neurological diseases. DBS is a widely used clinical treatment for patients with neurological diseases. However, traditional neural electrodes for DBS, such as PtIr electrodes, induces large artifacts around the electrodes, making it difficult to observe the position of the DBS electrode under MRI, and thus excluding the possibility of using MRI to check the position of the electrodes implantation and then adjust the position accordingly. Another issue with the traditional electrodes for simultaneous use with MRI, is the heating effect due to induced eddy current in the electrodes under magnetic field. The heating effect may damage the brain tissue surrounding the traditional metal electrodes implanted in the patients, thus damaging the patients' function related to the heat-damaged tissue, causing immeasurable loss to the patients.[71] In addition, even if the electrodes are acceptable to use in MRI scan without safety concern, the distortion of image due to MRI incompatible electrodes cause a problem in the localization of the DBS

electrodes. Lee et al. examined the DBS electrode position in the image from MRI scan and the from CT scan. The results suggested significant discrepancy between the position of the electrodes estimated with these two different methods.[72] Therefore, our CNT fiber electrodes could be utilized in this situation to address the problems. (b) Simultaneous neural recording & DBS & MRI. Though DBS plays an important role in the treatment of neurological disorders, the mechanisms is still an intriguing topic. Combining the three general modalities - neural recording, DBS and MRI- will help in addressing the unknown facts of the mechanisms of DBS treatment and thus leading to improvements in the treatments. (c). Simultaneous neural recording and MRI. This enables mapping of recording signals with the positions in the tissue being recorded using MRI. Functional MRI provides a wealth of information by reflecting the blood oxygenation level dependent (BOLD) signal on large areas of brain neural activity. However, the exact relationship between the two different sources of brain signals, the BOLD signal and the electrical signal, is still a matter of debate.[73] The simultaneous functional MRI and neural electrophysiological recording technique will greatly help on understanding the mechanism of the brain information representation and transmission by combining the two kinds of brain signals.

(5) The developed electrodes enable simultaneous neural recording & DBS & optogenetics study. The CNT fibers produced much smaller light artifacts in neural recording, favouring its application in combining with optogenetics technique with at least two advantages: (a) Reduced electrode size. The optical fiber is generally more than 100 μm in diameter, damaging a wide range of tissues on the implantation path especially used together with another ~ 100 μm diameter recording electrode. Therefore, the small size of

CNT fiber electrodes offers an advantage in combining with optogenetics by downsizing the total tissue damage area and minimize the loss of neurons. (b) Reduced light-induced artifacts. For simultaneous optogenetic modulation and neural recording, one issue to consider is the light-induced electrical artifacts produced by the electrode when giving stimulation light. The light-induced electrical artifacts are resulted from the difference in photoexcitation at the interface of two materials, in this case, the interface of the electrode and tissue. Compared with other electrodes made with metal, the CNT fiber has much smaller electrical artifacts induced by light, thus favouring its use in combining optogenetics technique with neural electrophysiological recording.

1.4.2 Innovations

Innovations of the thesis are stated and demonstrated in this subsection by comparing with state-of-the-art studies in the field of neuroscience and neural engineering.

(1) For the first time to demonstrate months of stable chronic single unit neural recording with CNT fiber electrodes across multiple animals.

CNT fiber, combing excellent electrochemical, mechanical, optical and magnetic properties, has become a hotspot of materials for neural interface since its appearance. Among the many studies of CNT fibers for neural interface, the study of Flavia Vitale et al. [70] poses a similarity to my thesis study. However, my study demonstrates multiple new innovations and much more convincing and much better results, especially for the most critical part of the results, compared with their research. (a). We proposed MRI compatibility of the CNT fiber electrodes for enabling simultaneous MRI study with neural recording, which is of great significance as stated in the above subsection (b). The Flavia

Vitale study did not fabricate an actual CNT fiber electrode for neural recording, instead, they used one CNT fiber electrode together with three NiCr-Au electrodes to form a tetrode for neural recording, which sacrificed one of the most valuable properties of the CNT fibers, the softness and flexibility, the most critical properties for the electrodes' longevity in neural recording. (c) The CNT fiber they used for fabricating electrodes for neural signals is made of 12.6 μm diameter. We downsized the size to 5 μm diameter CNT fibers by improving the electrochemical properties of the fibers. (d) The spikes of 'single unit' reported in their study are equally spaced, which is similar to a 20 Hz noise, which is very doubtful to be single unit signals. Therefore, the results of the chronic study of 2 weeks post implantation is also doubtful. (e) In my study, the recording capability is verified by high quality stimulation responsive signal detection in brain regions, with 15 μm and 5 μm CNT fiber electrodes. The chronic single unit detection is effective for more than 6 months.

(2) Demonstrating CNT fiber electrodes' MRI compatibility with 7.0 T MRI.

The MRI compatibility of CNT fibers is mainly due to that the magnetic susceptibility of the CNT fibers is very close to that of tissue. Studies from Luming Li lab illustrated the magnetic artifacts of CNT fibers wrapped to a 1.3 mm diameter polyurethane tube under a 3.0 T MRI scan.[67, 68] Here in my thesis study, several improvements for testing the MRI compatibility of CNT fibers were made. (a) The CNT fiber electrodes for MRI artifacts evaluation were directly implanted into the brain as the way they were in actual use for neural recording or neural stimulation. One reason for Luming's studies for wrapping CNT fibers onto a tube is possibly that they plan to use the CNT fiber electrode with the tube together to make a 1.3 mm diameter electrode as illustrated in Figure 19. However, for my study, the CNT fiber electrodes is to be used as a standalone material,

which makes the best use of the CNT fibre's softness and flexibility. In my MRI compatibility study, the total size of the CNT fiber electrodes are 25 μm, with the generated artifacts from MRI scan directly represent the real artifacts of the advanced standalone CNT fiber electrodes. (b) The study in Luming Li group used 3.0 T MRI scan. We used 7.0 T MRI, which has better spatial resolution and a more demanding requirements for the materials being scanned. In fact, we examined the CNT fibers' artifacts under a 3.0 T MRI scan, no images of CNT fibers could be found, which proved the CNT fiber electrodes' MRI compatibility. In summary, the study in Luming Li group demonstrated the MRI artifacts of CNT fibers together with a tube inside under 3.0 T MRI. My study demonstrated the artifacts of standalone CNT fiber electrodes under 7.0 T MRI.

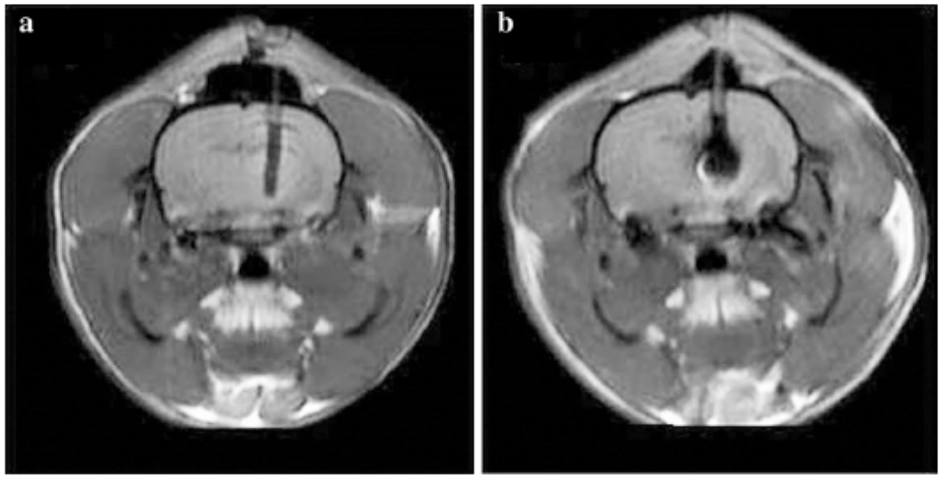

Figure 19. An example of MRI artifacts comparison of CNT fibers wrapped to a 1.3 mm tube and PtIr electrode. Figure from [68]

(3) Downsizing the CNT fiber electrodes to an ultrasmall size and demonstrating in electrophysiological recording in vivo.

In my thesis study, the CNT fiber electrodes were downsized to a 5 μm dimeter CNT fiber core and the stably electrophysiological recording ability was validated by recording for continuously three straight hours. The previously reported smallest diameter CNT fiber electrodes are 12.6 μm.[70] For other ultrasmall fiber electrodes, a carbon fiber electrode with a total diameter of 8.4 μm.[27] Though with similar diameters, my CNT fiber electrodes outweighs the carbon fiber electrodes in mechanical properties and electrochemical properties.

(4) Proposing and having preliminary studied electrophysiological recording with CNT fiber electrodes in MHb region, where densely packed small neurons near the third ventricle posing a challenge to electrophysiological neural recording in this area.

The MHb brain area in mammals is involved in behavioral processes related to aversive, appetitive stimuli, such as the stress, pain and drug like nicotine. Reliable and stable recording in MHb area can greatly improve our understanding of this brain area.[74-76] However, the near ventricle position, the small neuron size and the densely packed way of neurons in MHb area make it difficult to achieve good electrophysiological recording results from MHb. As far as I know, there is no single unit electrophysiological recording in MHb area for behavioral study. The softness and ultrasmall size of CNT fiber electrodes makes them possible to address the challenge in MHb recording.

(5) Proposing the CNT fiber electrodes for combing with optrodes in optogenetics study.

The neural recording capability demonstrated in my thesis and the CNT fiber electrodes much-reduced light induced electrical artifacts, together with the small size and

soft nature of the electrodes, provide advantages in reduced tissue damage, more healthy survived neurons around the optrodes and electrodes for neural recording and stimulation, if the CNT fiber electrodes being utilized with optrodes for optogenetics study.

1.5 Thesis Organization

Chapter 1 is the introduction and Chapter 6 is the conclusion. Chapter 2 to chapter 5 are the main parts of the thesis, each divided into four subsections: introduction, methods, results and discussion, and summary. The specific organization is as follow: (1) Chapter 1 introduces the fundamentals of the thesis study, including the complexity of brain study, the signals in the brain and the neural electrodes. Then the fundamentals, such as the electrochemical requirements, mechanical considerations and sources of electrode failures, are presented. For better illustrate the significances and innovations of the thesis, previous relevant studies on CNT fibers are presented, followed by the summarized significances and innovations of the thesis. (2) Chapter 2 demonstrates the electrode fabrication procedures, implantation method and characterizations of morphology, electrochemical, mechanical properties and in vivo histological studies of the CNT fiber electrodes. (3) Chapter 3 further characterized the MRI artifacts study on the CNT fiber electrodes with PtIr electrodes as a control study. (4) Electrophysiological recording serves as the most important characterization for evaluation the performances of neural recording electrodes in vivo. Chapter 4 focuses on neural recording studies using 15 μm CNT fiber electrodes in rats, including three different acute recording tasks demonstrating multiple advantages of the electrodes, and several chronic recording examples showing the excellent chronic performances of the CNT fiber electrodes. (5) In chapter 5, the electrodes are downsized with a 5 μm CNT fiber core, instead of 15 μm or larger. The smaller recording site gives

the electrode a higher spatial resolution, which facilitate detecting and sorting neurons from clusters of densely distributed groups and small neurons which fire spikes with low amplitude. In vivo neural recordings are also demonstrated for the ultrasmall sized electrodes. (6) Chapter 6 summarized the advantages and disadvantages of the developed CNT fiber electrodes in the thesis and proposes future scientific directions with specific ideas presented.

CHAPTER 2. FABRICATION, IMPLANTATION AND CHARACTERIZATION OF CNT FIBER ELECTRODES

2.1 Introduction

2.1.1 Fabrication of CNT fiber electrodes

The fabrication process includes preparing CNT fibers, soldering CNT fibers to connectors, coating fibers with parylene-C and exposing recording sites of the achieved CNT fiber electrodes.

2.1.2 Implantation of CNT fiber electrodes

The tiny size renders CNT fiber electrodes a very small bending stiffness, which makes it impossible for CNT fiber electrodes to be inserted directly into brain tissue by themselves. Therefore, strategies are needed to implant soft CNT fiber electrodes.

2.1.3 Characterization of CNT fiber electrodes

At present, the electrodes were mainly tested and evaluated in the following aspects: external morphology, electrochemical properties, mechanical strength and histological studies of biocompatibility of electrodes.

2.2 Methods

2.2.1 Fabrication methods

(1) Preparing CNT Fibers

CNT fibers were prepared by drawing and twisting from spinnable CNT array like making a thread.[77] The spinnable CNT arrays were grown by the method of chemical vapor deposition. Briefly, SiO_2/Si wafers were deposited by a thin Fe film, which acts as the catalyst. 300 sccm C_2H_4, 200 sccm H_2 and 1000 Ar gas filled in the space where the wafers stayed for about 15 min. CNT arrays were grown on the wafers under 660-750° C temperature. The achieved CNTs are double- or triple-walled CNTs with the diameter of about 6 nm. Then, a home-made device was used to spinning CNT fibers out of the CNT arrays by drawing and twisting millions of tiny CNTs. Upon twisting, a drop of glycol or ethanol was applied to the newly formed end of the CNT fibers to condense them. The resulted CNT fibers can reach more than 30 meters long.

In order to further improve the electrochemical performance, the CNT fibers were placed in 65% boiling nitric acid for at least 3 min. Then the fibers were rinsed with DI water for several times.

(2) Soldering and Insulating CNT Fibers

To assembly CNT fiber electrodes, there are two options: do the insulation first and then do the soldering or do the two things in the reverse order. Both methods work. Here I will introduce the method of doing the soldering first. Soldering the CNT fibers with tin to connectors, whether male or female pins or a printed circuit board, depending on how to connect the electrodes to the electrophysiological recording system. Then, wrapping or using other tricks to protect the connecting part of the CNT fibers from insulation and then do the insulation to the soldered CNT fiber and connectors. Then, a thin layer of epoxy was

applied to the soldered connecting part of the assembly to further secure the connection between the two.

For the insulation, we deposited 2.5 μm parylene-C on the soldered CNT fiber and connectors in a Parylene Coater (PDS 2010 LabCoater, Specialty Coating Systems, USA). Parylene-C is a widely used biomaterial for insulation and encapsulation. With the chemical vapor deposition polymerization method, parylene-C can be deposited on the surface of a material with a controllable thickness ranging from 1 to 100 μm.[78] Briefly, a dimer was used as the starting substance and heated up in the oven until it vaporized and then the gas reached to the chamber where it deposited on the target in the chamber. The target chamber was at room temperature, which was a very convenient condition for assembly of electrodes, requiring no high temperature or pressure.

To expose the recording sites, the CNT fibers were then cut with a Gillette razor blade. The remaining length of the CNT fibers was decided by the application context of the electrodes, and usually the length was 2~ 8 cm. The procedures are shown in **Figure 4**.

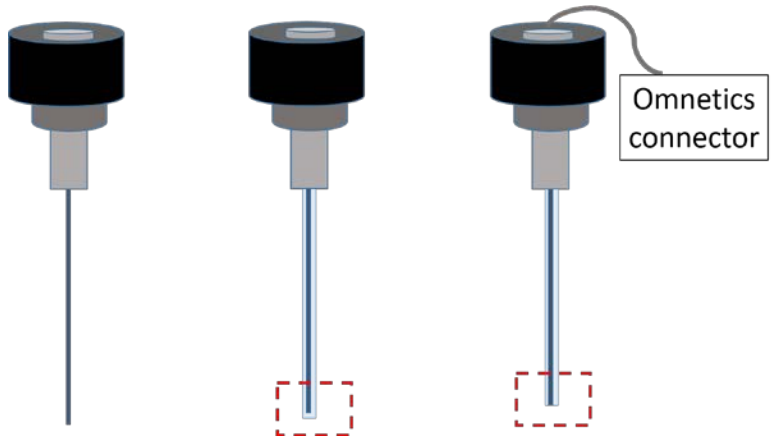

Figure 20. Schematic drawing of CNT fiber electrodes fabrication. The blue line represents the CNT fiber. The left image shows the soldering of CNT fiber to a pin. The middle image

shows the parylene-C coated CNT fiber electrode. The image on the right shows the CNT fiber electrode after the tip exposed by a blade and the pin connected to an Omnetics connector for signal transmission.

2.2.2 Shuttle-assisting Implantation methods

The implantation method was to bring in the electrodes together with rigid tungsten wires into the brain tissue and then pull out rigid tungsten later after their adhesive glue dissolved.

Firstly, we chose a material with a suitable stiffness and size as the shuttle. Because the tungsten wire is relatively stiff and has no cytotoxicity, we chose to use tungsten wires as a shuttle. Considering that too thick tungsten wires cause too much tissue damage and too thin tungsten wires do not have enough stiffness, we finally chose 50 um diameter tungsten wires. Then, the next step is to glue the CNT fiber electrodes to tungsten wires with materials that are biocompatible and dissolvable or degradable in vivo. 3% - 8% polyethylene oxide (PEO) solution was utilized as the adhesive and the concentration of PEO could be adjusted according to the preliminary experimental results. It should be noted that PEO solution is volatile so try to cover the PEO solution immediately after use. Otherwise, the concentration of PEO solution will increase so that the volume of PEO used for combining CNT fiber electrodes and tungsten wire would be too much, which will cause unnecessary excessive tissue damage when implanted into brain tissue. The best solution is to make PEO solution when needed. For assembling CNT fiber and tungsten wires, briefly, fill 3%-8% PEO solution into an open container, such as a Petri dish, and then dip a segment of tungsten wire in PEO solution for one or two times. At this time, the tungsten wire is covered with a small amount of PEO solution. Then the CNT fiber

electrode is held up with tweezers about 3-6 mm in length, and this small segment is carefully moved to attach to the tip of the tungsten wire, and make sure that the tip of the CNT fiber and the tungsten as close as possible, but the tip of the CNT fiber must not exceed the tip of the tungsten wire, otherwise, the CNT fiber will be separated from the tungsten wire before being inserted into the brain tissue. After this 3-6 mm segment is affixed, affix the remaining parts of the CNT fiber far from the tip along the tungsten wire and ensure that the upper segment of the CNT fiber electrode is at least 1 cm longer than the tungsten wire. The extra length of the CNT fiber electrode is designed to facilitate the separation of CNT fiber electrodes and tungsten wires after subsequent implantation. If the length of the CNT fiber electrode is the same as that of the tungsten wire, the CNT fiber electrode will easily move along with a slight movement of the tungsten wire, which make it impossible to guarantee the accuracy of the electrodes' implantation position during the extraction of the tungsten wire shuttle.

As the CNT fiber electrodes and the tungsten wires are assembled, a substrate is needed to support them so as to facilitate the operation of the implantation. Stiff materials such as a cardboard, copper mesh or hard plastics can be served as substrates. In addition, another feature that the substrate needs to satisfy is to vertical-calibration-doable to ensure the accuracy of implant position. After finding a suitable substrate, a double-sided adhesive tape should be pasted onto the substrate, the CNT fiber electrode/PEO/tungsten wire assembly can then be vertically pasted onto that, and the exposed non-pasted double-sided adhesive part can be covered with a pad of degreased cotton or other materials to prevent the CNT fiber electrode from accidentally being touched on the sticky adhesive tape, resulting in the electrode not able to be completely separated from the substrate and cannot

be successfully implanted into the brain tissue. After the assembled electrode/PEO/tungsten wire is placed on the substrate, it is necessary to suspend the assembly vertically for at least 10 minutes, so that the PEO solution can flow downward slowly to the tip of the electrode under the force of gravity, and further strengthen the combination of the CNT fiber electrode and tungsten wire. It should be noted that the assembly cannot be placed sideways, in order to avoid causing the PEO solution to aggregate to a side, so as to avoiding the CNT fiber electrode and the tungsten wire combination not glued tightly enough.

The next step is to implant the electrodes. Before implantation, ensure that there is no excessive fluid on the surface of craniotomy of the brain tissue, otherwise the CNT fiber electrodes and the tungsten wire shuttle may be separated before successful implantation. In addition, it is better to connect the electrode and the voltage amplifier connector in advance, otherwise the connecting procedure after implantation will probably shake the electrode and lead to unnecessary tissue damage and imprecise implantation location. When ready, the assembly is implanted at a fast speed, which is required to prevent the implantation failure owing to the separation of CNT fiber electrode and the tungsten wire shuttle due to the dissolution of PEO glue in tissue.

Immediately after implantation, 1×phosphate buffered saline (PBS) solution or artificial cerebrospinal fluid (CSF) is dripped into the craniotomy window to keep the tissue wet on the one hand, and to accelerate the dissolution of PEO, the adhesive for electrodes and tungsten wires on the other hand. Observe whether the out-of-brain-part of the electrodes are separated from the tungsten wire shuttle or not. If they are not separated yet,

PBS solution should be applied onto the non-separated position. If the assembly is still not separated after applying several drops of PBS solution or artificial CSF, it is necessary to carefully try to separate the CNT fiber electrode from the tungsten wire shuttle manually with tweezers or toothpicks, so that the lower end of the CNT fiber electrode is close to the tissue rather than attached to the tungsten wire shuttle. It takes about 5-10 minutes for the separation between the CNT fiber electrode and the tungsten wire shuttle.

The next step is to extract the tungsten wire out of the brain tissue and leave the CNT fiber electrode in its original implanted position. Pay attention not to touch the CNT fiber electrode in the process of tungsten wire handling, otherwise the location of the electrode site will be inaccurate and the brain tissue might get injured. Usually, there is more PEO at the combining tips of CNT fiber electrode and tungsten wires, and the tips are the most critical positions for ensuring the complete separation of CNT fiber electrode and tungsten wires. As long as the tip is separated, even if there is not a complete separation in the upper section, the CNT fiber electrode and the tungsten wire shuttle will be completely separated in the process of pulling up the tungsten wire under the friction of the tissue and the tungsten wire. But if the tips are not separated, the entire CNT fiber electrode and the tungsten wire will be lifted up together, thus changing the expected implantation position of the CNT fiber electrode. When the tungsten wire is completely pulled out of the tissue, it is necessary to observe and evaluate whether the CNT fiber electrode is bent. Generally, CNT electrodes will bend to a certain extent, because CNT fiber electrodes are longer than tungsten wires. At this point, the bending CNT fiber needs to be pulled up slowly until straightened. Then the tip position of the CNT fiber electrode will start to change accordingly when pulling up the CNT fiber electrode. Draw the CNT

fiber electrode to an appropriate position as required. So far, the implantation of CNT fiber electrodes has been completed.

2.2.3 Characterization methods

(1) Morphology examination

We examined the morphology of the CNT fibers under SEM (Hitachi S-4800 operated at 1-2 kV acceleration voltage, Japan).

(2) Electrochemical properties characterization

The electrochemical characteristics of the interface between electrodes and tissue are of great significance to microelectrodes. When recording neural signals, if the impedance of the electrode is too large, the neural signal will be lost; if the impedance is too small, the background noise will increase and the signal-to-noise ratio will decrease; therefore, the impedance characteristics of the electrode should be evaluated, and the evaluation of the impedance characteristics of the electrode is also a common non-invasive method to examine the integrity and stability of the implanted electrode.

As saline is the main component of body fluids, it is generally believed that the impedance between electrodes and physiological fluids can be expressed by the impedance between electrodes and saline. There are two methods of impedance measurement, one is the two-electrode system, the other is the three-electrode system as shown in **Figure 7**. The measurement system of two electrodes only has working electrodes and counter electrodes. Working electrodes are the electrodes we study, and the counter electrodes are used to form circuit loop. The platinum electrode with large surface area is generally used as counter

electrodes. When the current flows through the two electrodes through the electrolyte, the working electrodes and the counter electrodes will polarize, and the electrode potential deviates from the equilibrium potential to produce an overvoltage, which will affect the measurement results of the system and cause errors in the measured electrode impedance. In order to make the measurement more accurate, a third electrode, called a reference electrode, is introduced into the two-electrode system. The reference electrode is used to measure voltage without passing current. The ideal reference electrode is characterized by low impedance and does not produce obvious polarization overvoltage when current flows through it. Simply speaking, in a three-electrode system, the role of the counter electrode is to form a circuit loop with the working electrode, and the role of the reference electrode is to let us measure the potential of the working electrode. Therefore, the three-electrode impedance measurement method is more accurate than the two-electrode system. People often use a large area of Pt electrode as the counter electrode, and Ag/AgCl or calomel electrode as the reference electrode.

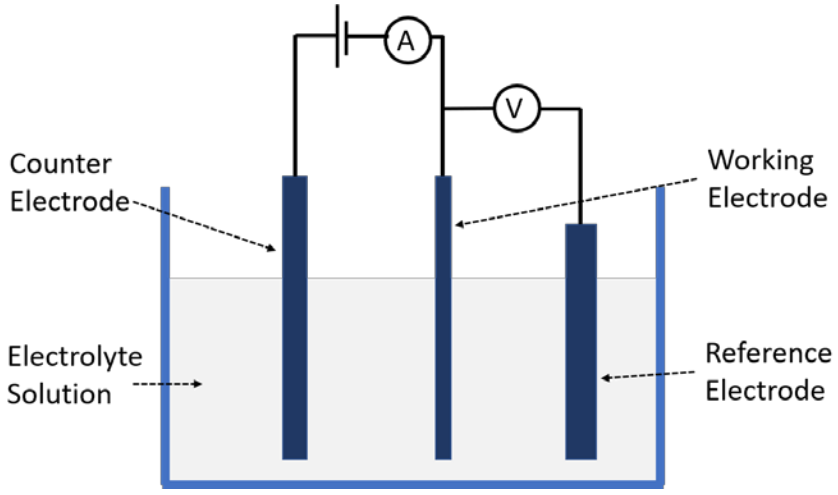

Figure 21. The three-electrode impedance test system.

Charge storage capacity and charge injection limit are two other critical parameters for evaluating neural electrodes for stimulation. Cyclic voltammetry is usually used to measure the charge storage capacity. Briefly, this method applies a range of voltage at a certain scanning rate repeatedly once or more times on the working electrode while recording the current-potential curve over time. The voltage range is the range that prevents the reduction or oxidation reaction on the electrodes. If the first half of the potential is scanned in the direction of cathode, and the electroactive substance is reduced on the electrode to produce reduction waveform, then when the second half of the potential is scanned in the direction of anode, the reduction product will be oxidized again on the electrode to produce oxidation waveform. Therefore, a triangular wave scanning completes a cycle of reduction and oxidation process, so this method is called cyclic voltammetry, and its current-voltage curve is called cyclic voltammetry. By calculating the area contained in the closed CV curve, we can obtain the charge storage capacity of the neural electrode.

EIS and CV were performed using CHI 660e electrochemical workstation (CH Instruments, USA) in 1× phosphate buffered saline (PBS, pH 7.4) at room temperature in a three-electrode system, where the counter electrode was Pt and the reference electrode was Ag/AgCl. The parameters for EIS were set as follows: Initial potential = 0.22 V, Amplitude = 0.007 V, Quiet Time = 2 s, automatic sensitivity scale setting, 12 measurement points were evenly distributed for frequency ranges 10-100 Hz, 100-1k Hz, 1k- 10k Hz, 10k – 100k Hz. Parameters for CV scanning were set as follows: Initial Potential = 0.8 V, High Potential = 0.8 V, Low Potential = -0.6 V, Final Potential = 0, Initial Scan Polarity set as Negative, Scan Rate = 0.05 V/s, Sweep Segments = 4, Sample

Interval = 0.001 V, Sensitivity = 1.e-007. The charge storage capacity was computed as the integral of the negative current recorded in the second cycle. For measurement of charge injection limit, a pulse stimulator (Model 2100, A-M Systems, USA) was utilized to apply symmetric square current pulses to the electrodes at a frequency of 130 Hz. The pulses last for 60 μs each period. The potential transients were recorded by an oscilloscope (DSO5202P, Hantek, China). The potential excursion (Vexc) was calculated as the total voltage (Vtot) subtracted by the initial access voltage (Vacc) as shown in **Figure 8**. The current amplitude was recorded when Vexc equalled -0.6V. Then the charge injection limit was determined by the total charge delivered divided by the total surface area of the neural electrodes. Where total charge was the product of current amplitude and pulse lasting time in each cycle.

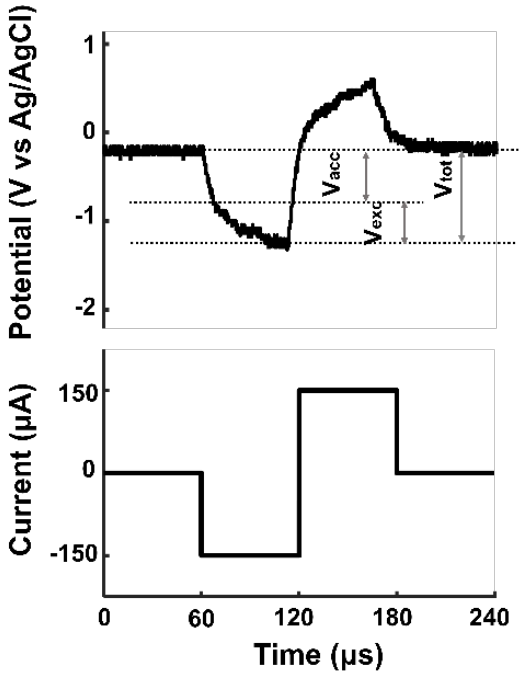

Figure 22. An example of voltage change over time responding to a biphasic current pulse in a complete period.

The tested CNT fiber electrodes include the 20 μm CNT fiber electrodes with and without nitric acid treatment, the 5 μm CNT fiber electrodes treated with nitric acid. PtIr electrodes are of a diameter of 25 μm.

(3) Mechanical characterization

An important factor affecting the performance of CNT electrodes is the mechanical strength of the electrodes. Electrodes with mechanical strength close to that of brain tissue are less likely to cause relative movement between electrodes and tissues during animal breathing, running, etc. In this case, less tissue damage and inflammation would be caused, thus enabling electrodes to perform well in long-term neural recording or stimulation. Moreover, smaller relative motions also make it possible for electrodes to record signals from the same or the same group of neurons over a long period of time. This is important for many studies, such as the study of the long-term response or adaptation of a neuron or synapse to certain stimulus.

Bending stiffness describes the resistance of a material against bending deformation. Both the inherent Young's modulus and the size of the material will affect the bending stiffness. Bending stiffness is often used to characterize the mechanical properties of neural electrodes.[79]

Bending stiffness of CNT fiber electrodes and PtIr electrodes were both calculated using a core-shell model, where CNT fiber and PtIr wire as core and insulated parylene-C layer as shell. The following equation was used for calculation of bending stiffness:

$$K = E_{core}\frac{\pi d_i^4}{64} + E_{shell}\frac{\pi d_o^4}{64}[1 - (\frac{d_i}{d_o})^4]$$

Where E represents the Young's Modulus. E_{core} and E_{shell} refers to the Young's Modulus of core (CNT fiber or PtIr wire) and shell (parylene-C). Young's modulus of 5um and 20um CNT fiber electrodes were measured with a single column model Instron 5843. The values of Young's modulus were 22 GPa and 10 GPa, respectively. The different mechanical properties of 5 μm and 20 μm CNT fibers are attributed to the different twisting angles

during the preparation of materials. The values of various parameters used to calculate bending stiffness are listed in Table 1.

Table 1. Parameters for bending stiffness calculation.

Electrode material	Young's modulus (GPa)	d_i (μm)	d_o (μm)
CNT fiber (5 μm diameter)	10	5	10
CNT fiber (20 μm diameter)	22	20	25
PtIr wire	236[70]	25	30
Parylene-C	2.76	-	-

(4) Histological studies

We performed histological studies six and twelve weeks after implantation of electrodes to evaluate the inflammation response of brain tissue to chronically contralaterally implanted PtIr and CNT fiber microelectrodes. Six and twelve weeks after the implantation of electrodes, rats were anesthetized and undergone transcardiac perfusion with about 150 mL PBS and about 250 mL 4% paraformaldehyde (PFA) solution. The complete brain was then obtained by removing the skulls around it with tweezers and immersed in a tube of 4% PFA for at least 24 h in 4 °C refrigerator. The brain sample were then cut into small cubes and immersed in 15% sucrose solution until totally sinking to the bottom of the tube. Then the brain cubes were transferred in 30% sucrose solution and immersed inside until fully sinking to the bottom of the tube at 4 °C. A small amount of optimal cutting temperature (OCT, Tissue-Tek, US) compound were applied to cryoprotect the brain cubes and the cubes were stored at -80 °C after that until being sectioned. Frozen

sectioning were performed with a cryotome device (Leica CM1950, Germany) and the sections were stored in 1×PBS and then soaked in 5 mg/mL sodium borohydride solution for about 30 min and then rinsed 3 times with PBS, followed by 3% bull serum albumin (BSA) immersion for two hours at 4 °C and washed with PBST for at least 3 times. Then the sections were incubated with primary antibodies overnight at 4 °C. The antibodies include 1:1000 GFAP (glial fibrillary acidic protein, targeting astrocytes, Abcam #ab4674, US), 1:500 Iba1 (rabbit anti-ionized molecule 1 of calcium binding adaptor, targeting microglia, Wako# 019-19741, Japan) and 1:1000 NeuN (mouse anti-neuronal nuclear, targeting nuclei of neurons, Millipore #MAB277, US). After thorough wash of the primary antibodies the next day, sections were incubated in secondary antibodies for 2 h at room temperature. The second antibodies were Alexa Fluor 647 (donkey anti-rabbit, 1:500, Jackson Immunoresearch, US), Alexa Fluor 568 (goat anti-chicken, 1:500) and Alexa Fluor 532 (goat anti-mouse, 1:500, Invitrogen, US). In addition, DAPI (6-diamidino-2-phenylindole, Sigma-Aldrich, US) was also added together with those three second antibodies. Finally, the sections were transferred onto glass slides and embedded in Prolong Gold Gel (Invitrogen, US) and were ready for imaging.

A confocal system (UltraView VoX, PerkinElmer, US) was utilized to take 20× images of the sections. The results were colorized with Volocity Software (PerkinElmer, US). Fluorescence intensities of the immunomarkers were calculated as a function of distance. The distance was defined as the relative distance to the centre of the implants, which was defined as shown in Figure 10. The fluorescence intensities were calculated segment by segment. Each segment was a ring with outer diameter 40 μm larger than inner diameter and the inner diameter increased 20 μm segment by segment. The average

intensities of GFAP and Iba1 in a ring area were standardized by dividing the intensity value in the background region, which was defined as ~400 μm away from the implant centre. Image J software was used to count neurons ring by ring. The neuron lost zone was calculated by the distance from the implant centre where the neuron density reached or more than 80% of the background neuron densities. Both CNT fibre and PtIr electrodes were implanted with a 50 μm tungsten shuttle.

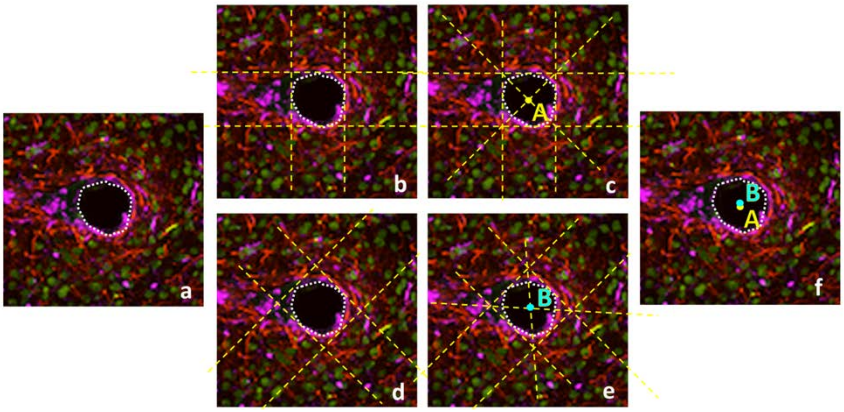

Figure 23. Schematic diagram of finding the center (distance x=0 μm) of the implant. (a) The white dashed enclosed line indicates the border of the hole formed by the implant in the superimposed images of GFAP/Iba1/NeuN. (b-c) Two vertical and two horizontal lines tangent to the white circle were drawn in b. and the intersection point A was marked in c. (d-e) Four line at a angle of 45° tangent to the white circle were drawn in d. and the intersection of the diagonal B was indicated in e. (f) The center of the implant tract was defined as the midpoint of A and B.

2.3 Results and Discussion

2.3.1 The Morphology of CNT Fiber Electrodes

Figure 6a. shows the lateral view of the CNT fibers. The twisting angles could be inferred from the clear texture of the fibers. The left 20 μm CNT fiber has a twisting angle of ~18°and the right 5 μm CNT fiber with a twisting angle of ~ 5°. Figure 6b. shows the CNT fibers is very flexible and soft and could be wrapped like a thread on a Teflon tube.

Figure 6c. shows an assembly of a four-channel CNT fiber electrode array and the inset shows the recording tip of the electrodes. The picture shows that there is no insulation layer wrapping the recording tip. The blade exposed recording tip has a large specific surface area owing to the porous structure of CNTs and the thread-like structure, resulting in the excellent electrochemical properties of the CNT fiber electrodes.

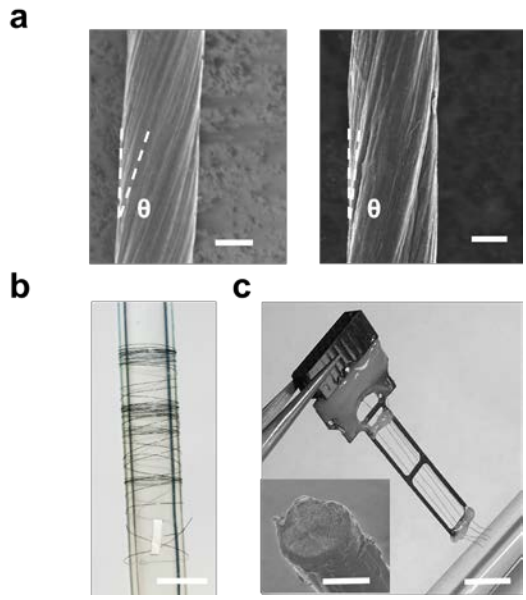

Figure 24. Images of CNT fiber electrodes. a. shows the lateral image of 20 μm and 5 μm CNT fibers under SEM with the scale bar 10 μm and 2 μm respectively. b. shows 2.5 μm parylene-C coated 20 μm CNT fibers wrapped on a tube. Scale bar, 5 mm. c. shows four CNT fiber electrodes placed against a glass stirring rod. Scale bar, 5 mm. The inset shows the SEM image of the tip, or the recording site of the electrode. Scale bar, 10 μm.

2.3.2 The CNT Fiber Electrodes Implantation Demonstration

The implantation process was shown in **Figure 5** where four electrodes were inserted simultaneously into a brain phantom, which was 6% agar gel.

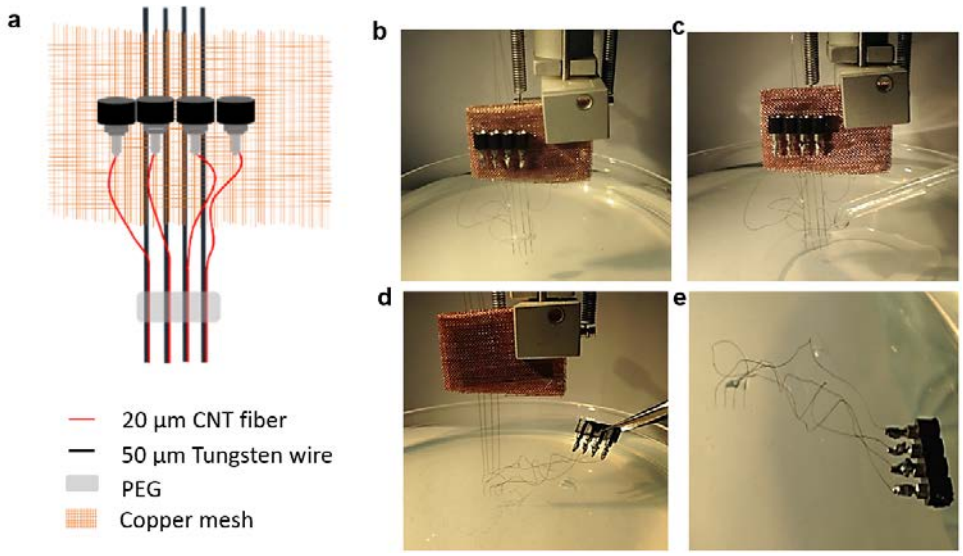

Figure 25. Implantation scheme of CNT fiber electrodes. (a) Schematic drawing of 4 channel CNT fiber electrode array with an interval of ~500μm. The 4 channels are fixed together with PEG, which is dissolvable in PBS. PEO is used to temporarily attach the CNT fibers to tungsten wires. (b-e) shows the implantation process. (b) The electrode array was inserted in the agar gel with desired depth, held by the stereotaxic apparatus. (c) 1× PBS was applied around the implantation site to help dissolve PEO. (d) The tungsten wires were lifted vertically by the stereotaxic apparatus after the PEO was completely dissolved. (e) The CNT fiber electrodes remained in the agar gel.

There are many ways for implanting flexible electrodes. Magnetic-assisting implantation method,[80] microfluidic devices assisting implantation,[81], coating the electrodes with thermo-reversible polymer solution and stiffening the electrodes,[82] or inserting together with a rigid stiffener to drag the electrodes into brain tissue.[83] However, the shuttle-assisting implantation methods seem to be a best strategy at present, considering the success rate, the tissue damage level and the operational complexity.

2.3.3 Electrochemical Properties Results and Discussion

The results of EIS, CSC and CIL of CNT fiber electrodes and PtIr electrodes are shown in **Figure 9**. Figure 9a and 9b show that the impedance decreases with the increase

of frequency and the phase increases with the increase of frequency, which reflects the good high-pass phenomenon of the CNT fiber electrodes. Because the extracellular voltage of neural signals is about 50-500 μV and the frequency is about 1 kHz, the impedance performance of electrodes is usually evaluated by the impedance of electrodes at 1 kHz. The impedance at 1 kHz for 20 μm CNT fiber electrode, 20 μm CNT fiber electrode with nitric acid treatment, 5 μm CNT fiber electrode with nitric acid treatment and 25 μm PtIr electrode were 279.96±32.08 kΩ (n=8), 41.95±3.62 kΩ (n=8), 709.78±64.26 kΩ(n=8), 367.73±52.21 kΩ, (n=8). The values show superior impedance properties of 20 μm CNT fiber electrodes compared to PtIr electrodes with a similar diameter. The 5 μm acid treated CNT fiber electrodes have an impedance about twice that of 25 μm PtIr electrodes though, the impedance value is usually considered within the acceptable range for individual neural recording, especially given that the diameter of the recording site is only 5 μm. The nitric acid treatment removed impurities on the tip of CNT fiber electrodes and doped with the CNT fibers, therefore resulting in the better electrochemical properties of CNT fiber electrodes. Figure 9c shows that there is no redox peak for CNT fiber electrodes under the voltage from 0.8 V to -0.6 V, which indicates that the electrochemical interactions events at the CNT fiber electrode-tissue interface are mainly capacitive charging and discharging without Faradaic reactions. The CSCc of 20 μm CNT fiber electrodes, 20 μm CNT fiber electrodes treated with nitric acid, 25 μm PtIr electrodes are 278. 21±5.42 mC/cm2, 419.87±73.04 mC/cm2 and 2.36±0.36 mC/cm2. The charge injection limit of of 20 μm CNT fiber electrodes, 20 μm CNT fiber electrodes treated with nitric acid, 25 μm PtIr electrodes are 3.52±0.15 mC/cm2, 5.04±0.22 mC/cm2 and 0.15±0.01 mC/cm2. The CSCc

and CIL values show that CNT fiber electrodes clearly have markedly advantage over PtIr electrodes for neural stimulation.

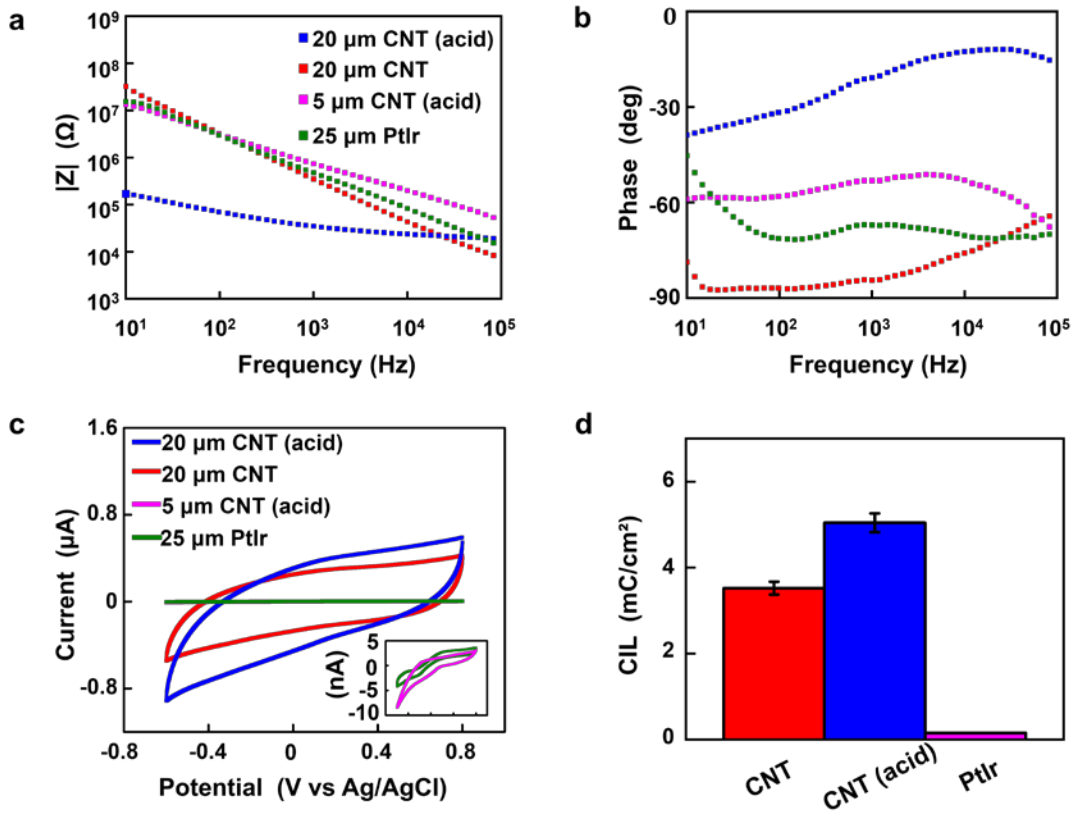

Figure 26. Electrochemical Properties of CNT Fiber Electrodes. Figure a and b are impedance magnitude and phase of EIS under 10- 100,000 Hz. Figure c and d shows the CV curve and charge injection limit of the electrodes. Error bars represent SEM (n=8).

2.3.4 Mechanical Characterization Results and Discussion

The bending stiffness of 20 μm and 5 μm CNT fibers is calculated to be 8.16×10^3 nN·m and 1.58×10^2 nN·m, respectively. These values are larger than the mechanical properties of the mesh electrodes reported by Lieber group and brain tissue, but much smaller than that of the same size PtIr electrodes (1.53×10^5 nN·m) and carbon fiber electrodes (3.9×10^4 nN·m) or silicon electrodes (4.6×10^5 nN·m).[26, 27, 79, 84, 85]

2.3.5 Histological Study Results and Discussion

Glial scar formed around the implant and the neuronal death near the recording sites are two main negative factors affecting the longevity of the microelectrodes for chronic neural recording.[49, 86] We observed a two-fold reduction compared to PtIr electrodes of astrocytes and microglia marked by GFAP and Iba1 respectively as shown in Figure 11, indicating less gliosis for the CNT fibre electrodes implant. The neuron lost zone for CNT fibre electrodes and PtIr electrodes were approximately 66±5 μm (n=6) and 109±5 μm (n=6) respectively (Figure 12a, d, e). The loss of neurons region for CNT electrodes is approximate to the implantation footprint, which is 20 μm CNT fibre, with 2.5 μm parylene-C insulation layer and a 60 μm tungsten shuttle, indicating that no obvious further neuron loss zone formed after the acute injury of implantation process. In the 12-week post implantation data shown in Figure 14, a ~1.7-fold reduction of intensity for GFAP around the CNT fiber electrodes was observed compared to PtIr electrodes while the intensities of Iba1 for both electrodes were clearly reduced compared to data in 6-week post implantation and the values became comparable between CNT fibre and PtIr electrodes. As for the neuron lost zone, no statistically significant further neural degeneration compared to 6-week post implantation was observed for CNT fibre electrodes while ~1.3-fold neuron lost zone was observed around the PtIr electrodes. These results demonstrate an improved and stable neural interface between CNT fibre electrodes and neural tissue than stiff metal electrodes like PtIr.

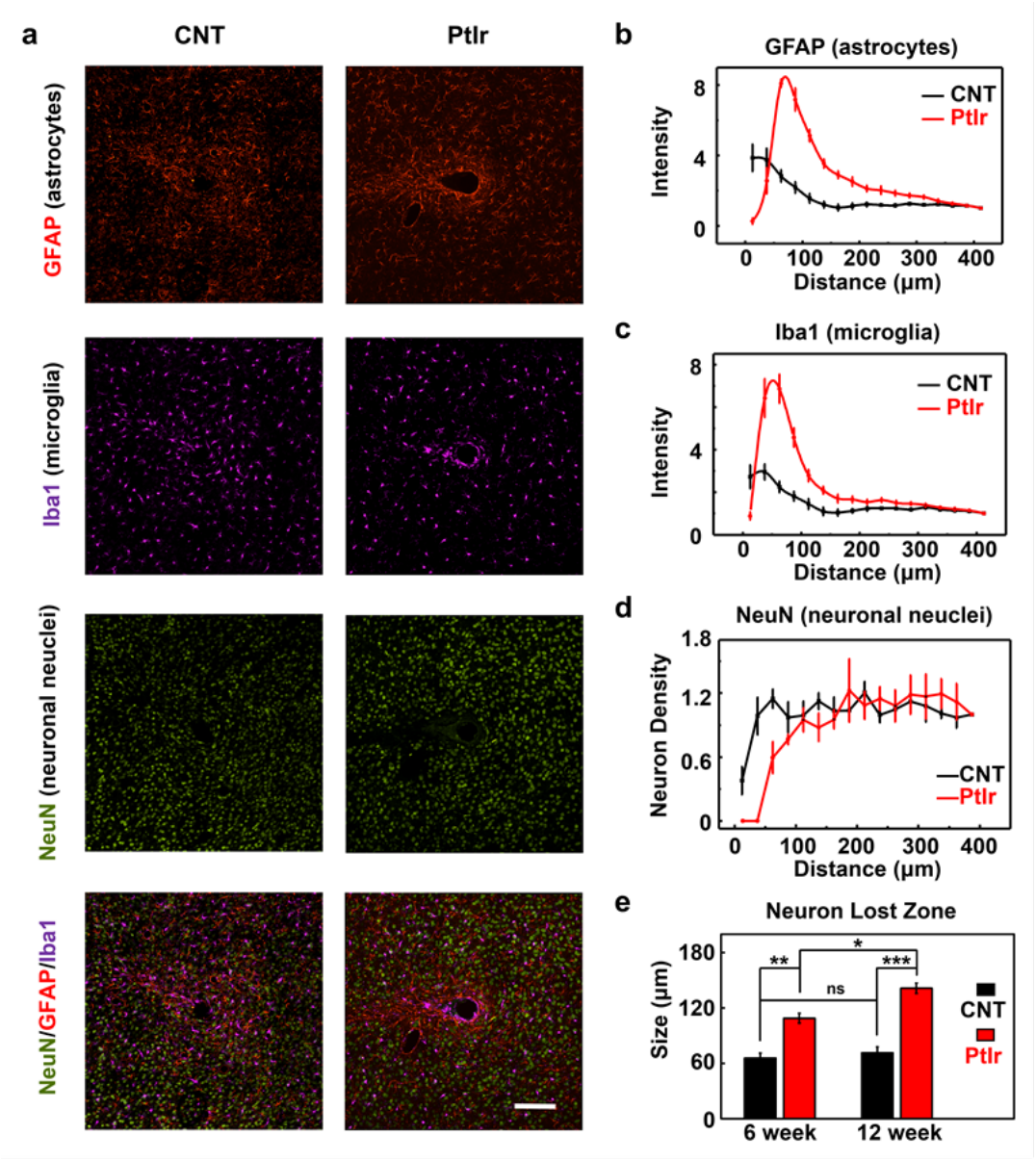

Figure 27. Immunohistochemistry analysis of brain tissue reaction 6-week post implantation for CNT fiber electrodes. (a) Immunofluorescence photos of a 20 μm CNT fiber electrode (left) and a 25 μm PtIr electrode (right), both with a 2.5 μm parylene-C insulation layer. GFAP, Iba1 and NeuN were labeled using red, purple and green colors respectively. The images on the bottom row were merged images of those three markers. Scale bar, 100 μm. (b, c) Normalized fluorescence intensities of GFAP and Ibal as a function of distance. Error bars represent SEM (n=6). (d) Neuron density as a function of distance with a bin size of 25 μm. Error bars represent SEM (n=6). (e) Neuron lost zone represented by equivalent diameter for both CNT fiber and PtIr electrodes post 6- and 12-week implantation. The error bars represent SEM, n=6. ($p < 0.001$ for ***, $p < 0.01$ for **, $p < 0.05$ for *, $p > 0.05$ for no significance, one-way ANOVA).

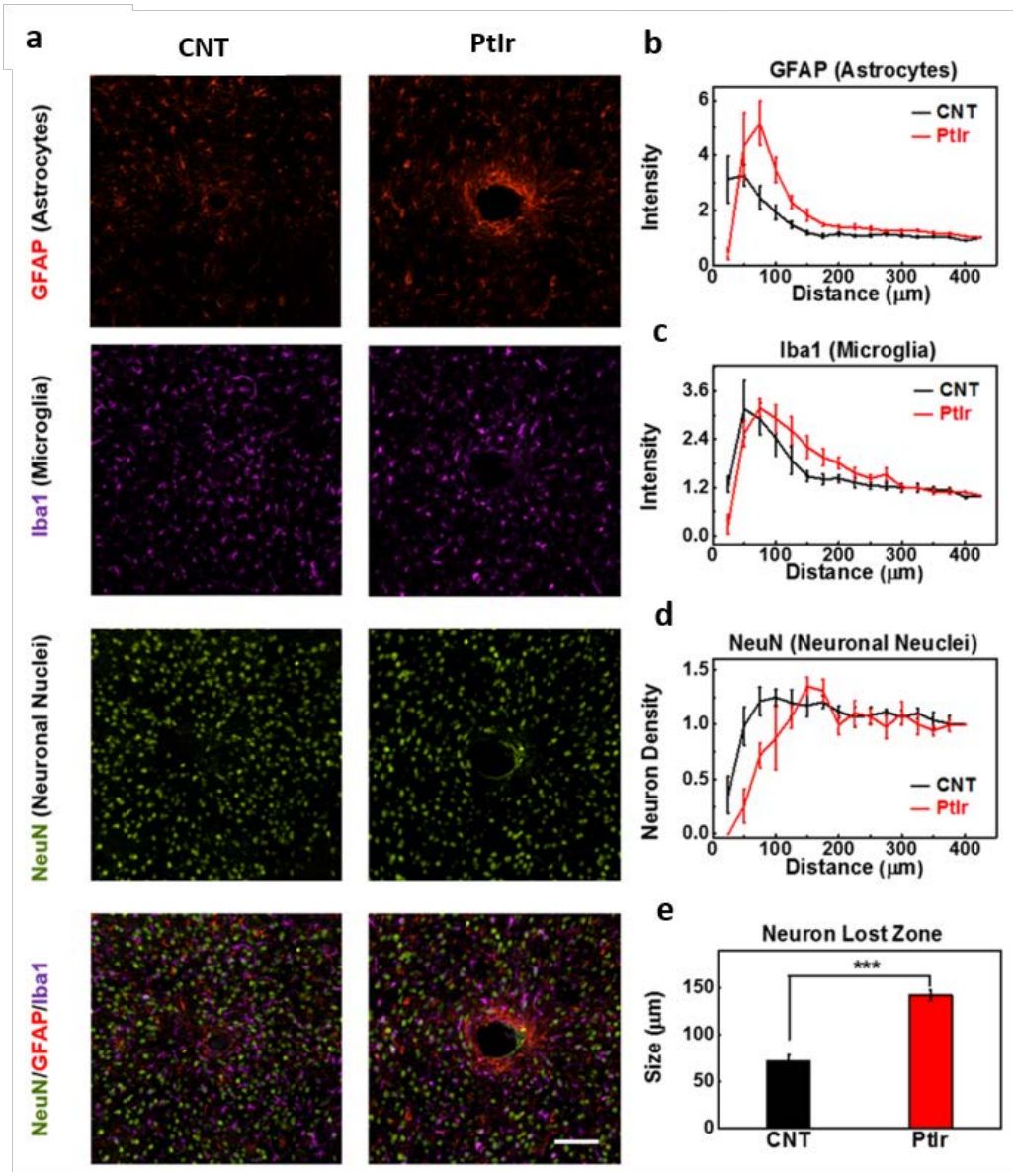

Figure 28. **Immunohistochemistry analysis of brain tissue reaction 12-week post implantation for CNT fiber electrodes.** (a) Immunofluorescence photos of a 20 μm CNT fiber electrode (left) and a 25 μm PtIr electrode (right), both with a 2.5 μm parylene-C insulation layer. GFAP, Iba1 and NeuN were labeled using red, purple and green colors respectively. The images on the bottom row were merged images of those three markers. Scale bar, 100 μm. (b, c) Normalized fluorescence intensities of GFAP and Ibal as a function of distance. Error bars represent SEM (n=6). (d) Neuron density as a function of distance with a bin size of 25 μm. Error bars represent SEM (n=6). (e) Neuron lost zone represented by equivalent diameter for both CNT fiber and PtIr electrodes post 6- and 12-week implantation. The error bars represent SEM, n=6. ($p < 0.001$ for ***, one-way ANOVA).

2.4 Summary

This chapter details the fabrication procedures, the shuttle assisted implantation method, and the characterization of the achieved CNT fiber electrodes. The fabrication procedures of the CNT fiber electrodes clearly describe the electrode design, insulation layer coating, methods of exposing recording sites, etc., accompanied by a schematic description. Due to the softness and flexibility, the CNT fiber electrodes cannot be directly implanted into the brain like a rigid metal electrode or a silicon electrode. In fact, the implantation is a major challenge for the development of soft electrodes, so the implantation strategy of CNT fiber electrodes is explained in detail here. A shuttle-assisted implantation method is utilized, where the flexible electrode and a stiff rod acting as a shuttle are combined tightly with a biocompatible glue and then inserted together into the tissue, and then the shuttle is extracted out of the tissue after the separation of the shuttle and electrodes due to the dissolve of the glue between them. The implantation design scheme, the choice of shuttle material, the assembly of electrodes and shuttle, the detailed steps of implantation, and the difficulties during implantation to be noted are all presented. Next, the properties of CNT fiber electrodes are characterized, including (1) morphological characterization. The porous surface structure of the CNT fibers accounts for the good electrochemical properties of the CNT fiber electrode. (2) The electrochemical characterization with EIS, CV and CIL testing, of CNTs demonstrates the low impedance, high charge storage and high charge injection capability of CNT fiber electrodes, and theoretically proves the advantages of CNT electrodes in neural recording and neural stimulation. (3) The result of bending stiffness characterizing the mechanical properties demonstrated the flexibility of the CNT fiber electrodes, which can partly explain the

decrease of the inflammatory response. (4) Histological studies on the inflammatory response of CNT fiber electrodes 6 weeks and 12 weeks after implantation confirmed that the CNT fiber electrode induced less severe inflammatory responses than conventional electrodes, resulting in thinner glial scars and smaller neuron lost zone, which facilitated neural signal recordings of the electrodes.

CHAPTER 3. IN VIVO MRI ARTIFACTS STUDY OF CNT FIBER ELECTRODES

3.1 Introduction

MRI compatible microelectrodes are critical for anatomical or functional MRI and electrophysiological recording mapping. This chapter characterized the MRI compatibility of CNT fiber electrodes. The methods include: (1) T1- and T2-weighted 7.0 T MRI scan with CNT fiber electrodes and the control electrodes implanted in rat brans and the analysis. (2) Calculation of eddy currents, current-decaying time constants, skin depths of electrodes. Then the results and discussions are presented, followed by a summary of this chapter.

3.2 Methods

3.2.1 MRI Scanning and Results Analysis Methods

We characterized the MRI compatibility by assessing the artifacts size of CNT fiber and PtIr micro electrodes implanted in rat brains with a 7.0 T Bruker MRI (Bruker, Germany). 25 μm PtIr microwires and 20 μm CNT fiber microelectrodes were insulated with about 2.5 μm parylene-C. Both electrodes were contralaterally implanted in the rat brains. With the animal's head in the MR scanning coil in anesthesia, T1- and T2- weighted MR scanning was performed at a scanning interval of 0.8 mm per slice. The scanning parameters were set as follows: TR = 350 ms, TE = 11 ms, matrix = 122 ×92 and field-of-view = 40 cm × 40 cm for T1 scanning; TR = 2510 ms, TE = 41 ms, matrix = 240 ×320 and field-of-view = 40 cm × 40 cm for T2 scanning. The edges of the artifacts were detected

using canny edge detector with Matlab and the size of the artifacts were defined as the equivalent diameter of a circle with the same geometrical area as the that inside the detected edges of the artifacts as shown in Figure 10.

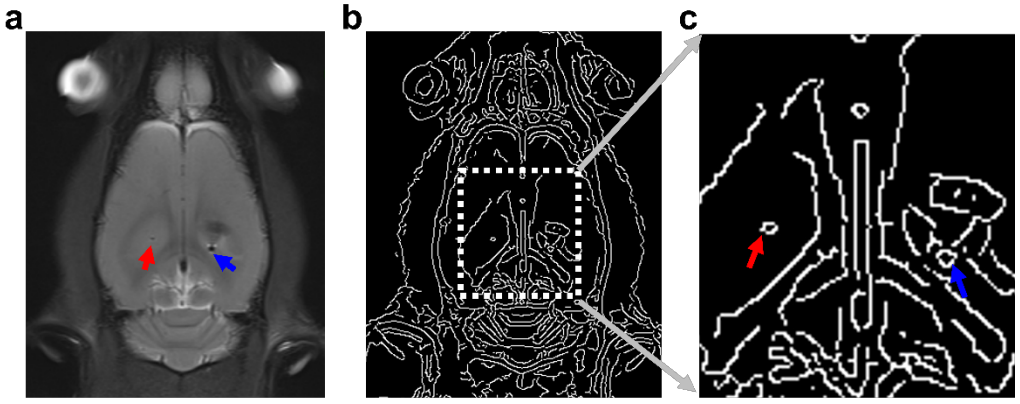

Figure 29. An example demonstrating the measurement of the artifact size in MRI. (a) This is the original MRI image used in the demonstration for measuring artifact size. The red arrow points to the CNT fiber and the blue arrow points to the PtIr electrode. (b) The generated edge image of the original image with Canny edge detector in Matlab (Mathworks, USA). (c) An enlarged image of the white dotted frame in b with the same color code used as in a. The white enclosed area indicates the artifact. The size of an artifact is defined as the equivalent diameter of a circle with the same geometrical area.

3.2.2 Calculation of Eddy Currents

Another source of artifacts during MR scanning results from eddy current, which is generated due to time-varying magnetic field B. The maximum eddy currents I_{max}, skin depth δ and decaying time constant τ were calculated for both electrodes made of CNT fibers and PtIr in a 7.0 T MR coil.

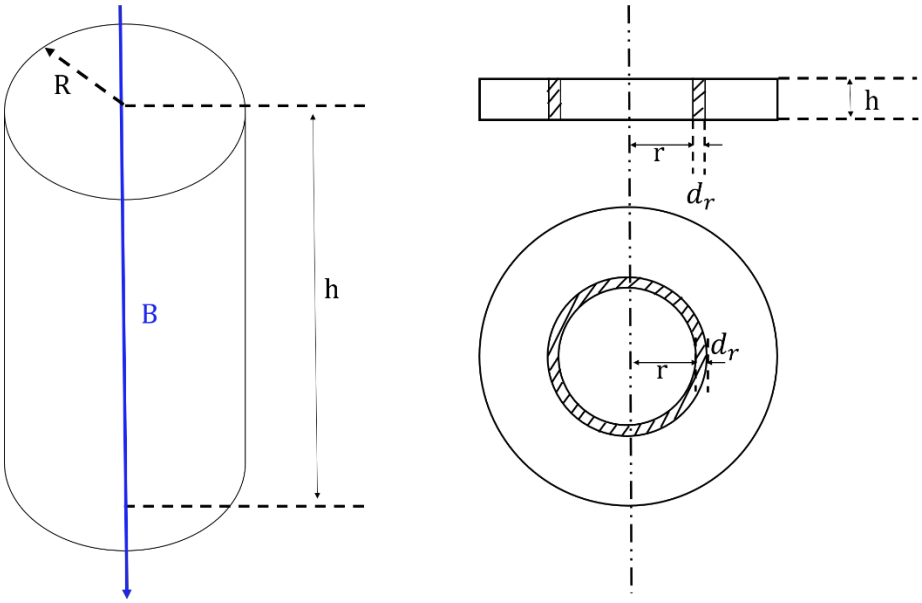

Figure 30. The schematic diagram of the model used to calculate eddy current.

The radius and length of electrodes were represented by R and h, where $R_{CNT} = 10\ \mu m$, $R_{PtIr} = 12.5\ \mu m$ and $h \approx 4\ mm$. The geometrical model used for calculation is shown in Figure 12. A small ring with radius r, width d_r and length h was taken from the electrode. The electromotive force ε_i generated from the time-varying magnetic field was calculated by

$$\varepsilon_i = -\oint \frac{dB}{dt} \cdot dS$$

The magnetic field B is perpendicular to the ring, so

$$\varepsilon_i = -\frac{dB}{dt} \int dS = -\frac{dB}{dt} \cdot \int 2\pi r dr \ = -\frac{dB}{dt} \pi r^2$$

Referring to the definition of material's resistance, the small ring has a resistance

$$dRES_{ring} = \rho \frac{2\pi r}{h dr}$$

Referring to Ohm's Law, we got the current

$$dI = -\frac{dB}{dt} \cdot \frac{h}{2\rho} r dr$$

Then, we got the total eddy current inside the cylinder by integrating

$$I = \int dI = -\frac{dB}{dt} \cdot \frac{h}{2\rho} \int_0^R r\, dr = -\frac{1}{4\rho} \frac{dB}{dt} R^2 h$$

And

$$max(-\frac{dB}{dt}) = SR_{max} \cdot X_{max}$$

Here the slew rate $SR_{max} = 1160\, T/m/s$, the distance between the coil center and the sample center X_{max} = 15.5 cm. The material resistivity of CNT fiber and PtIr are $\rho_{CNT} = 2 \times 10^{-5} \Omega \cdot m$, $\rho_{PtIr} = 2.4 \times 10^{-7} \Omega \cdot m$. [67]

$$I_{max} = \frac{SR_{max} \cdot X_{max}}{4\rho} R^2 h$$

The eddy currents

$$I_{\max\_CNT} = 0.9\, \mu A$$

$$I_{\max\_PtIr} = 117.1\, \mu A$$

And the current increases with time t as

$$I(t) = I_{\max}(1 - e^{-\frac{t}{\tau}})$$

And then it decays as

$$I(t) = I_{\max} \cdot e^{-\frac{t}{\tau}}$$

The electrode placed inside the magnetic coil has an inductance *L*

$$L = \frac{\mu_0 h}{2\pi}\left(ln\frac{2h}{r} - 0.75\right)$$

Where $\mu_0 = 4\pi \times 10^{-7}\ H/m.$ [SI 10] representing the magnetic permeability of vacuum.

The resistance of the sample

$$RES_{sample} = \frac{E}{I_{max}}$$

The decay time constant τ [67]

$$\tau = \frac{L}{RES_{sample}}$$

Then the decaying time constants are

$$\tau_{CNT} = 76\ ns$$

$$\tau_{PtIr} = 6060\ ns$$

Skin depth δ represents the penetration depth of an electromagnetic wave beneath the surface of a conductor.[67]

$$\delta = \sqrt{\frac{2\rho}{\omega\mu}}$$

Where ω represents the angular frequency, μ represents the magnetic permeability

$$\mu = \mu_0 \mu_r$$

And μ_r represents the relative magnetic permeability.

For the 7.0 T MRI, radial frequency $f = 300$ MHz, $\omega = 2\pi f = 1.884 \times 10^9\ rad/s$. The susceptibility of PtIr χ=231 ppm, and the relative permeability $\mu_r = 1 + \chi = 1 + 231 \times 10^{-6} \approx 1$. The susceptibility of CNT fiber χ= -26 ppm, and the relative permeability $\mu_r = 1 + \chi = 1 - 26 \times 10^{-6} \approx 1$. Therefore, $\mu = \mu_0 \times \mu_r \approx \mu_0 = 4\pi \times 10^{-7}\ H/m$ for both CNT fiber and PtIr electrodes. Then we get

$$\delta_{CNT} = 130\ \mu m$$

$$\delta_{PtIr} = 14.2\ \mu m$$

3.3 Results and Discussion

Previous study investigated the MRI artifact properties of CNT fibers wrapping to a 1.3 mm polyurethane tube in 3.0 T magnetic resonance scanning with the CNT fibers wrapping onto a tube made of polyurethane. The results showed reduced 62% and 74% artifact reduction under gradient echo and spin echo sequences scanning.[67]

The artifact for 20 μm CNT fibers is 268.4±29.9 μm (n=5) while that of PtIr microwires is 675.1±22.5 μm (n=5) in T2-weighted images. The artifact of PtIr microwires is 922.5±59.2 μm (n=5) in T1-weighted MRI images while that of CNT fibers is barely visible as indicated in Figure 11e. The results indicate that CNT fiber electrode caused much reduced magnetic field distortion than the PtIr microwire electrodes. The CNT fiber

electrodes with much-reduced artifact make it possible to visualize and identify the brain tissues in the vicinity of the implanted electrodes, which is important and necessary for precisely mapping MRI results with electrophysiological recording results from the electrodes, benefiting many applications such as verifying the placement of electrodes, identifying pathological abnormalities using MRI when electrodes already implanted in patients.[87-90]

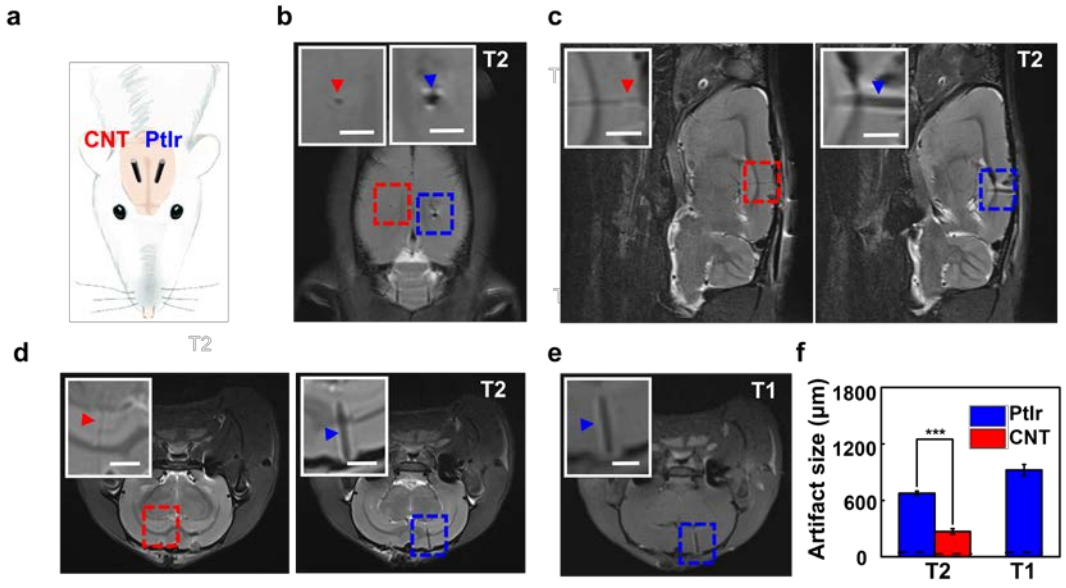

Figure 31. In vivo MRI artifact comparison of CNT fiber electrodes and PtIr electrodes. (a) Schematic drawing of CNT fiber and PtIr microwire electrodes contralaterally implanted in a rat used for MRI artifact assessment studies. (b-d) MRI image in horizontal, sagittal and coronal planes in a T2-weighted scan. Both CNT fiber and PtIr microwire were coated with a parylene-C layer with the same thickness. The red and blue frame were zoomed in in the insets. Scale bar, 1.5 mm. The CNT fiber and PtIr electrodes are shown in two planes in the sagittal and coronal planes. (e) T1-weighted MRI image of the rat in coronal plane. The CNT fiber electrodes are invisible. The blue frame indicates the artifact. Scale bar, 1.5 mm. (f) Artifact sizes of CNT fiber and PtIr microwire electrodes in T1- and T2-weighted images. Error bars indicate S.E.M. n=5, *** $p<0.001$, One-way ANOVA. All CNT fiber electrodes and PtIr wire electrodes were coated with 2.5 μm parylene-C.

The magnetic susceptibility difference between the electrodes and brain tissue is usually thought to be the main cause of MRI artifacts.[91] The susceptibility of PtIr microwire electrodes is 231 ppm[67] and $\Delta\chi$ is 240 ppm between PtIr and water (-9.05 ppm). The susceptibility of carbon atom in graphite materials is highly anisotropic diamagnetic with 70 times greater orthogonal susceptibility than the in the parallel direction (χ=-8.5 ppm). CNT fibers are reported with a diamagnetic susceptibility of about -26 ppm.[87] In fact, the real magnetic susceptibility of the CNT fibers we used might be different from the estimation due to the different growth conditions and the different structure of CNT fibers such as with different twisting angles. However, we can speculate that the susceptibility of CNT fiber is much closer to that of tissue than the PtIr electrodes as indicated from the much-reduced artifacts. Another research in our lab reported a MRI compatible Graphene-Cu electrode showed smaller artifact in T2-weighted images than that of the 20 μm CNT fiber electrodes. This makes sense considering that the magnetic susceptibility of copper (-9.63 ppm) is much closer to water/tissue. What is more, slight iron might exist in the CNT fibers since the iron acts as catalyst for CNT's growth. The remaining iron could compromise the MRI compatibility of CNT fibers.

The skin depth of the CNT fiber (130 μm) is much deeper than the diameter (20 μm). And the skin depth of PtIr (14.2 μm) is smaller than the diameter (25 μm). Besides, it can be seen that the induced eddy current has a fast decaying rate comparing to the repetition time or echo time parameters in our MRI system (For T1-weighted scanning, *TE* = 11 ms, *TR* = 350 ms; for T2-weighted scanning, *TE* = 41 ms, *TR* = 2510 ms). In a word, the induced eddy current can be neglected for both electrodes in generating MRI artifacts.

3.4 Summary

MRI compatibility is an important feature of neural electrodes, as it allows simultaneous neural recording, DBS and MRI, greatly desired for not only fundamental neuroscience studies, but also for clinical use. In this chapter, CNT fiber electrodes and PtIr electrodes with similar size were contralaterally implanted in rats for MRI artifacts study. T1- and T2- weighted scanning modes with a 7.0 T MRI scanner showed significant reduction in artifacts size induced by CNT fiber electrodes, compared with PtIr electrodes. The magnetic field distortion caused by magnetic susceptibility difference between electrode-tissue interface is considered as the dominant explanation for the MRI compatibility performance of CNT fiber electrodes, as CNT fiber has much closer susceptibility to tissue than PtIr. The eddy current, another factor possibly partly accounting for the MRI compatibility of the electrodes, was well studied in the chapter, including the calculation of maximum eddy current amplitude, the current decaying time constant and the depth the eddy current in the implant. The results showed that the CNT fiber electrodes have ~ 1% eddy current amplitude, ~ 1% current decaying time constant and ~ 1/10 skin depth compared with those of the PtIr electrodes. In addition, the eddy current values of CNT fiber electrodes and PtIr electrodes are quite small and the effects on artifacts can be neglected. Note that the actual PtIr electrodes are generally more than 100 μm in diameter, here we used a much smaller sized PtIr electrodes for better comparing the artifacts caused by different materials, PtIr and CNT fibers.

The inherent MRI compatibility of CNT fiber material, together with the small size of the CNT fiber electrodes attributed to the excellent electrochemical properties due to

porous structure, result in the MRI compatibility of the CNT fiber electrodes. The CNT fiber electrodes have broad application prospects for MRI compatible researches.

CHAPTER 4. IN VIVO NEURAL RECORDING WITH CNT FIBER ELECTRODES

4.1 Introduction

Electrophysiological recording serves as the most important characterization for evaluation the performances of neural recording electrodes in vivo. This chapter focuses on the acute and chronic neural recording studies of CNT fiber electrodes in rats.

Standardizing and performing high-quality surgery are essential to the results of electrophysiological experiments. The general methods presented include electrode preparation procedures, animal and surgery tools preparation, anesthesia of animals, the surgery, electrophysiological recording and post-surgery procedures, and the recorded data analysis methods. For each of the different recording purposes, the different parts of the procedures are described in each result section, to get rid of the confusion of general procedures.

Multiple recording results are shown, demonstrating the recording abilities of CNT fiber electrodes. These recordings include: (1) Whisker responsive single unit recordings in rats' whisker pathway. (2) Multiple-depths neural recording. (3) Chronic neural recording results over months.

4.2 Methods

4.2.1 Electrode Preparation

The impedance of CNT fiber electrodes at 1kHz should be measured before operation and the measurement result should be less than 1 MΩ. If the impedance of the electrode is tens of MΩ, which is much larger than 1 MΩ, it may be that the welding of the electrode and connector is not done well. In this case, the electrode needs re-welding and another electrode should be used instead. If the impedance of the CNT fiber electrode is between 1 MΩ and 5 MΩ, it may be that the recording site of the electrode is not clean. For example, parylene-C covers a part of the end surface that should have been exposed when the tip is exposed by blade cutting. In this case, it would help to apply current or voltage stimulus to clean up the cross-section without exceeding the charge capacity range of the electrode so as to expose a new area of the electrode until the impedance of the electrode is less than 1 MΩ. Another method for decreasing the impedance is to cut across the CNT fiber electrode near the tip to produce a new recording site and measure the impedance again. When a suitable impedance is obtained, the CNT fiber electrode needs to be disinfected in a sealed container. Steam sterilization at high temperature may destroy the structure of CNT fiber itself, so it is not suitable for CNT fiber electrodes. Ultraviolet or gas disinfection or other disinfection methods without destroying the CNT fiber electrodes should be utilized to sterilize the electrodes. After sterilization, the CNT fiber electrodes should be kept in a sealed sterilization bag until being used.

CNT fiber have good biocompatibility in animals, so CNT fiber electrodes can be used in animal experiments.[92-95] Regarding to CNT fiber probe, personnel should also be aware of potential hazards of carbon nanotube fiber. CNT fiber is already used in many in vivo studies (including in rat brain[96, 97]). The CNT fiber for the probe in this work is about 5-40 microns in diameter and more than 10 cm in length. It’s made of millions of

tiny CNT tubes by twisting and condensation. The CNT fiber is then encapsulated with parylene-C, a widely used biocompatible polymer in medical instruments, especially as an encapsulation material for implanted neural prostheses.[98-100] However, since the tiny carbon nanotubes, which constitutes the CNT fiber and are inside the CNT fiber, has potential consequences if inhaled by personnel, according to a review[101], which said that "If they are sufficiently thin, even very long fibers can readily penetrate to the distal lung, traveling into the lung by aligning their longitudinal axis with the airstream.' And NIOSH recommends an exposure limit of 1 μg/m3 of CNT and CNF. Attention should be paid to the potential hazard. Exposure should be limited and hazard should be considered similar to asbestos. Besides, the CNT fiber should be treated as sharps.

4.2.2 Animal and Surgery Tools Preparation

Rodents are currently the gold standard model for the study of neural system and sensory processing. They have mammalian neurological characteristics similar to human beings, as well as rich literary basis, which can be used for historical comparison and background knowledge. For these reasons, rodents are the ideal model system for this study. Adult Sprague-Dawley rats (Charles River laboratory) were used throughout the acute and chronic electrophysiological recording studies. All procedures are approved by the Committee of Animal Care and Use Institutions at Peking University and the Georgia Institute of Technology. It is necessary to allow received animals acclimatized for at least three days before operation. The animals should be weighed before surgery to determine the amount of anesthetic, and a clean cage should be taken to place the animal after surgery. And for the cage, be careful not to have something rugged or sharp, to prevent the implant on the head from being hit after surgery.

The surgery room should avoid the circulation of personnel. Surgical tools, including tweezers, scissors, cotton-tipped applicators and gauze sponges, should be sterilized in a sealed sterilization bag. After the animal's head hair is shaved or removed with hair removal cream, it needs to be disinfected in the exposed skin area, that is, alternating three times using alcohol and chlorhexidine for disinfection, to be careful not to let the fluid drip into the animal's eyes. When the sterilized surgical tool is opened from a sealed bag, avoid contact with anything that is not sterilized or disinfected, and if the gloves worn by the operator come into contact with a location that is not sterilized or disinfected, the operator needs to disinfect the gloves with alcohol. If the surgical tool is contaminated on a large scale, such as falling into an area other than the extinction area, the surgical tool needs to be re-disinfected before it can be used. Any area that the animal may contact and which the operation needs to encounter should also be disinfected, including microscopes, drill bits for drilling the skull, operating tables, etc.

4.2.3 Anesthesia of Animals

In the induction chamber, 5%-3% isoflurane is used to anesthetize the animal until full anaesthesia. The method of testing the animal for complete anaesthesia is to observe whether the animal is inactive or not, and secondly to check the heart rate. If the rate of heartbeats is less than 1 time per second, it is basically confirmed that the animal has been completely anesthetized.

The animal is then transferred to the nose cone on the operating table for 1%-3% anesthesia, and the animal is simultaneously anesthetized with fentanyl cocktail by intravenous injection at the tail vein. Fentanyl cocktail is made by 5 μg/kg fentanyl, 150

μg/kg dexmedetodomine, 2 mg/kg midazolam and mixed to 1 ml/kg solution with aseptic saline. For the tail vein fentanyl injection, a 24-gauge catheter is used to pierce through the tail vein and bandage is used to wrap and keep the catheter and tail together and an injection plug is applied to the catheter for continuously injecting fentanyl cocktail. When using catheter to insert into the tail vein, start with position close to the end of the tail and gradually move the insertion position to the upper end of the tail if not successfully plugged into the vein, which can prevent the blood from coming out of the pervious inserted position so that the animal doesn't bleed too much. The animal is placed on a thermostat controlled heating pad, which is set to 37 degrees Celsius. A temperature probe is inserted into the rectum to monitor the animal's body temperature. The depth of anesthesia can be monitored by observing pupil dilation and reactions to offensive stimuli (pinching the toe or tail), breathing frequency, and heart rate per minute. When heart rate and breathing frequency are low, stable and unresponsive to offensive stimulation, animals are considered to be in a stable state of anesthesia. In general, the animal's heart rate remains at < 300 beats per minute, ideally ~ 250 beats per minute. When the heart rate drops below 200 beats per minute, the animal is thought to be anesthetized too deeply. Since the initial heart rate of anesthesia in different animals is not consistent, the depth of anesthesia could not be judged by one observation alone, but multiple observations should be combined to evaluate the depth of anesthesia.

4.2.4 Surgery

In order to prevent surgical lights from shining on the animal's eyes and causing the animal to feel uncomfortable or even wake up, the animal's eyes should be evenly coated with ophthalmic ointment gel. The ophthalmic ointment gel should be appropriately

replenished during the surgery to keep the animal's eyes moist and comfortable. The next step is to fix the animal’s head to the stereotaxic device with two ear bars and the bar on the top of the animal’s nose. The ear bars should be adjusted appropriately until the animal is firmly secured. The test method is to gently press or push the animal's head to see if it is moving and to take further adjustments until it’s stably secured. This step is critical because if the animal's head is not securely fixed, it can lead to the inability to precisely locate the expected implantation position.

Before the surgery, a dose of analgesia (0.03 mg/kg buprenorphine) is injected through the abdominal cavity to relieve the pain sensation caused by the surgery on the animal. After shaving the hair on the animal's head and disinfecting the exposed skin, cut the opening skin in the appropriate area with the sterilized scissors, and use appropriate device to remove the connective tissue from the skull and remove the excess blood away with several cotton-tipped applicaters to expose the clearly visible skull. If the animal keeps bleeding from the skull, bone wax can be used to seal the bleeding points and stop the bleeding.

The next step is to nail three to four sterilized small screws in the skull, for facilitating the fixation of the implant in latter part of the surgery and being used for connecting grounding wires. Use a drill bit to drill a small hole in the skull that is close to or slightly larger than the screw diameter, and then nail the screw until the bottom of the screw has just touched the brain tissue. Surgeons should pay attention to the depth of the screws. If the screw is fixed too shallow, it is easy to loosen off and cannot be used for grounding. If the screw is fixed too deep, it may cause injury to the brain tissue or even hemorrhage of the brain. In addition, it is best not to nail the screw directly into the skull

without drilling a small hole, because it requires a greater force on the skull with this way, which may cause greater damage to the brain tissue. Then take a conductive electric wire of about 5-10 cm long and remove about 1 cm long the insulating layer with a lighter or other tools at both ends of the wire. Wrap tightly one end of the wire surrounding the nailed screw with the assistance of tweezers and the other end to the grounding line. In order to prevent the failure of the electrophysiological signal recording experiment caused by damage of grounding wire, another electric wire could be wrapped to another screw with the same method.

The next is to do the craniotomy. Rulers are used to measure the distance from bregma or lambda points on the skull under microscope to determine the craniotomy area on the skull. Generally, the craniotomy size is about 1 mm to 3 mm in length. Draw lines or other markers to mark the craniotomy window to assist drilling. A larger drill bit may be used initially until close to the bottom of the skull and then replace with a smaller drill bit for fine carving. Try not to drill too hard, in order to avoid causing brain tissue damage and thus affecting the electrophysiological recording for the animal. In addition, avoid continuous drilling at the same position to prevent the potential heat damage to the brain tissue. Doing the craniotomy in a correct manner is critical for the success of the experiment, take cautions to minimize unnecessary damage to brain tissue during the process.

The CNT fiber electrode is too soft to be inserted into the brain tissue through the dura, so the dura must be removed with fine tweezers or syringe needles before the electrode is implanted. The dura is a layer of connective tissue, which is right above the brain tissue. Therefore, in the process of removing the Dura, special care should be taken not to touch the brain tissue. Use one hand do the operation with tweezers or syringe

needles, and the other hand holding the operating hand to prevent the hand from shaking as to enhance the stability of the operation. Carefully rip a small hole or slit from the dura and clear the dura membrane further. Or, if possible, remove only a small fraction of the dura and make sure to insert the electrode through the area without dura in the implantation procedure of the surgery.

4.2.5 Electrophysiological Recording and Post-surgery Procedures

After implanting the electrode into the expected position, the electrophysiological signals recorded by the electrode can be observed by a software such as Open Sorter. At this point, if the noise in the recorded data is large, source of the noise should be examined and be eliminated by corresponding methods. One of the sources of noise is electricity on the socket, shutting down unwanted instrumentation in the operating room and unplugging the corresponding plug would help in this situation. Another source is that the electrophysiological recording system does not have a good electrical shielding, copper mesh or foil paper can be used to cover the relevant area of the whole system. Also, check whether the grounding wire is well connected to the ground, try to change the position of the grounding wire and see if the noise disappears. In a few cases, the noise may result from by electrode breakage, where the electrode needs to be replaced.

For detecting stimulation responsive neural electrical signals, deflection is applied to rats' whiskers. Firstly, trim the whiskers of interest to a length of about 15 mm from the whisker root on the face. The interested whisker is then inserted into a tiny tube in a galvanometer system (galvanometer optical scanner model 6210 H, Cambridge Technology) and ensure that the end of the part of the whisker outside of the tube is about

10 mm away from the whisker root on the face as shown **in Figure 16**. Then the whisker is deflected along the rostro-caudal axis by an actuator, which is programmed using Simulink in Matlab (MathWorks, USA) to control the voltage applied to the tube at a sampling rate of 1 k Hz so as to control the amplitude and speed of the deflection (National Instruments).

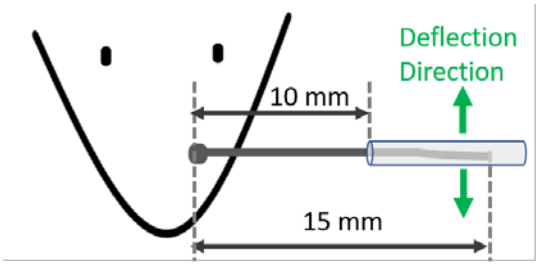

Figure 32. Schematic drawing of whisker stimulation system. The tube is deflected by a Matlab controlled actuator.

After the electrode is inserted in an expected position and desired neural electrophysiological signal is detected, the next step is to fix the electrode on the animal's head. The flexible CNT fiber electrode should be lowered until the connecting pin of the electrode is about 1 cm above the brain tissue. Gently carve fine lines with a knife on the skull to increase the roughness of the skull surface so as to strengthen the connection between the skull and dental cement. Then use the UV curable dental cement to build a wall little by little around the craniotomy window. Pay attention not to directly looking at the light to avoid potential eye damage. The wall should be built more inwardly with the increase of building layers as shown in **Figure 17** until the upper end of the dental cement wall seamlessly connected together. The CNT fiber electrodes are built inside the walls with the connecting pin part of it embedded in the wall and part of it outside of the wall. At this time, a hollow space is formed above the craniotomy window. In the process of

applying dental cement, it is necessary to carefully operate, as far as possible to avoid contacting with inserted CNT fiber electrode and causing changes of the location of the CNT fiber electrode, which then leads to the inaccuracies of the electrophysiological recording position. In addition, the grounding wire also needs to be buried in the dental cement with a segment of connecting part outside of the cement. To further protect the CNT fiber electrode and the grounding wire, a small cover, such as part of a small tube, could be used to cover the exposed parts of the electrode and grounding wire and only uncover them when performing electrophysiological recording.

Figure 33. The way to build a hollow dental cement wall by gradually shrinking toward the center above the craniotomy window to enclose the CNT fiber electrodes inside.

Animal’s vital signs should be monitored throughout the procedure, including heart rate, breathing frequency and body temperature, etc. After the surgery, put the animal in a clean cage with food and water, record the animal's post-surgery state and keep a close watch for the next few days. Once wound infection or other abnormal phenomenon of an animal is observed, immediately consult the veterinarian about the measures that should be taken and take notes.

4.2.6 Data Analysis Methods

Offline Sorter software (Plexon) was used for spike detection and single units sorting. The original detected voltage data was high-pass filtered at 250 Hz together with a 60 Hz notch. The voltage threshold for detecting spikes was set at three times of the RMS of the noise. The intercepted segment of each spike was confined to 1.2-1.3 ms. Another value for defining the spikes is called pre-threshold, which is the time length defined before the valley of the spikes, used as an alignment tool for the many detected spikes. The pre-threshold for the spikes data was set to 0.45 ms. The spike sorting methods were valley-seeking algorithms or by manually selecting spikes clusters from the principal component analysis results of the spikes.

4.3 Results and Discussion

4.3.1 Acute Neural Recording of Whisker Responsive Signals in VPm

Firstly, I will introduce the whisker system in rodents. Rats use the whisker system to locate and discriminate objects in the environment. The whisker system is a commonly used model system in research, such as studying information transmission in somatosensory pathway, neural activity adaptation to repetitive stimuli, sensorimotor integration.[102-104] Figure 21 is a schematic view of whisker distribution on a rat's face. The four rightmost whiskers are called α, β, γ and δ, respectively, and the other whiskers are divided into 5 rows from the middle of the face to the bottom, namely group A, B, C, D and E, and whiskers in each row are named 1,2,3,4… from the back to front respectively, such as examples of row A showed in the figure.

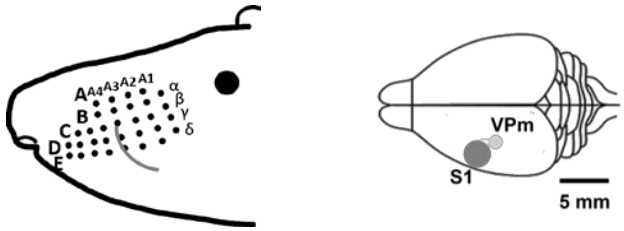

Figure 34. Schematic drawing of location and structure of the whiskers on the rat face (left) and whisker responsive regions in the rat brain (right).

When a whisker is deflected, the VPm in the thalamus and the S1 of the sensory cortex respectively have specific areas responding to the specific stimuli to every whisker as shown in Figure 22. Therefore, the electrophysiological recording of the CNT fiber electrodes in the VPm or S1 barrel cortex regions is a good way to verify the accuracy of the electrode implantation position, as the electrodes can record whisker responsive neural signals only when the electrodes are placed in the responsive area of the deflected whiskers.

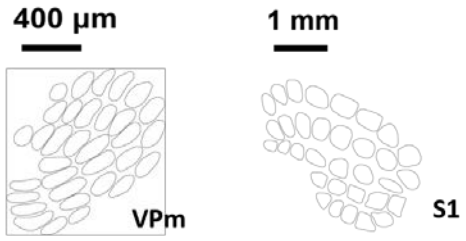

Figure 35. Schematic drawing of barreloids in VPm of a coronal slice (left) and barrels in S1 of a tangential slice in an adult rat.

In a typical experiment for whisker responsive signals detection from VPm, a CNT fiber electrode is inserted in whisker responsive VPm in thalamus to record neural activity responding to whisker deflection. The craniotomy was set at 2-4 mm caudal to grema, 2-4 mm lateral to the midline to access to the barreloids in VPm. The implantation depth of electrodes to reach barreloids usually falls within the range of 4700 μm to 5200 μm. For

the data shown in Figure 15, Whiskers were deflected periodically one at each time. Each session contains 100 trials. It is approximately 5 s in each trial, including a deflection of whisker at a speed of 1200°/s, then 10 stimuli of 900°/s at a frequency of 10 Hz in 1 s and followed by another 1200°/s deflection 100 ms later. Figure c shows the voltage response of two trials of the recorded voltage data when deflecting whisker D2 and whisker C3 respectively. It can be seen from the second row that most of the spikes were generated as the stimulus appeared, and it can be considered that the neuron recorded in VPm region by the electrode is mainly corresponding to the whisker D2. When we took the whisker D2 out of the tube, and applied the same stimulus to the whisker C3 adjacent to the D2 in VPm region, and then we can see from the third row that the correlation between the spikes firing of the neuron and the deflection stimulus clearly declines, which means that the spikes in row 3 were more likely to be generated by spontaneous firing of neurons, not by responding to deflection of whiskers.

To further analyse the correlation between stimuli and the recorded signals, spike waveforms of single unit were sorted from the 100 trials deflecting whisker D2. Figure 15 a. shows the average waveform of a sorted single unit with an amplitude of 372 μV and a high signal-to-noise ratio of ~30. The signal-to-noise ratio was calculated by the half of the peak-to-valley voltage difference of the average spike waveform divided by twice the standard deviation of the noise level as the equation

$$\mathbf{SNR} = \frac{Peak - Valley}{2 * Std(noise)}$$

The raster plot of 100 trials of this unit and the peri-stimulus time histogram (PSTH) are shown in figure 15 b. By comparing the spike counts following the first and second 1200°/s

stimuli, it is apparent that the number of spikes produced by the second one following 10 consecutive stimuli is significantly reduced, indicating the adaptation of neurons to persistent stimuli. This is consistent with the adaptation of neurons responding to stimulation in other literatures.[105, 106] These results indicate that the 15 μm CNT electrode can be accurately positioned to an expected implantation site and that an excellent signal-to-noise ratio can be achieved so as to sort detected waveforms into single units.

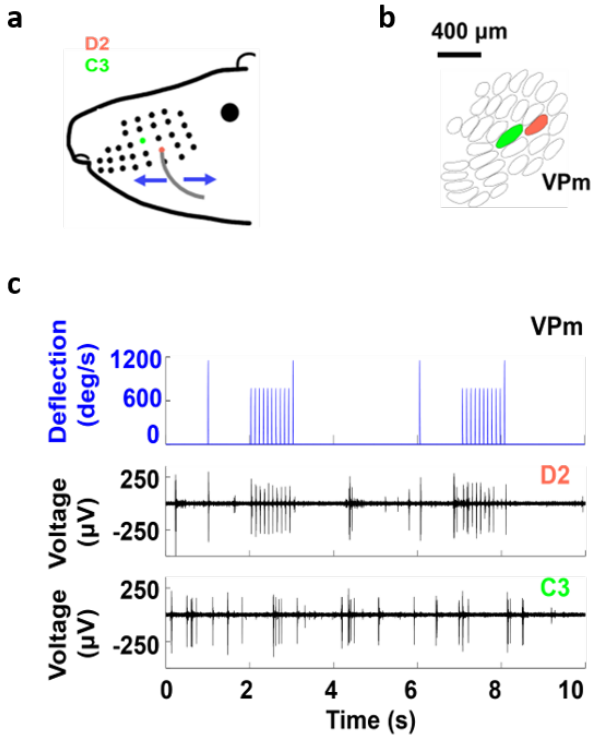

Figure 36. Whisker responsive neural recording in VPm using CNT fiber electrodes. In this part, whisker D2 and C3 were respectively deflected while a CNT fiber electrode was recording at the same position in VPm. a. shows the position of whiskers D2 and C3 on the rat's face. b. shows the barreloids in VPm where whisker D2 and C3 were represented in red and green respectively. The first row in blue in c. shows two trials of deflection stimulation of the galvanometer system. The second and third rows in c. shows the recorded voltage when deflecting whisker D2 and whisker C3 respectively.

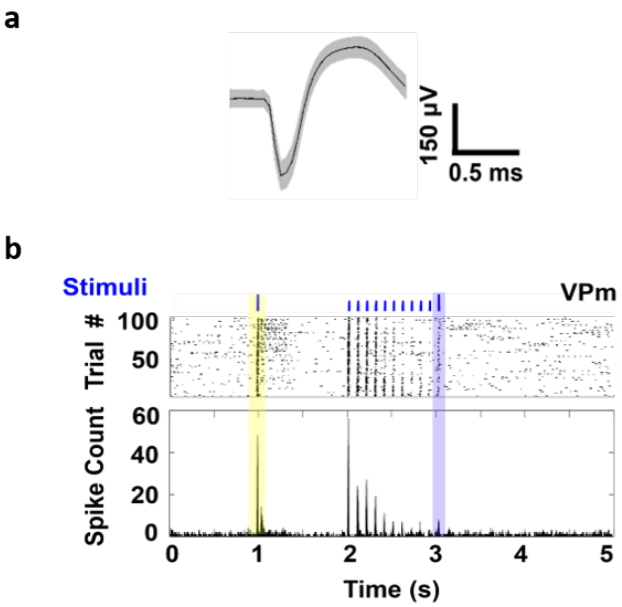

Figure 37. Spike waveform, raster plot and PSTH of individual neuron in VPm recorded by a 15 µm CNT fiber electrode. The black line in a. shows the average spike waveform of sorted unit and the grey band denotes ±1 SD. Raster plot and PSTH of the 100 trials are shown in b. where the yellow and blue bands denote the positions of first and second 1200°/s deflection.

Besides single unit, the LFP from the CNT fiber electrodes in VPm also clearly showed the neural activity's adaptation to frequent deflection on whiskers as shown in Figure 25. The recorded data were filtered with a bandpass filter by 0.5-300 Hz. The amplitude of the valleys following each stimulation shows a decreasing response of neurons following multiple stimulation. Therefore, the 15 µm CNT fiber electrodes can record with high SNR both whisker responsive single unit and LFP in the VPm.

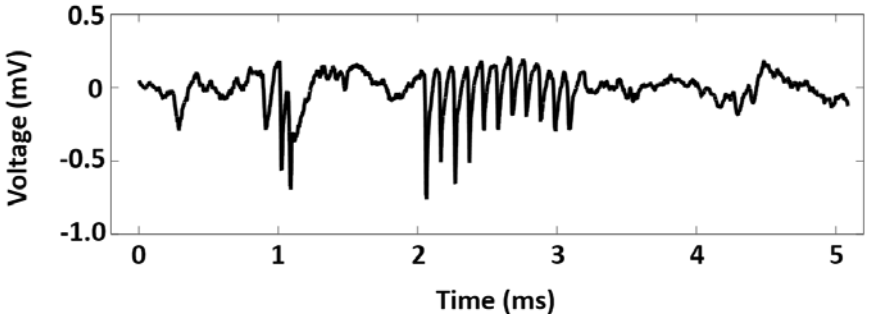

Figure 38. Whisker responsive LFP from CNT fiber neural electrodes. The figure shows LFP of one trial with the same stimuli as in Figure 15.

4.3.2 Acute Neural Recording of Whisker Responsive Signals in S1

Information transmission in VPm and S1 are two well studied vibrissae pathway in rodents. The challenge of neural recording in VPm is to precisely locate VPm owing to the smaller size and the deeper position of VPm. The tolerance for the deviation from the expected position is much smaller when the electrodes are implanted. The whisker responsive barrels in S1 is bigger and lie in a shallow depth of ~700-1200 μm, which reduces accuracy requirements for electrode placement. However, the challenge for neural recording in S1 lies in the surgery and the electrochemical properties of the electrodes. Because the position of S1 is extremely shallow, it is more difficult to avoid damage to brain tissue during surgery, for example, if the force applied on the brain during drilling to create the craniotomy is too hard or keep drilling in the same position for a long time, the brain tissue might get injured during these processes, leading to neuronal damage and even no neuroelectric activity. In addition, the neurons in S1 have a smaller amplitude of action potentials, which requires better electrochemical performance and higher spatial resolution of the electrodes. In my research, both 15 μm and 5 μm CNT fiber electrodes were utilized to perform the electrophysiological recording in S1. As can be seen from figure 26,

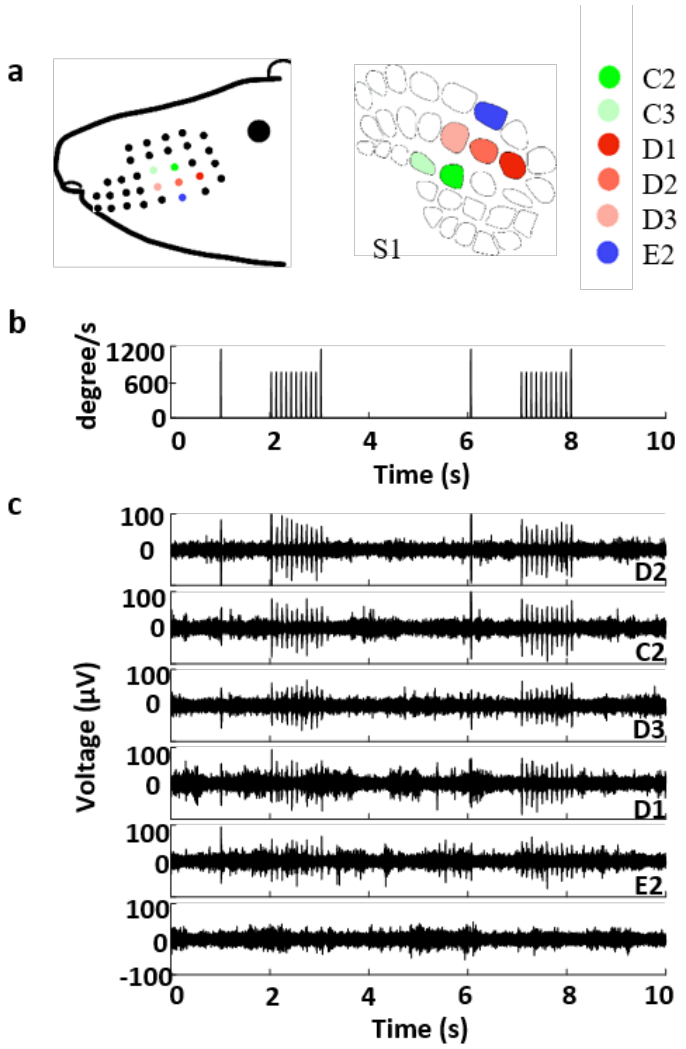

Figure 39. Whisker responsive neural recording in S1 using CNT fiber electrodes. a. (left) shows the positions of these five whiskers on the rat's face. a. (right) shows the corresponding barrels in S1 and the five whiskers were indicated by different colors. b. two trials of deflection stimulation applied on the whiskers or applied beside whiskers as control. c. neural signals recorded by a 15 μm CNT fiber electrode placing in the same position while stimulating on different whiskers as indicated in the right corner of the voltage traces. For the last trace in c., no whisker was inside the tube of the galvanometer system while the tube was deflected in the same way as shown in b.

electrodes of both size can record neural activities responding to deflection stimuli on whiskers. In figure 26c., the primary responsive whiskers were whiskers D2 and C2 while whiskers D3, D1 and E2 were less responsive than them. The last voltage trace shows no

obvious spikes following the stimulation when stimulating on the air, demonstrating that the signals recorded when stimulating other whiskers were not mechanical noise.

4.3.3 Multi-depth Neural Recording

The high tensile strength of CNT fiber neural electrodes makes it possible to retract and move the electrodes after inserted in the brain tissue. This is a great advantage for soft and flexible electrodes which are associated with less inflammatory responses and the ability to fine-tuning the implantation position of the microelectrodes after implantation offers advantage for both recording and stimulating neural electrodes. The advantages include: (1) selecting cells that have particular response properties; (2) seeking cells that might have been silent for some time during the insertion by moving electrodes back and forth; (3) monitoring changes of single neurons in small population undergoing neuronal plasticity; (4) seeking neurons in pairs or triplets in different brain regions to probe neuronal connectivity and tracts; (5) recording from multiple brain regions with single microelectrode such as recording neurons along the banks of sulci at multiple different depths.

The CNT fiber microelectrodes were demonstrated to be movable along the insertion direction after inserted by adjusting the depth to move them upward as shown in Figure 27. In a typical electrophysiological recording experiment, a CNT fiber neural electrode was inserted into the brain to a pre-determined depth at ventral posterolateral thalamic nucleus (VPL) in an anesthetized rat. The insertion strategy was the same as described in previous parts of the thesis. After retracting the tungsten shuttle, the CNT fiber microelectrode was retracted from the depth of -6838 to -2160 μm (relative to the surface

of the brain tissue in the craniotomy) utilizing a hydraulic micromanipulator with a sub-micron spatial resolution. The signals along the retraction process was recorded at five different depths across five different brain regions including VPL, field CA2 of the hippocampus and the trunk region of primary somatosensory cortex S1Tr. The high SNR of the electrophysiological recording at these five different depths demonstrates that retracting the CNT fiber electrodes along the insertion track did not result in disturbance to the neurons in pretty close proximity to the CNT fiber electrode, especially indicated from the three very close depths -2160, -2166 and -2169 μm depths. These results demonstrate that CNT fiber microelectrodes are strong enough to be dragged post implantation into the brain tissue and adaptive electrode-neural interface is formed while the electrodes are still soft and flexible for enhanced neural integration, which can be used for chronic timescales. In the future, motorized microdrives could be integrated with CNT fiber microelectrodes to enable reliable fine-tuning and autonomous implantation of electrodes in freely-behaving animals, essential for many fundamental neuroscience studies.

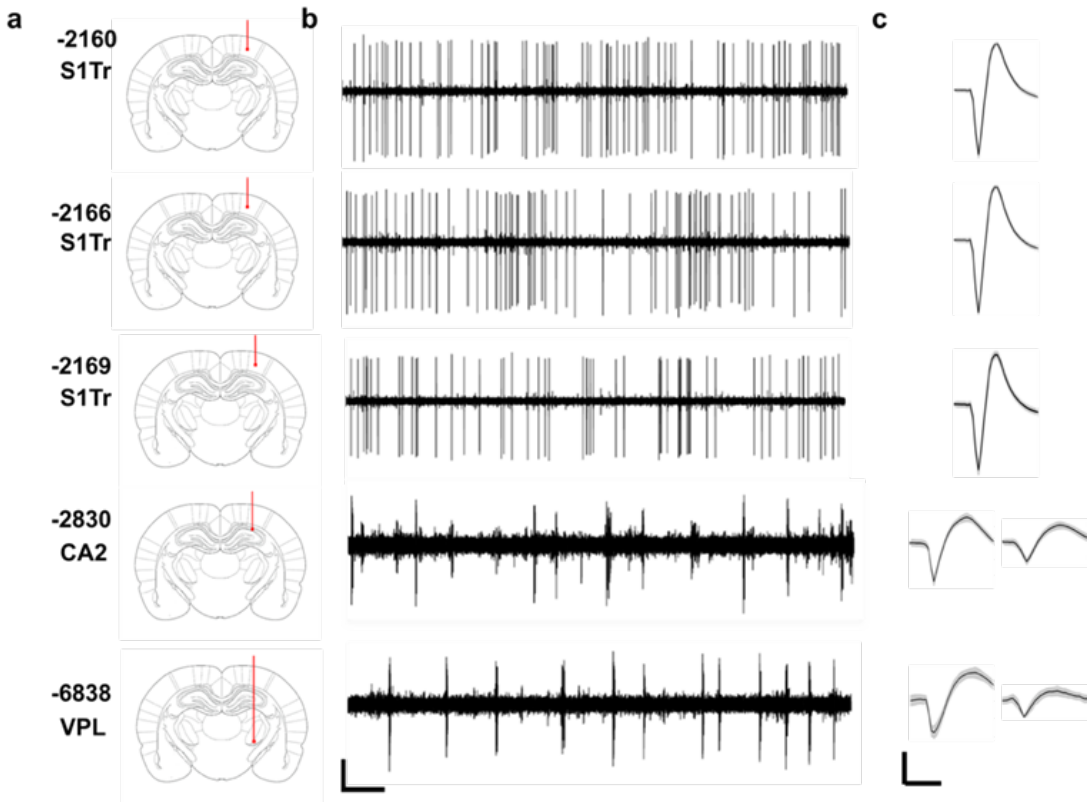

Figure 40. Multi-depth neural recording with CNT fiber microelectrodes. a. schematic drawing shows the depth and brain regions at each recording depth in the coronal plane. The numbers on the left indicate the depth (μm) coordinate at each recording site with each corresponding brain nuclei shown below the numbers. b. shows the representative voltage traces of neural recording at each depth. The horizontal bar is 500 ms and the vertical scale bar is 200 μV. For recording at each depth, the waveforms of isolated single units are shown in c. with gray bands denoting ±1 S.D. with the horizontal scale bar of 0.5 ms and vertical scale bar of 200 μV.

Note that the voltage traces at depth -2830 and -6838 μm show bigger noise level, which were mainly resulted from AC power-line contamination, as demonstrated in the power spectral density plot of these five recordings in Figure 28. The dominant noise comes from the 60 Hz noise and the magnitude for recordings at depth -2830 and -6838 μm is significantly higher than that of the other three recordings.

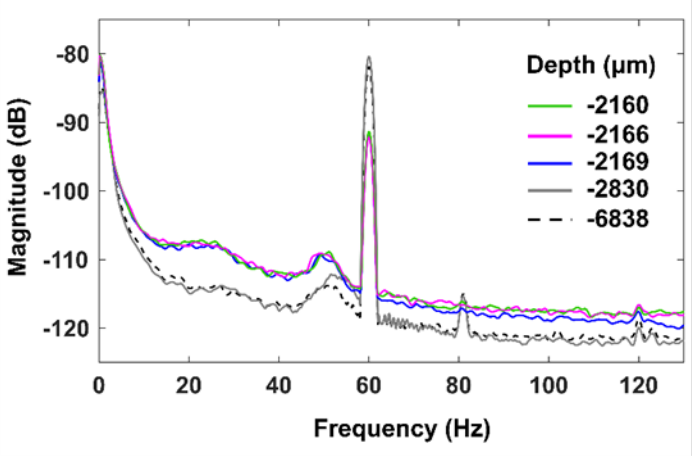

Figure 41. Power spectrum density plot of the neural activity voltage signals at the five different recording depths as indicated: -2160, -2166, -2169, -2830, -6838 μm.

4.3.4 Chronic Neural Recording

The most convincing evidence for verifying the effectiveness of CNT fiber electrodes is to test whether the CNT fiber electrodes can record stably over a long period of time. I performed survival surgery and chronic electrophysiological recording on anesthetized rats and record from spontaneous firing neurons using 15 μm CNT fiber microelectrodes. The results show that the CNT fiber electrodes are effective for up to 4~5 months in stably and continuously detecting sortable single unit neural signals with a high SNR.

Results from a representative chronic neural recording are shown in figure 29. One 15 μm CNT fiber microelectrode was implanted in thalamus and performed neural electrophysiology every one to two weeks for about four months. The data recorded from this microelectrode was sorted to identify single unit spikes and the results showed that it can reliably record single unit spikes over this four-month period. The average spike waveforms of detected and sorted single units were shown in Figure 29a. in different colors.

The different colors represented different sorted units clustered by the results of principal component analysis (PCA) recorded across day 1 to day 117. The PCA results of the sorted spikes of units from each recording session at different days form a cluster from day 17 to day 117, which is #3 and #4 as indicated by red in the figure. All the waveforms of each recording sessions through the 4 months were used for PCA study. To represent the PCA results for each of the unit using one parameter, D=sqrt ($PC1^2$ + $PC2^2$) was calculated for all the waveforms of each recording session. The distance between two different PCA results was defined as the difference of the average D, measured in the unit of standard deviation in the preceding recording session's D distribution. The average position shift of the units' centers between every consecutive electrophysiological recording session was calculated to be ~ 2.90 standard deviation of the cluster. Note that the distance for the single units in red color from day 65 to day 88 (#7- #12) was 1.05 standard deviation. The small distance between PCA results suggests that these single units in red color are likely recorded from the same neuron, which means that the electrode remained in proximity to the same neuron for the chronic recording days, especially from day 65 to day 88. To further support this claim, the peak-to-valley amplitude, noise level, SNR and peak-to-trough time were calculated for the units in red color with the results shown in Figure 29c. As can be seen, the four statistical parameters were basically stable across day 17 to day 117. The amplitude was 49±7 μV, the SNR was 4.2±0.7, the noise level was about 6.0±0.9 μV and the peak-to-trough time was 0.46±0.06 ms. The stable spike amplitude through the four-month recording period was clearly distinct from many reported neural electrodes where the amplitudes decreased as the increase of the days post implantation.[107, 108] The stable single unit recording results, in addition to the results of histological studies

showed before, indicated that a more stable electrode-tissue interface was formed for CNT fiber microelectrodes.

However, the confirmation of whether the signals were from the same neurons was not easy and it needs more convincing evidences, which warrants further research and study in the future. Here we observed two notable phenomena. Firstly, some units reappeared and disappeared in different recording sessions. For example, the blue unit on day1, the cyan unit on day 37, the magenta unit on day 65 and the black unit on day 88 just appeared once, and the red unit appeared in day 35 and reappeared on day 45 but disappeared on day 37. There are multiple possible reasons for these phenomena. For example, (1) the electrode had slightly moved in day 37 and detected another neuron or the same neuron as in day 35 and day 45 but with a different shape owing to the disturbance of the relative positions between the recorded neuron and the implanted electrode. (2) The neuron detected in day 35 silenced in day 37 while another neuron started firing in day 37, which was the cyan unit and the red neuron fired again in day 45. The other notable phenomenon was that the firing rate of the red unit across day 17 to day 117 varied a lot as shown in Figure 32. Even if we just considered the red unit, the firing rate still varied from ~0.2 Hz to ~1.5 Hz. As mentioned before, spike firing timing or firing rate is a critical parameter for the use of action potential data recorded from electrodes. The waveforms are usually only used to assist sorting spikes into different single units, or to say different neurons. The key information from action potential data is the firing timing. Inconsistent firing rate might result from the different anesthesia depth of animals across multiple different recording sessions on different days.[109-113] Future studies should do better

control on the depth of anesthesia and consider the firing rate as an important parameter in evaluating the stability of neuron recording.

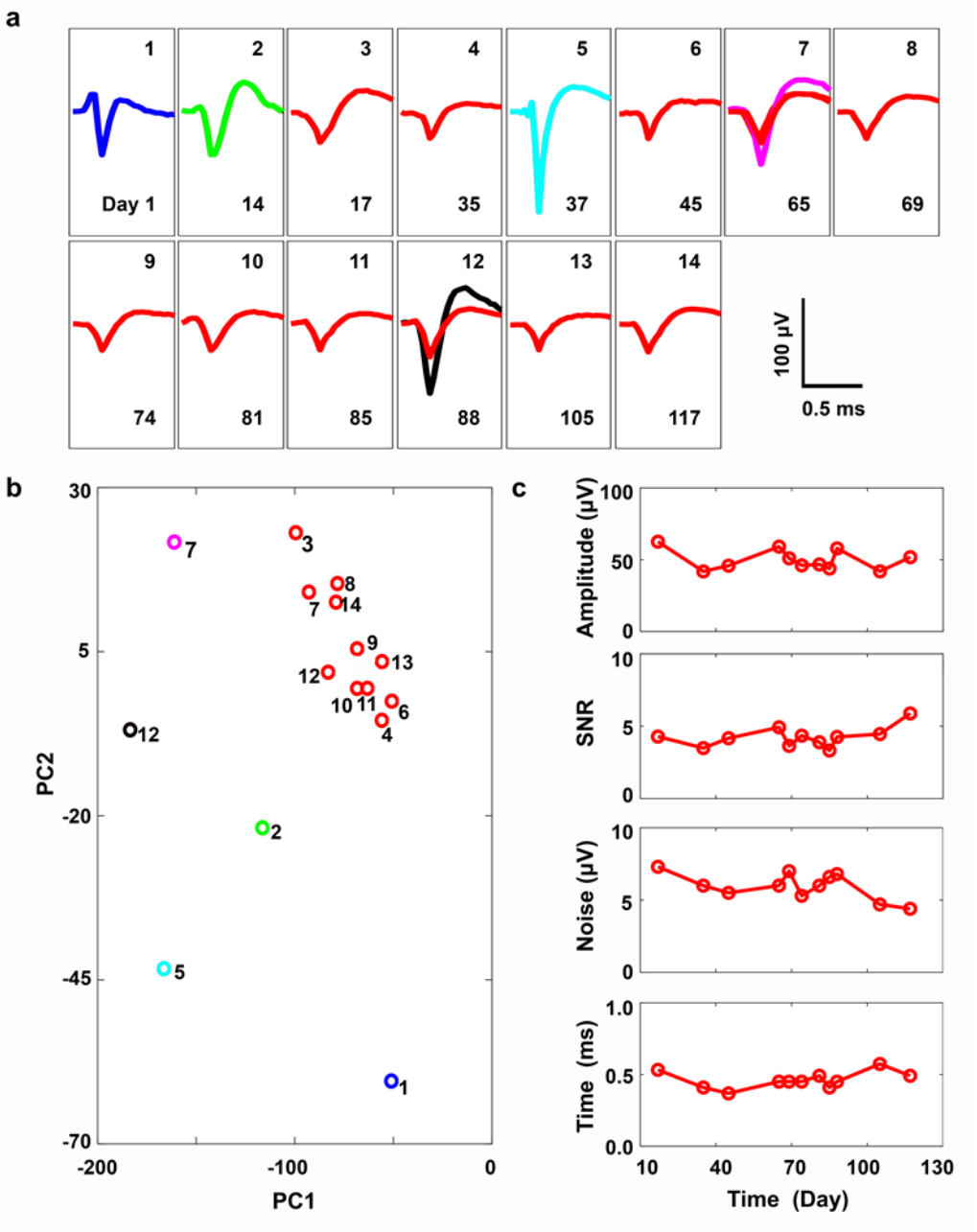

Figure 42. A representative chronic electrophysiology recording from a 15 µm CNT fiber microelectrode. (a) average spike waveforms of individual neurons from day 1 to 117 after surgery detected by a 15 µm CNT fiber microelectrode. The number in upper right corner represents the recording sessions and the number in the lower right corner represents the

amount of days post-implantation. The different colors represent different unit groups decided by PCA results as shown in b. (b) average value of the first and the second principal components of all waveforms from every units shown in a. The numbers beside each colored dot are numbered in the same way as those in the upper corner in a. The different unit groups indicated by colors were manually selected according to the PC1 and PC2 results. (c) Average peak-to-valley amplitude, SNR, noise level and peak-to-valley time of the single unit in red as a function of recording time post-surgery.

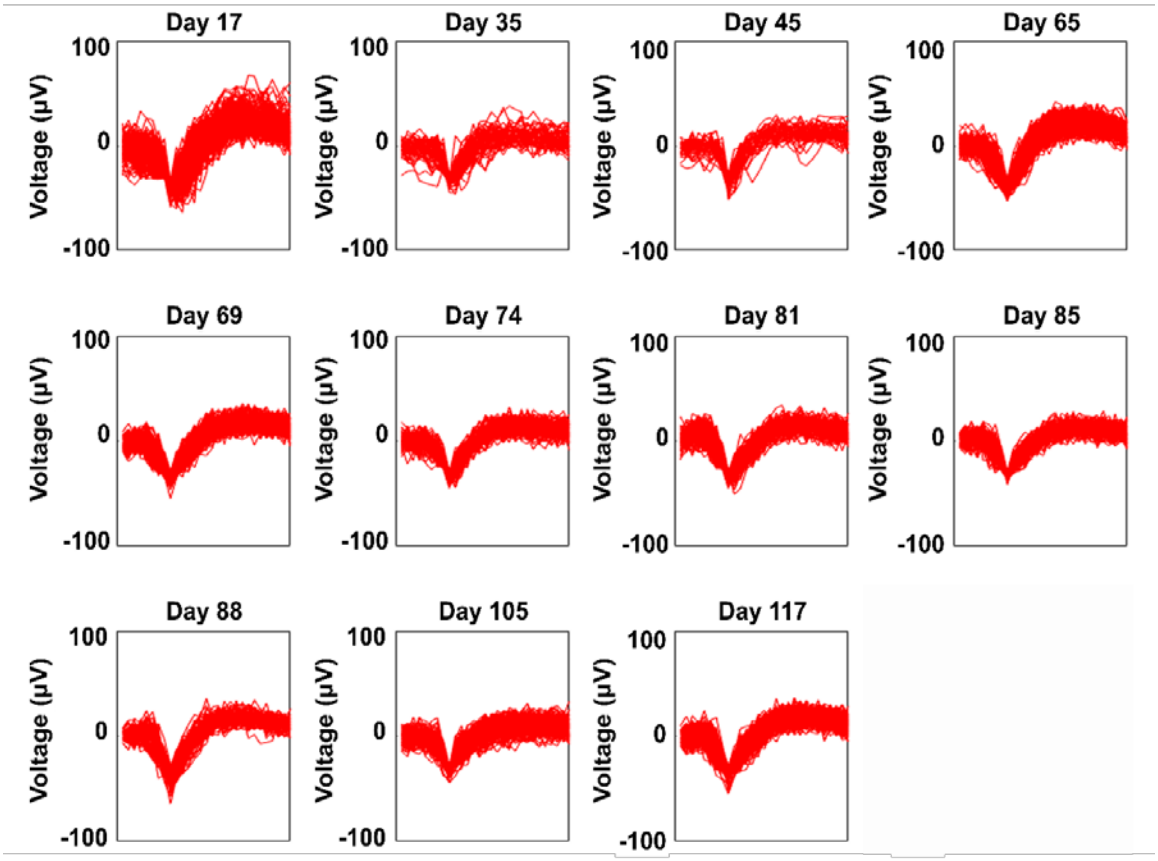

Figure 43. Superimposed waveforms of spikes from clustered red single units as shown in figure 29*c*. detected by 15 μm CNT fiber electrodes across day 17 to day 177 post-surgery. All the waveforms shown here were used in the calculation of PCA results. The horizontal axis represents time, which is 1.2 ms for all of the waveforms.

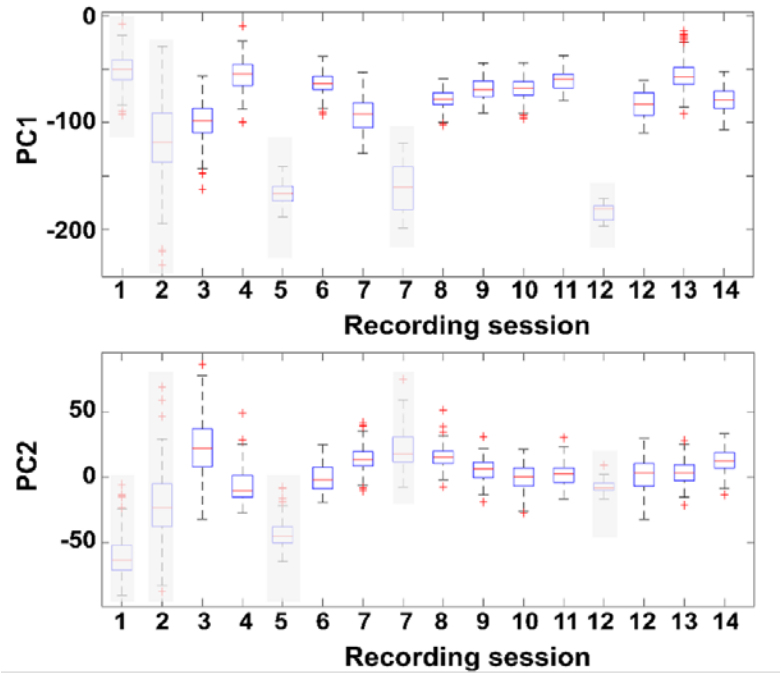

Figure 44. Boxplots of the first and second principal components separately for further comparing the single units from different recording days. The boxes without shadows are those clustered units in red as shown in other figures. Note that two boxes exist for recording session #7 and #12 as there are two single units detected on these two days. The horizontal axis represents the recording session and the vertical axis represents the value of either PC1 or PC2. For the boxes, the upper and lower borders indicate the positions of the first and the third quartiles. The red lines inside the boxes show the position of the median value. The black lines above and below the boxes represent the maximum and minimum non-outliers respectively. The red '+' marker indicates outliers in the samples.

Another three chronic electrophysiological recording examples of 15 μm CNT fiber microelectrodes are shown in Figure 33 with the longest recording day reaches day 188, which is about six months. The amplitude in rat 4 on day 145 reached about 400 μV, further confirmed the long-term effectiveness of CNT fiber neural electrodes.

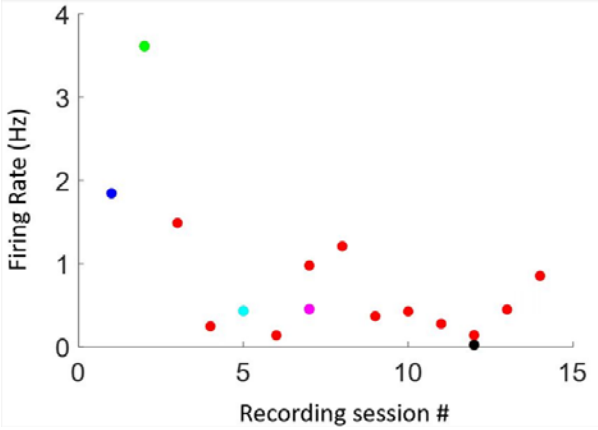

Figure 45. Firing rate of different recording sessions shown in Figure 21 a. The same color code was applied to indicate single units in different groups.

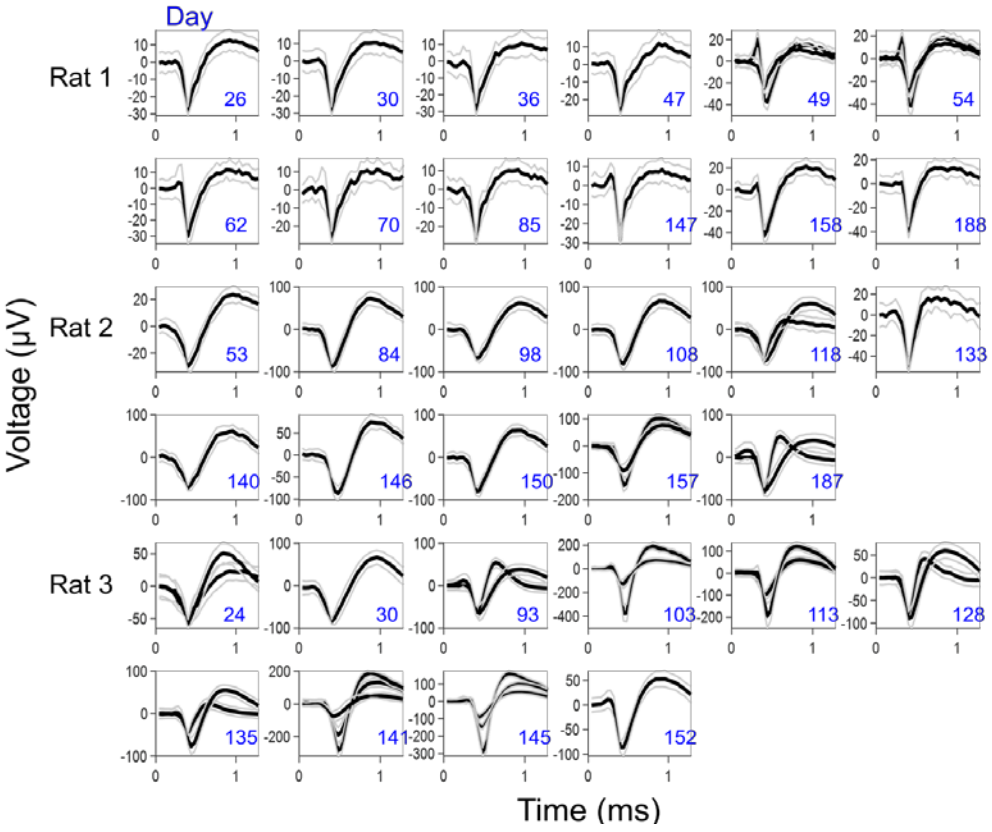

Figure 46. Three other electrophysiological recordings using 15 μm CNT fiber microelectrodes. The horizontal axis represents the total time length of the waveforms. The vertical axis represents the voltage of spikes. All recordings were on anesthetized rats under isoflurane and from spontaneous firing of neurons. For each sorted unit in each recording

session, the average waveforms are shown with black line and the standard deviation of the waveforms were shown with grey line. In some recording sessions, multiple single units were detected and showed. The blue numbers in the lower right corner represent the amount of days post-implantation.

4.4 Summary

Four representative electrophysiological recordings were demonstrated in this chapter, using electrodes made from 15 μm CNT fibers. (1) The whisker responsive signals recorded in VPm demonstrated the CNT fiber electrodes' ability for precisely targeting planned brain areas in the brain, as the whisker responsive region in VPm is small and relatively deep in the brain, posing a challenge in electrode targeting. (2) The action potential amplitudes from firing of neurons in S1 are relatively small compared with those recorded from VPm. Therefore, the recordings in S1 served as a good example of the CNT fiber electrodes' signal detection sensitivity. (3) The multi-depth recording results demonstrated the CNT fiber electrodes' ability of fine-tuning the implantation position of the microelectrodes after implantation, which offers advantage for both recording and stimulating neural electrodes. (4) The chronic recording examples from four representative rats showed the longevity of the CNT fiber electrodes for recording single unit signals. One of the chronic recording results were studied in detail, with principal component analysis performed and four different features of the sorted single units calculated. The results showed a possibility that some of the recorded single units for that rat recorded for 4 months were from the same neuron.

The above recording results validated multiple outstanding advantages of the CNT fiber electrode for neural recording.

CHAPTER 5. DOWNSIZING ELECTRODES WITH A 5 MICRON CNT FIBER CORE

5.1 Introduction

The smallest electrodes we fabricated were with a 5 μm diameter CNT fiber core. The smaller recording site gives the electrode a higher spatial resolution, which facilitate detecting and sorting neurons from clusters of densely distributed groups and small neurons which fire spikes with low amplitude. Another advantage is the small bending stiffness resulted from the small diameter of CNT fibers. Bending stiffness is proportional to the fourth power of the diameter. The 5 μm CNT fiber has about 1% bending stiffness of the 15 μm ones. Materials with small bending stiffness have reduced inflammatory response when implanted in brain tissue, thereby increasing the longevity of electrodes and causing less damage to neurons nearby.

However, the problems brought by smaller size of the CNT fibers are the poorer electrochemical properties and more difficulty in electrodes implantation. Therefore, the methods subsection introduces the techniques for the treatment of 5 μm CNT fiber electrodes used for neural recording. The electrochemical properties and three representative in vivo neural recording results are shown in the results.

5.2 Methods

5.2.1 Electroplating on CNT Fiber Electrodes

PSS or poly(3,4-ethylenedioxythiophene) polystyrene sulfonate (PEDOT: PSS) was electroplated to the 5 μm CNT fiber electrodes to lower the impedance of the 5 μm CNT fiber electrodes.

Three chemicals, 10 mL ultrapure water, 200 mg PSS, 10.7 μL EDOT were needed for making 10 mL PEDOT: PSS solution. Fresh PEDOT solution, usually made within one week, should be used for electroplating. The steps for making the PEDOT: PSS solutions are: (1) Decant some ultrapure water into a beaker, use a pipettor to draw excessive water out to make exactly 10 mL water. (2) Add the 200 mg PSS into the water. (3) Note that the EDOT is super toxic. Add 10.7 μL EDOT to the mixed water and PSS in a fume hood. (4) Put a stir bar inside the mixed solution and leave it on a stir plate for mixing. This procedure takes more than three hours, so usually just leave the beaker on the stir plate overnight. (5) After the solution is mixed uniformly, store the PEDOT: PSS solution in the refrigerator at 4 ℃ before use.

For electroplating, 8 nA current was applied to the 5 μm CNT fiber electrode for 6 s in the PEDOT: PSS solution. The impedance was test at 1004 Hz by NanoZ instrument. If there is not significant differences between the pre-PEDOT coating and post-PEDOT coating of the CNT fiber electrodes, one possible reason is that the electric circuit is broken in somewhere, and another possible reason is that the PEDOT: PSS solution should be replaced.

5.2.2 Impedance Stability Test

For testing impedance stability, the recording sites of 5 μm CNT fiber electrodes were immsered in 1×PBS solution for 50 days. The impedance before and after PBS

immersion were tested at 1004 Hz. Note that measurements should be taken to avoid evaporation of water resulted condensation of the PBS solution.

5.2.3 Implantation Precautions

The animal surgery and electrodes implantation of 5 μm CNT fiber electrodes are about the same as that of the CNT fiber electrodes with larger diameters. But the implantation of 5 μm CNT fiber is more difficult, considering the much smaller diameter resulting in much softer of the electrodes. Ensure to wait enough time for the CNT fiber electrodes/ Tungsten shuttle assembly to be dried before implantation. The success rate of implanting 15 μm CNT fiber electrodes is higher than that of implanting 5 μm CNT fiber electrode, and the implantation process of 5 μm CNT fiber electrode is more difficult. Because 5 μm CNT fiber electrode is more easily blocked out by the brain tissue when entering, and more easily pulled out with the tungsten wire extraction. Therefore, for the implantation of 5 μm CNT fiber electrodes, the concentration of PEO and the time of airing should be well controlled. In addition, the winding of CNT electrodes and tungsten wires should be avoided as far as possible in the process of assembling 5um electrodes, and they should be placed side by side as possible. Attention to these small techniques can greatly improve the success rate of electrode implantation.

Note that 5 μm CNT fiber electrodes are electroplated with PEDOT: PSS, therefore, unlike 15 μm CNT fiber electrode, the 5 μm ones cannot be only cut by blade to expose another recording site, but also need be electroplated for exposed new recording site. Therefore, multiple electrodes should be prepared for the animal experiment, in case

the electrode does not work and another electroplating of the electrode increases unnecessary waiting time for the animals under surgery.

5.3 Results and Discussion

5.3.1 Impedance Characterization Results

The impedance of 5 μm CNT fiber electrodes post PEDOT: PSS coating were tested at 1004 Hz. The impedance of original CNT fiber electrodes post blade cut varies a lot. The examples in Figure 47 show two extreme original impedances: ~50 MΩ (a) and ~ 1.1 MΩ (b). The final impedance post electroplating is about 0.4~0.6 MΩ, appropriate for neural recording.

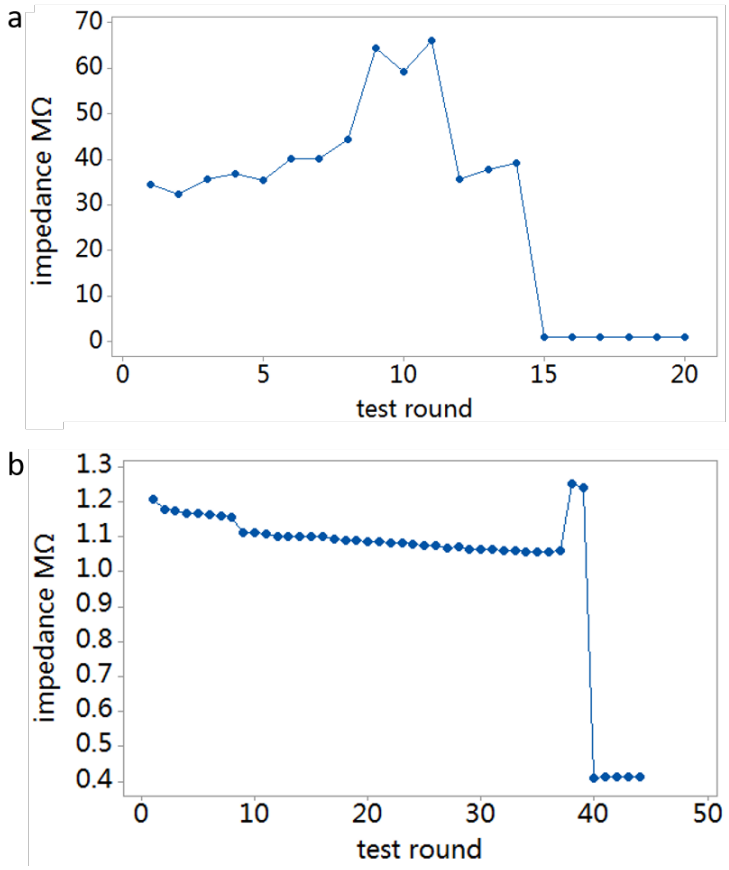

Figure 47. Two examples of impedance test of 5 μm CNT fiber electrodes at 1004 Hz.

Figure 48 shows the stability results of the impedance by PEDOT electroplating of 5 μm CNT fiber electrodes. 7 samples are shown in the figure. The blue, orange and grey line represent initial impedance before PEDOT coating, after PEDOT coating and followed by 50 days immersion in PBS respectively. The PEDOT electroplating technique greatly decreases the impedance of the electrodes as shown from the blue dots and the corresponding orange dots. The orange dots and the corresponding grey dots show that the impedance of the electrodes after 50 days immersion in PBS is still acceptable for neural recording, though there is a slight impedance increase for each of the 7 electrodes.

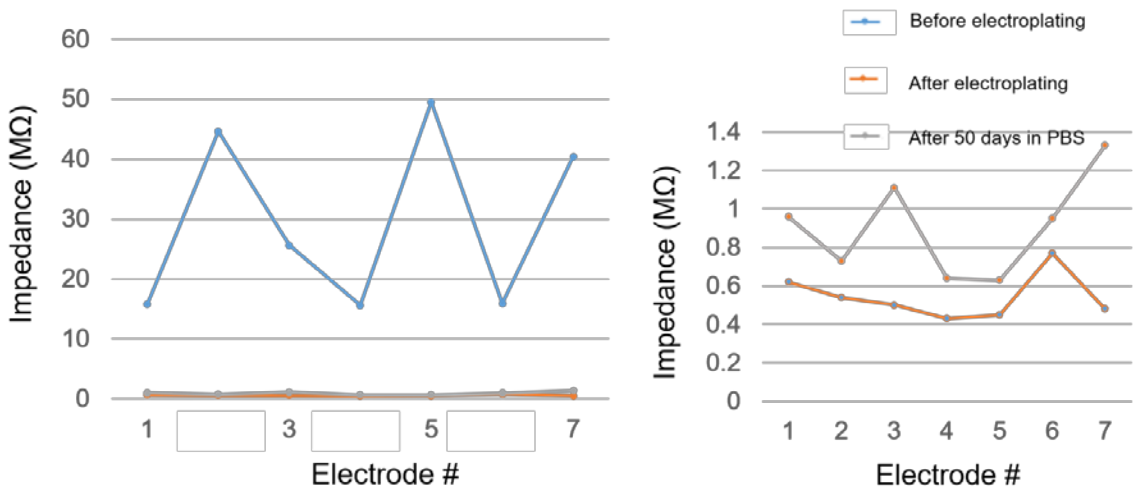

Figure 48. Impedance changes of 5 μm CNT fiber electrodes.

5.3.2 Acute Neural Recording

5 μm CNT fiber electrodes was used for detection of whisker responsive signals in S1. A representative result was shown in Figure 49. In Figure 49a, The blue trace shows the two periods of deflection stimulation applied on the whiskers. The black traces show neural signals recorded by a 5 μm CNT fiber electrode placing in the same position in the brain while the Galvanometer stimulating on whiskers D2 and C3 respectively. Figure 49b shows the responsive brain areas in S1 for whisker D2 and C3 and the average waveform for the sorted single unit for whisker D2 responsive signal.

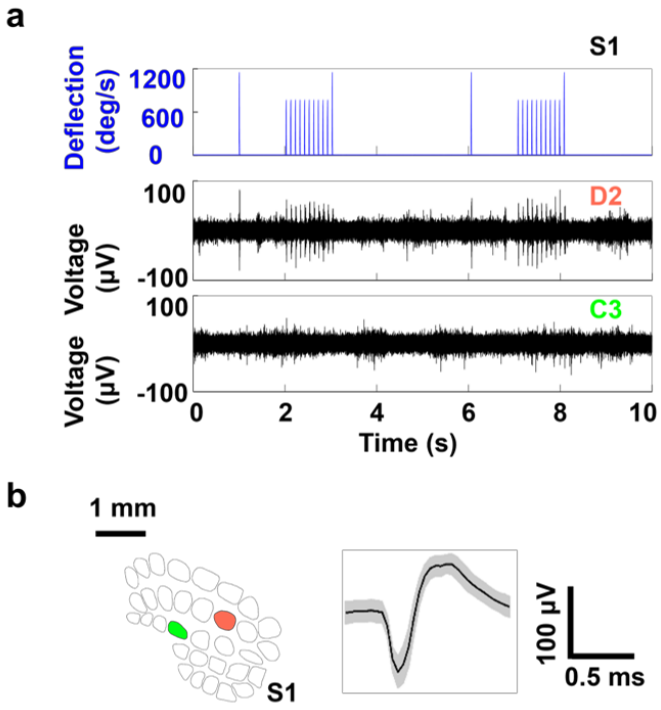

Figure 49. Whisker responsive neural recording in S1 using 5 μm CNT fiber electrodes.

The amplitude of the spikes in Figure 49 is relatively low compared with those detected from 15 μm CNT fiber electrodes. However, in another experiment, the 5 μm diameter CNT fiber electrode recorded single-unit signals of 226.86±13.34 μV amplitude from CA2 of rat brain. All the amplitude values correspond to the valley-to-peak amplitude here. In summary, no systematic amplitude difference was observed between 5 μm and 15 μm diameter CNT fiber electrodes. Noise level comparison between electrodes made from 5 and 15 μm CNT fibers was shown in Figure 51. The noise level was calculated as the standard deviation of the voltage trace after subtracting the individual spike waveform included in that trace, same as described in Chapter 4. No significant difference was found for the 5 μm and 15 μm CNT fiber electrodes, $p > 0.05$, one-way ANOVA. n=15.

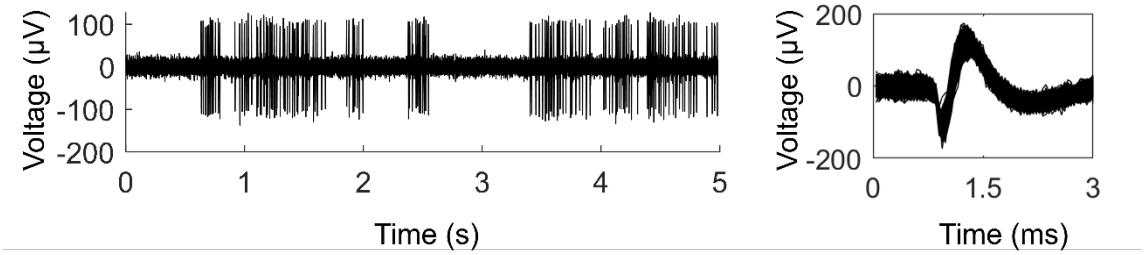

Figure 50. An example of neural recording with an electrode made with 5 μm diameter CNT fiber from CA2 in a rat brain.

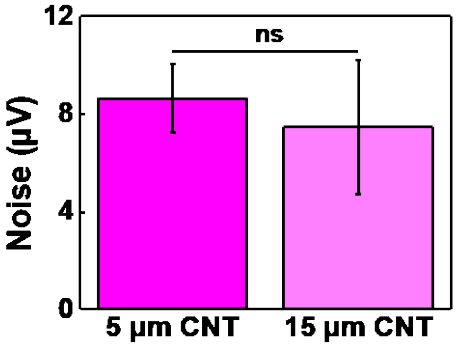

Figure 51. Noise comparison between different diameter CNT fiber electrodes.

5.3.3 Continuous Neural Recording for Three Hours

Small bending stiffness can reduce the inflammatory reaction that the electrode may cause, thereby increasing the effective duration of the electrode and the neurons around the electrode. The results in Chapter 4 show that the 15μm CNT fiber electrodes have a good performance in long-term individual neural recording. The 5 μm CNT fiber electrode has not been subjected to excessive chronic electrophysiological recording experiments yet. Here in Figure 34 shows an example of a three hours' continuous recording using a 5 μm CNT fiber electrode in CA3 in rat. The results demonstrate that the 5 μm CNT fiber

electrode is capable of recording stably and reliably for at least three straight hours. Further chronic neural recordings will be performed and evaluated in the future.

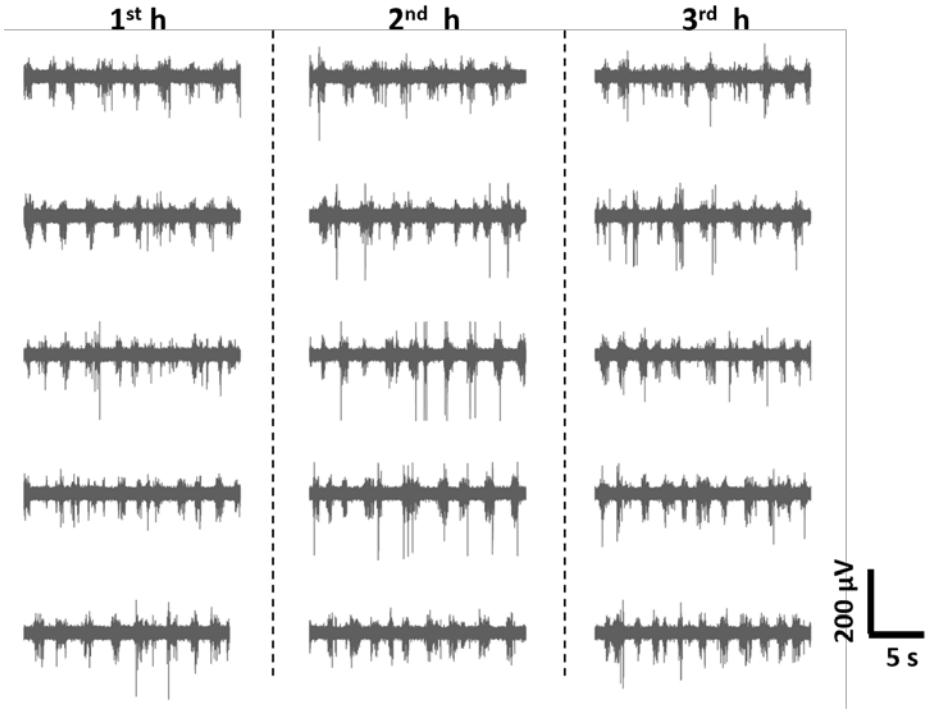

Figure. Continuous electrophysiological recording for 3 hours in CA3. The isoflurane anesthetized rat was continuously recorded for 3 hours in a row. Five 20 s-recording traces were shown for each hour and the traces were picked at intervals of about 10 minutes.

5.4 Summary

Ultrasmall electrodes made from 5 μm CNT fiber core were demonstrated in this chapter. The fabricating and implantation procedures different from those mentioned in Chapter 4 were presented, including PEDOT: PSS electroplating for improving impedance properties of 5 μm CNT fiber electrodes, the impedance stability test, and precautions to take for 5 μm CNT fiber electrodes implantation. The PEDOT: PSS coated 5 μm CNT

fiber electrodes exhibited stable impedance, sufficiently low for neural recording, through 50 days immersion in PBS solution.

The recording results confirmed the single unit recording capability of the ultrasmall CNT fiber electrodes. Plus, the ultrasmall sized electrodes allow for high spatial recording resolution, low tissue damage and mild inflammatory responses, and more electrodes being integrated in a limited space.

CHAPTER 6. CONCLUSIONS AND FUTURE DIRECTIONS

6.1 Conclusion

In the thesis, neural electrodes from 5-20 μm CNT fibers were fabricated and characterized on mechanical properties, electrochemical properties, neural tissue biocompatibility and MRI compatibility. Acute neural recordings performed in the whisker pathway on rats' brain using CNT fiber electrodes achieved high quality whisker responsive single-unit neural signals. Multi-depth neural recording demonstrated that CNT fiber microelectrodes were strong enough to be repositioned along the insertion path post implantation into the brain tissue and adaptive electrode-neural interface was formed. Chronic study on rats with CNT fiber electrodes demonstrated the longevity and stability of the CNT fiber electrodes for neural recording for as long as six months. Ultrasmall electrodes made with 5 μm CNT fiber cores also demonstrated superior single unit neural recording capability. The results presented in the thesis substantiated a huge potential of CNT fiber electrodes for use in neuroscience research where combining long-term electrophysiology recording with other neural technologies, such as MRI and DBS. Advantages and disadvantages of the CNT fiber electrodes are briefly listed below.

6.1.1 Advantages

(1) The developed CNT fiber electrodes enable simultaneous neural recording, DBS and MRI scan, as approved by the remarkable neural recording results, the outstanding electrochemical properties and the MRI compatibility.

(2) The single unit neural signals can be recorded in real time during the implantation of CNT fiber electrodes.

(3) The CNT fiber electrodes can record at multi-depth by moving the electrode during the implantation process for more precise positioning.

(4) The ultrasmall electrodes made with 5 μm CNT fiber core provide high spatial resolution, low tissue damage and potentially better longevity performances.

(5) The CNT fiber electrodes can record reliable single units for four to six months.

(6) The small light-induced electrical artifacts and small size of the electrodes make the CNT fiber electrodes good candidates for use in combining with optogenetics technique.

(7) The fabrication of the CNT fiber electrodes, without complicated processes, is relatively easy and simple compared with other electrophysiological neural probes.

(8) The CNT fiber electrodes can be reused by exposing a new recording site by blade cutting, saving researchers' cost on buying electrodes.

(9) The flexible CNT fiber electrodes is not easy to get damaged during use, compared to tungsten electrodes and carbon electrodes.

6.1.2 Disadvantages

(1) The shuttle assisting implantation procedure causes tissue damage on the insertion path. Although the damage is relatively small compared with some state-of-the-art electrodes like the mesh electrodes, which uses an injection needle to inject the electrodes inside the

brain.[30] But the damage is bigger than those caused by carbon fiber electrodes and other stiff electrodes.[27] There is an urgent need for better implantation strategies.

(2) Multiple-channel electrodes are desired. At present, most of the experiments utilized single-channel CNT fiber electrodes. The development of multi-channel CNT fiber electrodes would be very useful for electrophysiological neural signal recording in neuroscience study. However, the difficulty in developing multi-channel electrodes also mainly lies in the development of a more effective and less invasive implantation strategy.

6.2 Future Scientific Directions

Several future scientific directions are presented here regarding the neural recording application, multi-channel probe design, improvements for the current electrode design and multimodal applications.

6.2.1 Neural Recording Application in MHb

The MHb brain area in mammals is involved in behavioral processes related to aversive, appetitive stimuli, such as the stress, pain and drug like nicotine. Reliable and stable recording in MHb area can greatly improve our understanding of this brain area.[74-76] However, the near ventricle position, the small neuron size and the densely packed way of neurons in MHb area make it difficult to achieve good electrophysiological recording results from MHb.[114]

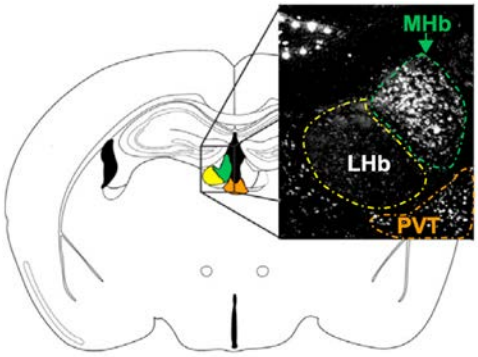

Figure 52. MHb in the mouse brain. The green area indicates the MHb, the yellow area indicates LHb and the orange indicated PVT. The black hollows represent ventricles in the brain. This figure was adapted from Edgar Soria-Gomez published paper in *Neuron*.[115]

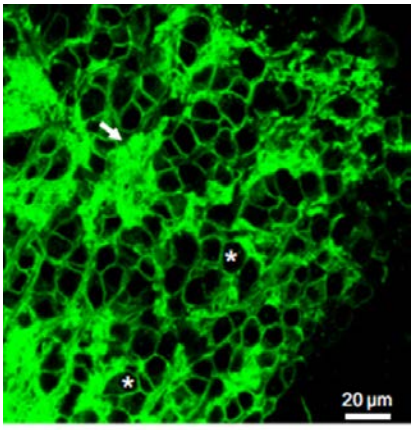

Figure 53. The densely packed neurons in MHb. The diameter of the neurons is ~12.5 µm. This figure was adapted from Jing Ren et al. published paper in *Neuron*.[114]

The critical issue about recording in MHb is to find a way of confirming the electrophysiology recording site. Optogenetics and histology techniques should be utilized to confirm the electrophysiology recording positions. The softness is the main feature that favors and makes it possible for CNT fiber electrodes to record from MHb area. The CNT fiber electrodes should be implanted with tungsten shuttle or with polymer coating method to stiffen the electrodes during insertion. 15 µm CNT fiber electrodes had been applied to perform electrophysiological recording in MHb. No reliable preliminary results have been

achieved so far. The strategy is to achieve successful acute experiments first on anesthetized mice, then on awake animals, and then to test the CNT fiber electrodes' performance for chronic neural recording in MHb area.

6.2.2 Multi-Channel Probe Design

As stated in the disadvantages of the thesis study, multi-channel electrodes are greatly desired for neuroscience study. Here I present two potential methods for multi-channel CNT fiber electrodes design.

For Design I in Figure 54, the recording sites are at the tips of the electrodes, same as the design in the thesis study. Four rows of four CNT fiber electrodes are aligned tightly to make a 16-channel electrode array. if 5 μm CNT fiber electrodes (with a total diameter of 10 μm) are used in this design, the size of the 16 electrodes array is about 40 μm ×40 μm. The advantage of this design is to pack many electrodes as a bundle within a limited space.

For Design II, instead of using the tip of the CNT fibers as recording sites, the recording sites are exposed by laser cutter at the sides of the CNT fibers. The procedure is to adjust the power and velocity parameters of the laser and design the laser track for burning off the parylene-C insulation layer, such as along the red dashed line, to expose the recording sites at different length of the electrodes, as indicated by the black dots. Regarding the feasibility of Design II, preliminary studies have been done on the laser cutting method. The results showed that by selecting appropriate parameters of laser cutting, it is doable to expose a proper sized window of the electrodes as recording sites. The design for adapting the position of the recording sites from the tips to at the sides,

decreases the contamination of the recording sites during implantation of the electrodes, as the tips are the parts that encounter the most friction during insertion, which causes great damage to the recording sites. The way of exposing the recording sites at the side of the electrodes will cause less damage of the recording sites of the electrodes during insertion into the brain, thus improving the recording abilities of the electrodes.

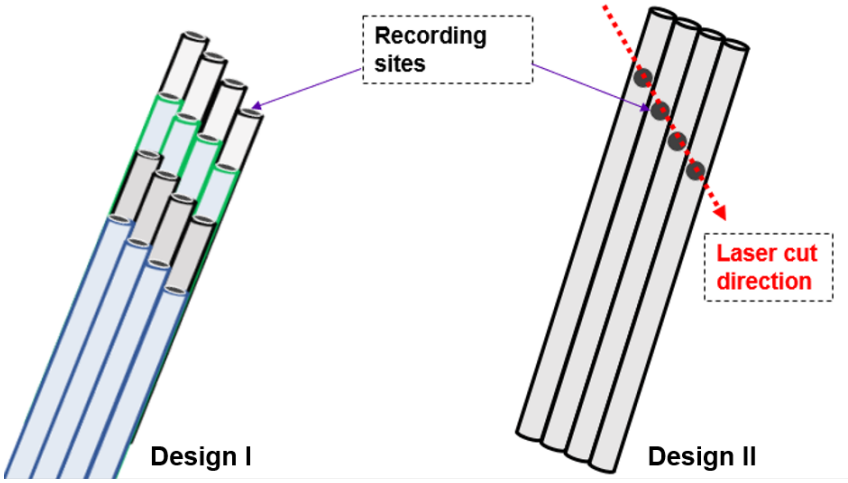

Figure 54. Two proposed design of multi-channel electrode arrays.

6.2.3 Improvements on the Current Electrode Design

(1) For the 15 μm to 20 μm CNT fiber electrodes, PEDOT: PSS is not electroplated, since the impedance already satisfies the requirements for neural recording and stimulation. However, by electroplating PEDOT: PSS on the recording sites of 15 μm to 20 μm CNT fiber electrodes, may obtain better electrical properties and thereby achieving better recording and stimulating performances.

(2) Consider adding anti-inflammatory drugs in the design of the CNT fiber electrodes. As the drugs may reduce the inflammatory responses and thus facilitate the chronic use of electrodes.

(3) Consider improving the implantation methods of the electrodes. Design I in Figure 55 replaces the 50 μm tungsten wire shuttle to a 7 μm carbon fiber shuttle, reducing the tissue damage during implantation. For Design II, the stiffness is controlled by voltage. When the voltage is off, the CNT fiber electrodes are flexible as they are, while the electrodes turn stiff when voltage is on. For Design III, the stiffness of the CNT fiber electrodes for insertion is gained by coating a very thin layer chemical. Though coating methods have been used widely, but usually the coating layer is too thick, compared with the size of CNT fiber electrodes themselves. With the development of advanced materials, hopefully, a thin layer (less than 10 μm) of coating materials will make the CNT fiber electrodes stiff enough for inserting into the tissue.

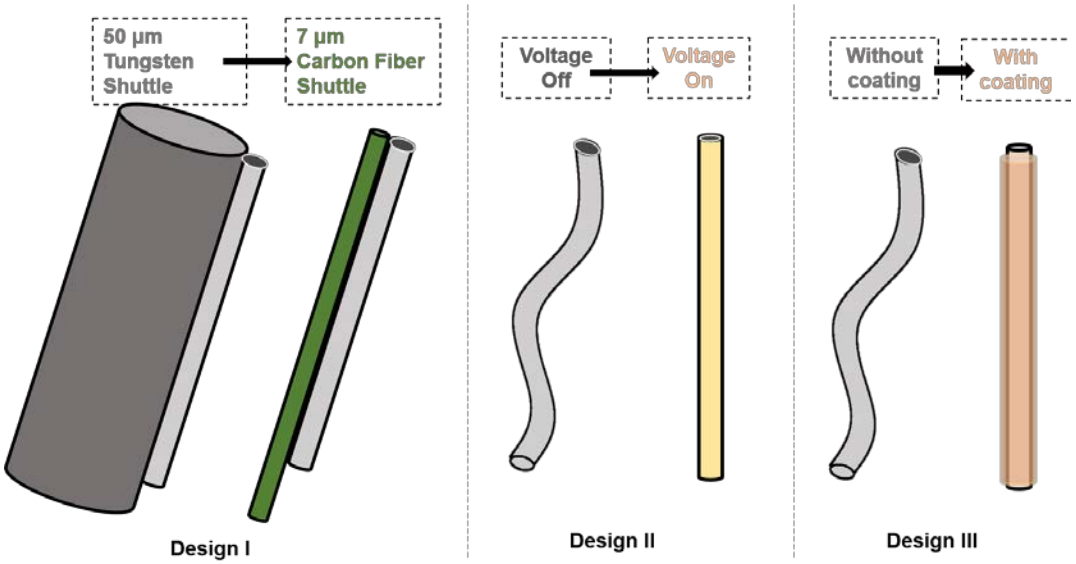

Figure 55. Three proposed implantation designs.

6.2.4 Multimodal Applications

The CNT fiber electrodes produce much less artifacts in MRI and much less electrical artifacts induced by light imaging than traditional metal electrodes. Future studies may use CNT fiber electrodes to combine multiple techniques together for neuroscience study.

6.3 Summary

In this chapter, advantages and disadvantages of CNT fiber electrodes are summarized and several future scientific directions are proposed.

Flexible CNT fibers have excellent mechanical, electrochemical properties, biocompatibility, and MRI compatibility as demonstrated in the thesis results. Acute and chronic electrophysiological recordings from CNT fiber electrodes demonstrated the long-term effectiveness of the electrodes for neural recording. Multiple excellent advantages of CNT fiber electrodes favour their use for combining with neural recording, MRI study, DBS and optogenetics. The results presented in the thesis substantiated a huge potential of CNT fiber electrodes for neuroscience research. They will probably play an important role in the future in neuroscience research and even for clinical use.

REFERENCES

1. von Bartheld, C.S., J. Bahney, and S. Herculano‐Houzel, *The search for true numbers of neurons and glial cells in the human brain: A review of 150 years of cell counting.* Journal of Comparative Neurology, 2016. **524**(18): p. 3865-3895.

2. Chung, J.E., et al., *High-density, long-lasting, and multi-region electrophysiological recordings using polymer electrode arrays.* Neuron, 2019. **101**(1): p. 21-31. e5.

3. Kording, K.P., *Of toasters and molecular ticker tapes.* PLoS Computational Biology, 2011. **7**(12): p. e1002291.

4. Zamft, B.M., et al., *Measuring cation dependent DNA polymerase fidelity landscapes by deep sequencing.* PloS one, 2012. **7**(8): p. e43876.

5. Glaser, J.I., et al., *Statistical analysis of molecular signal recording.* PLoS computational biology, 2013. **9**(7): p. e1003145.

6. Marblestone, A.H., et al., *Physical principles for scalable neural recording.* Frontiers in Computational Neuroscience, 2013. **7**(15): p. 137-137.

7. Ahrens, M.B., et al., *Whole-brain functional imaging at cellular resolution using light-sheet microscopy.* Nature methods, 2013. **10**(5): p. 413.

8. Ziv, Y., et al., *Long-term dynamics of CA1 hippocampal place codes.* Nature neuroscience, 2013. **16**(3): p. 264.

9. Farzadfard, F. and T.K. Lu, *Emerging applications for DNA writers and molecular recorders.* Science, 2018. **361**(6405): p. 870-875.

10. Henze, D.A., et al., *Intracellular features predicted by extracellular recordings in the hippocampus in vivo.* Journal of neurophysiology, 2000. **84**(1): p. 390-400.

11. Somogyvári, Z., et al., *Localization of single-cell current sources based on extracellular potential patterns: the spike CSD method.* European Journal of Neuroscience, 2012. **36**(10): p. 3299-313.

12. Shafi, M., et al., *Variability in neuronal activity in primate cortex during working memory tasks.* Neuroscience, 2007. **146**(3): p. 1082-1108.

13. Hromadka, T., M.R. Deweese, and A.M. Zador, *Sparse Representation of Sounds in the Unanesthetized Auditory Cortex.* PLOS Biology, 2008. **6**(1).

14. O'Connor, D.H., et al., *Neural activity in barrel cortex underlying vibrissa-based object localization in mice.* Neuron, 2010. **67**(6): p. 1048-1061.

15. Roxin, A., et al., *On the Distribution of Firing Rates in Networks of Cortical Neurons.* Journal of Neuroscience the Official Journal of the Society for Neuroscience, 2011. **31**(45): p. 16217-26.

16. Shoham, S., D.H. O'Connor, and R. Segev, *How silent is the brain: is there a "dark matter" problem in neuroscience?* Journal of Comparative Physiology A, 2006. **192**(8): p. 777-784.

17. Barth, A.L. and J.F.A. Poulet, *Experimental evidence for sparse firing in the neocortex.* Trends in Neurosciences, 2012. **35**(6): p. 345-355.

18. Peter, L., *The cost of cortical computation.* Current Biology, 2003. **13**(6): p. 493-497.

19. Chadderton, P., T.W. Margrie, and M. Häusser, *Integration of quanta in cerebellar granule cells during sensory processing.* Nature, 2004. **428**(6985): p. 856-860.

20. Sarpeshkar, R., *Ultra Low Power Bioelectronics: Feedback systems: fundamentals, benefits, and root-locus analysis.* 2010.

21. Harris, J.J., R. Jolivet, and D. Attwell, *Synaptic Energy Use and Supply.* Neuron, 2012. **75**(5): p. 762-777.

22. Gittis, A.H., S.H. Moghadam, and L.S. Du, *Mechanisms of sustained high firing rates in two classes of vestibular nucleus neurons: differential contributions of resurgent Na, Kv3, and BK currents.* Journal of Neurophysiology, 2010. **104**(3): p. 1625-1634.

23. Fattahi, P., et al., *A review of organic and inorganic biomaterials for neural interfaces.* Advanced materials, 2014. **26**(12): p. 1846-1885.

24. Fekete, Z., *Recent advances in silicon-based neural microelectrodes and microsystems: a review.* Sensors & Actuators B Chemical, 2015. **215**: p. 300-315.

25. Shi, J. and Y. Fang, *Flexible and Implantable Microelectrodes for Chronically Stable Neural Interfaces.* Advanced Materials, 2018: p. 1804895.

26. Lu, L., et al., *Soft and MRI Compatible Neural Electrodes from Carbon Nanotube Fibers.* Nano letters, 2019.

27. Kozai, T.D.Y., et al., *Ultrasmall implantable composite microelectrodes with bioactive surfaces for chronic neural interfaces.* Nature materials, 2012. **11**(12): p. 1065.

28. Luan, L., et al., *Ultraflexible nanoelectronic probes form reliable, glial scar–free neural integration.* Science Advances, 2017. **3**(2): p. e1601966.

29. Kim, D.H., et al., *Dissolvable films of silk fibroin for ultrathin conformal bio-integrated electronics.* Nature Materials, 2016. **9**(6): p. 511-7.

30. Hong, G., et al., *Mesh electronics: a new paradigm for tissue-like brain probes.* Current Opinion in Neurobiology, 2017. **50**: p. 33-41.

31. Tybrandt, K., et al., *High-Density Stretchable Electrode Grids for Chronic Neural Recording.* Advanced Materials, 2018. **30**(15): p. e1706520.

32. Viventi, J., et al., *Flexible, foldable, actively multiplexed, high-density electrode array for mapping brain activity in vivo.* Nature Neuroscience, 2012. **14**(12): p. 1599-1605.

33. Hong, G. and C.M. Lieber, *Novel electrode technologies for neural recordings.* Nature Reviews Neuroscience, 2019: p. 1.

34. Merrill, D.R., M. Bikson, and J.G. Jefferys, *Electrical stimulation of excitable tissue: design of efficacious and safe protocols.* Journal of Neuroscience Methods, 2005. **141**(2): p. 171-198.

35. Cogan, S.F., *Neural stimulation and recording electrodes.* Annu. Rev. Biomed. Eng., 2008. **10**: p. 275-309.

36. Lecomte, A., E. Descamps, and C. Bergaud, *A review on mechanical considerations for chronically-implanted neural probes.* Journal of neural engineering, 2018. **15**(3): p. 031001.

37. Muthuswamy, J., R. Saha, and A. Gilletti. *Tissue micromotion induced stress around brain implants*. in *2005 3rd IEEE/EMBS Special Topic Conference on Microtechnology in Medicine and Biology*. 2005. IEEE.

38. Polanco, M., S. Bawab, and H. Yoon, *Computational assessment of neural probe and brain tissue Interface under transient motion.* Biosensors, 2016. **6**(2): p. 27.

39. Lundqvist, M., et al., *Gamma and beta bursts during working memory readout suggest roles in its volitional control.* Nature communications, 2018. **9**(1): p. 394.

40. Parthasarathy, A., E.L. Bartlett, and S.G. Kujawa, *Age-related changes in neural coding of envelope cues: peripheral declines and central compensation.* Neuroscience, 2018.

41. Mellor, J., *Synaptic Plasticity at Hippocampal Synapses: Experimental Background*, in *Hippocampal Microcircuits*. 2018, Springer. p. 201-226.

42. Lacour, S.P., G. Courtine, and J. Guck, *Materials and technologies for soft implantable neuroprostheses.* Nature Reviews Materials, 2016. **1**(10): p. 16063.

43. Huang, S., et al., *Flexible Electronics: Stretchable Electrodes and Their Future.* Advanced Functional Materials, 2019. **29**(6): p. 1805924.

44. Guo, C.F., et al., *Highly stretchable and transparent nanomesh electrodes made by grain boundary lithography.* Nature Communications, 2014. **5**: p. 3121.

45. Woeppel, K., Q. Yang, and X.T. Cui, *Recent Advances in Neural Electrode-Tissue Interfaces.* Current opinion in biomedical engineering, 2017.

46. Zhao, S., et al., *Graphene encapsulated copper microwires as highly MRI compatible neural electrodes.* Nano letters, 2016. **16**(12): p. 7731-7738.

47. Kozai, T.D., et al., *Brain tissue responses to neural implants impact signal sensitivity and intervention strategies.* Acs Chemical Neuroscience, 2015. **6**(1): p. 48-67.

48. Tresco, P.A. and B.D. Winslow, *The challenge of integrating devices into the central nervous system.* Critical Reviews in Biomedical Engineering, 2011. **39**(1): p. 29.

49. Polikov, V.S., P.A. Tresco, and W.M. Reichert, *Response of brain tissue to chronically implanted neural electrodes.* Journal of neuroscience methods, 2005. **148**(1): p. 1-18.

50. Kozai, T.D., et al., *Reduction of neurovascular damage resulting from microelectrode insertion into the cerebral cortex using.* Journal of Neural Engineering, 2010. **7**(4): p. 046011.

51. Saxena, T., et al., *The impact of chronic blood–brain barrier breach on intracortical electrode function.* Biomaterials, 2013. **34**(20): p. 4703-4713.

52. Li, W.Z., et al., *Large-Scale Synthesis of Aligned Carbon Nanotubes.* Science, 1996. **274**(5293): p. 1701-1703.

53. Zhang, M., K.R. Atkinson, and R.H. Baughman, *Multifunctional Carbon Nanotube Yarns by Downsizing an Ancient Technology.* Science, 2004. **306**(5700): p. 1358-1361.

54. Vigolo, B., et al., *Macroscopic fibers and ribbons of oriented carbon nanotubes.* Science, 2000. **290**(5495): p. 1331-1334.

55. Dalton, A.B., et al., *Super-tough carbon-nanotube fibres.* Nature, 2003. **423**(6941): p. 703.

56. Ericson, L.M., et al., *Macroscopic, neat, single-walled carbon nanotube fibers.* Science, 2004. **305**(5689): p. 1447-1450.

57. Vigolo, B., et al., *Improved structure and properties of single-wall carbon nanotube spun fibers.* Applied Physics Letters, 2002. **81**(7): p. 1210-1212.

58. Miaudet, P., et al., *Hot-drawing of single and multiwall carbon nanotube fibers for high toughness and alignment.* Nano letters, 2005. **5**(11): p. 2212-2215.

59. Zhang, X., et al., *Spinning and processing continuous yarns from 4‐inch wafer scale super‐aligned carbon nanotube arrays.* Advanced Materials, 2006. **18**(12): p. 1505-1510.

60. Liu, K., et al., *Carbon nanotube yarns with high tensile strength made by a twisting and shrinking method.* Nanotechnology, 2009. **21**(4): p. 045708.

61. Tran, C.-D., et al., *Improving the tensile strength of carbon nanotube spun yarns using a modified spinning process.* Carbon, 2009. **47**(11): p. 2662-2670.

62. Miao, M., et al., *Poisson's ratio and porosity of carbon nanotube dry-spun yarns.* Carbon, 2010. **48**(10): p. 2802-2811.

63. Li, Y.-L., I.A. Kinloch, and A.H. Windle, *Direct spinning of carbon nanotube fibers from chemical vapor deposition synthesis.* Science, 2004. **304**(5668): p. 276-278.

64. Motta, M., et al., *High performance fibres from 'dog bone'carbon nanotubes.* Advanced Materials, 2007. **19**(21): p. 3721-3726.

65. Koziol, K., et al., *High-performance carbon nanotube fiber.* Science, 2007. **318**(5858): p. 1892-1895.

66. Wang, J., et al., *High-strength carbon nanotube fibre-like ribbon with high ductility and high electrical conductivity.* Nature communications, 2014. **5**: p. 3848.

67. Jiang, C., H. Hao, and L. Li, *Artifact properties of carbon nanotube yarn electrode in magnetic resonance imaging.* Journal of neural engineering, 2013. **10**(2): p. 026013.

68. Guo, Y., et al., *Biocompatibility and magnetic resonance imaging characteristics of carbon nanotube yarn neural electrodes in a rat model.* Biomedical engineering online, 2015. **14**(1): p. 118.

69. Dubin, R.A., et al., *Carbon nanotube fibers are compatible with mammalian cells and neurons.* IEEE transactions on nanobioscience, 2008. **7**(1): p. 11-14.

70. Vitale, F., et al., *Neural stimulation and recording with bidirectional, soft carbon nanotube fiber microelectrodes.* ACS nano, 2015. **9**(4): p. 4465-4474.

71. Chen, Y.-C., et al., *Ultra-high magnetic resonance imaging (MRI): a potential examination for deep brain stimulation devices and the limitation study concerning MRI-related heating injury.* Neurological Sciences, 2017. **38**(3): p. 485-488.

72. Lee, J.Y., et al., *Is MRI a reliable tool to locate the electrode after deep brain stimulation surgery? Comparison study of CT and MRI for the localization of electrodes after DBS.* Acta neurochirurgica, 2010. **152**(12): p. 2029-2036.

73. Gaglianese, A., et al., *Correspondence between fMRI and electrophysiology during visual motion processing in human MT+*. Neuroimage, 2017. **155**: p. 480-489.

74. Lecca, S., F.J. Meye, and M. Mameli, *The lateral habenula in addiction and depression: an anatomical, synaptic and behavioral overview*. European Journal of Neuroscience, 2014. **39**(7): p. 1170-1178.

75. Frahm, S., et al., *Aversion to Nicotine Is Regulated by the Balanced Activity of β4 and α5 Nicotinic Receptor Subunits in the Medial Habenula.* Neuron, 2011. **70**(3): p. 522-535.

76. Stamatakis, A.M., et al., *A unique population of ventral tegmental area neurons inhibits the lateral habenula to promote reward.* Neuron, 2013. **80**(4): p. 1039-1053.

77. Jia, J., et al., *A comparison of the mechanical properties of fibers spun from different carbon nanotubes.* Carbon, 2011. **49**(4): p. 1333-1339.

78. Hassler, C., T. Boretius, and T. Stieglitz, *Polymers for neural implants.* Journal of Polymer Science Part B, 2011. **49**(1): p. 18-33.

79. Xie, C., et al., *Three-dimensional macroporous nanoelectronic networks as minimally invasive brain probes.* Nature materials, 2015. **14**(12): p. 1286.

80. Jaroch, D.B., et al., *Magnetic insertion system for flexible electrode implantation.* Journal of Neuroscience Methods, 2009. **183**(2): p. 213-222.

81. Vitale, F., et al., *Fluidic Microactuation of Flexible Electrodes for Neural Recording.* Nano Letters, 2018. **18**(1): p. 326-335.

82. Singh, A., H. Zhu, and J. He. *Improving mechanical stiffness of coated benzocyclobutene (BCB) based neural implant*. in *international conference of the ieee engineering in medicine and biology society*. 2004.

83. Felix, S.H., et al., *Insertion of flexible neural probes using rigid stiffeners attached with biodissolvable adhesive.* Journal of Visualized Experiments, 2013(79).

84. Kim, T.-i., et al., *Injectable, cellular-scale optoelectronics with applications for wireless optogenetics.* Science, 2013. **340**(6129): p. 211-216.

85. Tyler, W.J., *The mechanobiology of brain function.* Nature Reviews Neuroscience, 2012. **13**(12): p. 867.

86. Winslow, B.D. and P.A. Tresco, *Quantitative analysis of the tissue response to chronically implanted microwire electrodes in rat cortex.* Biomaterials, 2010. **31**(7): p. 1558-1567.

87. Likodimos, V., et al., *Magnetic and electronic properties of multiwall carbon nanotubes.* Physical Review B, 2003. **68**(4): p. 045417.

88. Finelli, D.A., et al., *MR imaging-related heating of deep brain stimulation electrodes: in vitro study.* American journal of neuroradiology, 2002. **23**(10): p. 1795-1802.

89. Mobin, F., et al., *Correlation between MRI-based stereotactic thalamic deep brain stimulation electrode placement, macroelectrode stimulation and clinical response to tremor control.* Stereotactic and functional neurosurgery, 1999. **72**(2-4): p. 225-232.

90. Thani, N.B., et al., *Accuracy of postoperative computed tomography and magnetic resonance image fusion for assessing deep brain stimulation electrodes.* Neurosurgery, 2011. **69**(1): p. 207-214.

91. Schenck, J.F., *The role of magnetic susceptibility in magnetic resonance imaging: MRI magnetic compatibility of the first and second kinds.* Medical physics, 1996. **23**(6): p. 815-850.

92. Volder, M.F.L., De, et al., *Carbon nanotubes: present and future commercial applications.* Science, 2013. **339**(6119): p. 535-539.

93. Schmidt, A.C., et al., *Carbon Nanotube Yarn Electrodes for Enhanced Detection of Neurotransmitter Dynamics in Live Brain Tissue.* Acs Nano, 2013. **7**(9): p. 7864-7873.

94. Fabbro, A., et al., *Carbon Nanotubes: ArtificialNanomaterials to EngineerSingle Neurons and Neuronal Networks.* Acs Chemical Neuroscience, 2012. **3**(8): p. 611.

95. Malarkey, E.B. and V. Parpura, *Carbon nanotubes in neuroscience.* Acta Neurochirurgica Supplement, 2010. **106**: p. 337.

96. Liu, L., et al., *A simple functional carbon nanotube fiber for in vivo monitoring of NO in a rat brain following cerebral ischemia.* Analyst, 2017. **142**(9): p. 1452-1458.

97. Cao, F., L. Zhang, and T. Yang, *A novel N-doped carbon nanotube fiber for selective and reliable electrochemical determination of ascorbic acid in rat brain microdialysates.* Journal of Electroanalytical Chemistry, 2016: p. S1572665716305550.

98. Kim, J., et al., *Next-generation flexible neural and cardiac electrode arrays.* Biomedical Engineering Letters, 2014. **4**(2): p. 95-108.

99. Xu, H., et al. *Chronic multi-region recording from the rat hippocampus in vivo with a flexible Parylene-based multi-electrode array*. in *international conference of the ieee engineering in medicine and biology society*. 2017.

100. Castagnola, V., et al., *Parylene-based flexible neural probes with PEDOT coated surface for brain stimulation and recording.* Biosensors and Bioelectronics, 2015. **67**: p. 450-457.

101. Donaldson, K., et al., *Carbon Nanotubes: A Review of Their Properties in Relation to Pulmonary Toxicology and Workplace Safety.* Toxicological Sciences, 2006. **92**(1): p. 5-22.

102. Bosman, L.W., et al., *Anatomical Pathways Involved in Generating and Sensing Rhythmic Whisker Movements.* Frontiers in Integrative Neuroscience, 2011. **5**: p. 53.

103. Boloori, A.R. and G.B. Stanley, *The Dynamics of Spatiotemporal Response Integration in the Somatosensory Cortex of the Vibrissa System.* Journal of Neuroscience the Official Journal of the Society for Neuroscience, 2006. **26**(14): p. 3767.

104. He, J.V., Zheng, W. Qi, and G.B. Stanley, *Adaptive shaping of cortical response selectivity in the vibrissa pathway.* Journal of Neurophysiology, 2015. **113**(10): p. 3850-3865.

105. Wang, Q., R.M. Webber, and G.B. Stanley, *Thalamic synchrony and the adaptive gating of information flow to cortex.* Nature neuroscience, 2010. **13**(12): p. 1534.

106. Whitmire, C.J., et al., *Information coding through adaptive gating of synchronized thalamic bursting.* Cell reports, 2016. **14**(4): p. 795-807.

107. Sanchez, J.C., et al., *Structural modifications in chronic microwire electrodes for cortical neuroprosthetics: a case study.* IEEE Transactions on Neural Systems and Rehabilitation Engineering, 2006. **14**(2): p. 217-221.

108. Chestek, C.A., et al., *Long-term stability of neural prosthetic control signals from silicon cortical arrays in rhesus macaque motor cortex.* Journal of neural engineering, 2011. **8**(4): p. 045005.

109. Antkowiak, B., H. Hentschke, and K. Kirschfeld, *Effects of volatile anaesthetics on spontaneous action potential firing of cerebellar Purkinje cells in vitro do not follow the Meyer-Overton rule.* British Journal of Anaesthesia, 1997. **79**(5): p. 617-624.

110. Antkowiak, B. and C. Helfrich-Förster, *Effects of small concentrations of volatile anesthetics on action potential firing of neocortical neurons in vitro.* Anesthesiology, 1998. **88**(6): p. 1592-605.

111. Ries, C.R. and E. Puil, *Mechanism of anesthesia revealed by shunting actions of isoflurane on thalamocortical neurons.* Journal of Neurophysiology, 1999. **81**(4): p. 1795-801.

112. Aksenov, D.P., et al., *Effects of anesthesia on BOLD signal and neuronal activity in the somatosensory cortex.* J Cereb Blood Flow Metab, 2015. **35**: p. 1819-1826.

113. Massey, C.A., et al., *Isoflurane abolishes spontaneous firing of serotonin neurons and masks their pH/CO2 chemosensitivity.* Journal of Neurophysiology, 2015. **113**(7): p. 2879-2888.

114. Ren, J., et al. *Habenula "cholinergic" neurons co-release glutamate and acetylcholine and activate postsynaptic neurons via distinct transmission modes*. in *中国神经科学学会全国学术会议暨第五次会员代表大会*. 2011.

115. Soriagómez, E., et al., *Habenular CB1 Receptors Control the Expression of Aversive Memories.* Neuron, 2015. **88**(2): p. 306-313.